

LATTICE GAS DYNAMICS, VOLUME I VISCOUS FLUIDS

Jeffrey Yepez

Rome Laboratory/ER
31 Grenier Street
Hanscom AFB, MA 01731-3010

9 November 1995

DTIC QUALITY INSPECTED 2

APPROVED FOR PUBLIC RELEASE; DISTRIBUTION UNLIMITED.



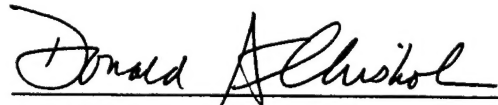
PHILLIPS LABORATORY
Directorate of Geophysics
AIR FORCE MATERIEL COMMAND
HANSCOM AIR FORCE BASE, MA 01731-3010

19980428 152

This technical report has been reviewed and is approved for publication



DONALD D. GRANTHAM, Chief,
Atmospheric Structure Branch
Contract Manager



DONALD A. CHISHOLM, Acting Director
Atmospheric Sciences Division

This report has been reviewed by the ESC Public Affairs Office (PA) and is releasable to the National Technical Information Service (NTIS).

Qualified Requestors may obtain additional copies from the Defense Technical Information Center (DTIC). All others should apply to the National Technical Information Service (NTIS).

If your address has changed, if you wish to be removed from the mailing list, or if the addressee is no longer employed by your organization, please notify PL/IM, 29 Randolph Road, Hanscom AFB, MA 01731-3010. This will assist us in maintaining a current mailing list.

Do not return copies of this report unless contractual obligations of notices on a specific document require that it be returned.

REPORT DOCUMENTATION PAGE			Form Approved OMB No. 0704-0188	
Public reporting burden for this collection of information is estimated to average 1 hour per response, including the time for reviewing instructions, searching existing data sources, gathering and maintaining the data needed, and completing and reviewing the collection of information. Send comments regarding this burden estimate or any other aspect of this collection of information, including suggestions for reducing this burden, to Washington Headquarters Services, Directorate for Information Operations and Reports, 1215 Jefferson Davis Highway, Suite 1204, Arlington, VA 22202-4302, and to the Office of Management and Budget, Paperwork Reduction Project (0704-0188), Washington, DC 20503.				
1. AGENCY USE ONLY (Leave blank)		2. REPORT DATE 9 November 1996		3. REPORT TYPE AND DATES COVERED SCIENTIFIC
4. TITLE AND SUBTITLE LATTICE GAS DYNAMICS, VOLUME I: VISCOUS FLUIDS			5. FUNDING NUMBERS PE 61102F PR 2304 TA CP WU 10	
6. AUTHOR(S) JEFFREY YEPEZ				
7. PERFORMING ORGANIZATION NAME(S) AND ADDRESS(ES) AIR FORCE RESEARCH LABORATORY/VSBE 29 RANDOLPH RD HANSCOM AFB, MA 01731-3010			8. PERFORMING ORGANIZATION REPORT NUMBER PL-TR-96-2122(I) ERP, NO. 1200	
9. SPONSORING/MONITORING AGENCY NAME(S) AND ADDRESS(ES) AIR FORCE OFFICE OF SCIENTIFIC RESEARCH MATHEMATICAL AND COMPUTATIONAL SCIENCES AFOSR/NM BOLLING AFB, DC 20331-0001			10. SPONSORING/MONITORING AGENCY REPORT NUMBER	
11. SUPPLEMENTARY NOTES				
12a. DISTRIBUTION AVAILABILITY STATEMENT APPROVED FOR PUBLIC RELEASE: DISTRIBUTION UNLIMITED			12b. DISTRIBUTION CODE	
13. ABSTRACT (Maximum 200 words) The theory and computation of lattice gas dynamics for viscous fluid hydrodynamics is presented. Theoretical analysis of these exactly conserved, discrete models is done using the Boltzmann approximation, a mean-field theoretical treatment. Theoretical results are then compared to numerical data arrived by exactly computed simulations of simple lattice-gas systems. The numerical simulations presented were carried out on a prototype lattice-gas machine, the CAM-8, which is a virtual finegrained paralld mesh architecture suitable for discrete modeling in arbitrary dimensions. Single speed and multi-speed lattice gases are treated. The new contribution is an integer lattice gas with many particles per momentum state. Comparisons are made between the mean-field theory and numerical experiments for shear viscosity transport coefficient.				
14. SUBJECT TERMS Lattice-gas Parallel computing Viscous fluid Computational fluid dynamics Discrete fluid Cellular automata			15. NUMBER OF PAGES 226	
			16. PRICE CODE	
17. SECURITY CLASSIFICATION OF REPORT UNCLASSIFIED	18. SECURITY CLASSIFICATION OF THIS PAGE UNCLASSIFIED	19. SECURITY CLASSIFICATION OF ABSTRACT UNCLASSIFIED	20. LIMITATION OF ABSTRACT SAR	

Contents

1	Introduction	1
1.1	Overview of the Lattice Gas Scheme	1
1.2	Background	3
1.3	Lattice Gas Attributes	7
1.4	Organization	10
2	Single-Speed Lattice Gas Theory	15
2.1	Microdynamics: An Exactly Computable Dynamical System	21
2.1.1	Preliminaries	21
2.1.2	Isotropic Lattice Tensors	22
2.1.3	Dynamical Transport Equation	25
2.1.4	Embedding in a Continuum	32
2.1.5	Hamiltonian	33
2.1.6	Hamilton's Equations	35
2.2	Mesoscopic Equilibrium: A Statistical Mechanics Treatment	39
2.3	Mesodynamics: A Mean-Field Treatment	44
2.3.1	Interpreting the Form of the Lattice Gas Pressure	47
2.3.2	Collision Operator in the Mesoscopic Limit	50
2.3.3	Jacobian of the Collision Operator	51
2.3.4	BGK Approximation	52
2.3.5	Eigensystem of the Jacobian of the Collision Operator	53
2.3.6	Collision Set Formulation of J	57
2.4	Bridging the Meso and Macroscales: Chapman-Enskog Expansions	58
2.4.1	Mach Number Expansion of the Fugacity	58
2.4.2	J Theorem	62
2.5	Macrodynamics	65
2.5.1	Derivation of the Continuum Equations	68
2.5.2	Recalculating the Shear Viscosity Transport Coefficient	70
2.5.3	Variation of Viscosity Minima with Lattice Coordination Number	72

3	The Simplest Lattice-Gas ($L=1$)	75
3.1	Introduction	75
3.2	Using the Tools of the Trade	77
3.2.1	Triangular Lattice	77
3.2.2	Mean-Field Calculation of the Shear Viscosity	82
3.2.3	An Example of a Deterministic Lattice-Gas	85
3.2.4	An Example of a Spurious Invariant	88
3.3	Some Numerical Fluid Experiments	90
3.3.1	Measurement of Shear Viscosity	90
3.3.2	Superposition of Sound Pulses	96
3.3.3	Kelvin-Helmholtz Instability on the CAM-8	98
3.3.4	Von Karman Streets on the CAM-8	99
4	Multispeed Lattice-Gas	103
4.1	Summary of Physical Assumptions	105
4.2	Microdynamics: An Exactly Computable Thermodynamical System	106
4.3	Statistical Mechanics of a Multispeed Lattice Gas System	107
4.4	Obtaining the Macroscopic Equations of Motion from the Fermi-Dirac Distribution Function	110
4.5	Determination of Expansion Coefficients	114
4.6	Momentum Flux Density Tensor	117
4.7	Thermohydrodynamic Sound Speed Measurements	118
4.8	Rayleigh-Bénard Convection on the CAM-8	122
5	Integer Lattice Gases ($L > 1$)	127
5.1	Microdynamics	129
5.2	Mesodynamics	130
5.2.1	Equilibrium Distribution	130
5.2.2	Boltzmann Equation	133
5.2.3	Chapman-Enskog Expansion	134
5.2.4	First Correction to the Equilibrium Distribution	136
5.2.5	Statistical Mechanics	138
5.3	Macrodynamics	147
6	The Simplest Integer Lattice Gas ($L = 2$)	149
6.1	Introduction	149
6.2	A Numerical Test of the Kinematic Shear Viscosity	152
6.3	Channel Sampling Algorithm	154

7 Conclusion	165
7.1 Discussion	165
7.2 Summary of Lattice Gas Systems for Viscous Fluids	167
7.2.1 Classical Integer Lattice Gas	167
7.2.2 Multispeed Lattice Gas	168
References	169
A The Cellular Automata Machine CAM-8	181
B Discrete Mathematics for Lattice Calculations	187
B.1 Discrete Fourier Transform	187
B.2 Integration by Parts on a Lattice	188
B.3 Discrete Green's Function	189
C The Parallel C-Star Language on the CM-5: A Network Communi- cations Test	191
D Mach Number Expansion of the Fermi-Dirac Distribution Function	195
D.1 Expanding the Single-Speed Fermi-Dirac Distribution Function	195
D.2 Single Particle Distribution Function from Symmetry	198
E Integer Lattice Gas Implementation	203
F Counting States in Quantum Mechanics	211

List of Figures

2.1	Fractional Occupation Versus Fugacity for a Classical Lattice Gas ($L = 1$)	61
2.2	Galilean Factor Versus Fractional Occupation for a Classical Lattice Gas ($L = 1$)	61
2.3	Kinematic viscosity for $D=2$ and $B=4,6,8$	73
3.1	Triangular Lattice Convention	77
3.2	FHP Collision Rules	82
3.3	FHP Momentum Profiles	90
3.4	FHP Viscosity Profiles by Poiseuille Flow	93
3.5	FHP Kinematic viscosity	94
3.6	Spectator Collision Rules	96
3.7	4-body Collision Rules	96
3.8	FHP Viscosity Profiles by Exponential Damping	97
3.9	FHP Sound Mode	98
3.10	Shear 7-bit CAM-8 Experiment	101
3.11	Von Karman Streets Simulation on the CAM-8	102
4.1	Standing Wave Density Profile	121
4.2	Sound Wave Damping	124
4.3	Sound Speed vs Energy	125
4.4	Rayleigh-Bénard Convection Cells	125
5.1	Bit Layout for an Integer Lattice Gas	129
5.2	Fractional Occupation Versus Fugacity ($L = 1$ to $L = 10$)	132
5.3	Galilean Factor Versus Fractional Occupation ($L = 1$ to $L = 10$)	136
5.4	Occupation Number Versus Fugacity for a Bose-Einstein Lattice Gas	144
5.5	Fractional Occupation Versus Fugacity for a Bose-Einstein Lattice Gas and an Integer Lattice Gas	146
5.6	Galilean Factor Versus Occupation Number for a Bose-Einstein Lattice Gas	147
6.1	Equivalence Class Example for an $L = 2$ Integer Lattice Gas	150

6.2	Log-Log Plot of the Decay Rate for an $L = 2$ Integer Lattice Gas . .	155
6.3	Kinematic Viscosity of an $L = 2$ Integer Lattice Gas	156
6.4	Von Karman Instability in an $L = 2$ Integer Lattice Gas	162
6.5	Von Karman Instability in an $L = 4$ Integer Lattice Gas	163
A.1	MIT Laboratory for Computer Science CAM-8 Prototype	182
A.2	CAM-8 System Diagram	183
C.1	Performance runs on a 256-node CM-5 for a hexagonal lattice embed- ded into a 3D mesh	193

List of Tables

2.1	Glossary of Model Constants	16
2.2	Glossary of Single-Speed lattice gas Variables	16
2.3	Statistical Mechanics Glossary of Variables	17
2.4	Statistical Ensembles	39
3.1	Streaming for 2D Hex Lattice Embedded a into 3D Mesh	79
4.1	Multispeed Lattice-Gas Glossary of Variables	104
5.1	Grand Partition Function Example	138

Preface

The work presented here is the culmination of many years of good influence by many very special people. Without their help I could not have made any substantial progress. I would like to acknowledge Dr Norman Margolus, Dr Bruce Boghosian, Dr Shiyi Chen, Dr Hugh Pendleton, and Dr Stan Heckman for useful discussions and collaborations. I would like to thank Harris Gilliam for computer help. I would like to thank Donald Grantham for his dedicated support in starting a new basic research initiative at our laboratory. My new initiative in lattice-gas research would not have happened without his initial encouragement. I would also like to thank Dr Charles Holland, Dr Marc Jacobs, and Major Scott Schreck of the Mathematical and Computational Sciences Directorate of the Air Force Office of Scientific Research for the vision to allow this basic research with the hope of improving the state-of-the-art of computational physics on parallel architectures.

Chapter 1

Introduction

1.1 Overview of the Lattice Gas Scheme

To simplify a molecular dynamics program, one might consider a completely discrete version of things.¹ In this simplest case, one would still like to correctly simulate the many-body system of N particles—that is, to capture all the relevant physical kinetics, at least at a course-grained “hydrodynamic” scale—yet one would also like the most severely restricted microscopic behavior. This is a minimalist’s delight. Each particle has a definite position within a crystallographic lattice and time advances in discrete units. Consequently, a particle can have only a certain value for its momentum; that is, it can only move along the lattice directions going from one site to the next, and so its velocity is quantized, $v=nc$, where n is a positive integer and $c = \ell/\tau$ is the ratio of the lattice cell size to smallest unit of time. A particle occupies a point on the lattice; it resides at a single site at a time. Given that a particle is a point, the extent of information needed to encode its existence is a single classical bit. If the bit is *on*, the particle is there. If the bit is *off*, the particle is not there.

But how many particles can reside at one site of the lattice at any particular time?

Received for publication, 9 November 1996.

A minimalist, in deference to Fermi-Dirac statistics, would immediately suggest an answer: the maximum number of particles that can simultaneously reside at a single lattice site must equal the maximum number of distinct momenta one is willing to keep track of. To use “quantum mechanical” terms, each particle occupies its own distinct local state.

In this way, the Pauli exclusion principle is enforced as there can be no more than a single particle per momentum state. As a particle in state α at some lattice site of the crystallographic space “hops” into state β , say at a neighboring site, a digital bit is moved from α and into β . So in lattice gas dynamics one simulates a system of *Boolean particles*. Global data permutations correspond to spatial translation and endow the bits with “kinetic energy”. Local and conditional data permutations correspond to collisional interactions between bits. Effectively, all the “computational work” is placed in the collisional interactions, since it is there that the decisions are made as to whether or not a set of Boolean particles should collide and if so how. This computational picture of particle dynamics is related to finite difference methods for solving partial differential equations [90, 23]. But the lattice gas methodology has an intrinsic value beyond finite difference schemes in that there is no internal source of error in the numerical treatment, it is therefore referred to as *exactly computable*.

To complete the introduction to lattice gases, some historical notes about the subject are presented and some computational attributes unique to lattice gases are discussed (this is provided as motivation to show why one might want to study lattice gases). The introduction concludes with a section outlining the organization of this volume on lattice gas dynamics for viscous fluid simulation.

1.2 Background

Let me briefly review some of the historical developments in the lattice gas field. An overview of the lattice gas subject has been given by Boghosian [14]. Lattice gases are a special case of cellular automata, popularized in the 1980's by Ed Fredkin [40] and by Stephen Wolfram [95, 96]. An early treatment of the cellular automata subject is presented by Tommaso Toffoli and Norman Margolus in their book on cellular automata machines [92]. Following the cellular automata paradigm, lattice gases are ideally suited for fine-grained parallel processing.

Simple implementations of a discrete molecular dynamics on a square lattice were investigated in the early 1970's by the French, in particular Yves Pomeau and coworkers [48]. By the late 1970's, cellular automata research was underway at the Information Mechanics Group at MIT on reversible computation by Edward Fredkin, Tommaso Toffoli, and Norman Margolus [88, 40, 62]. The idea of building special-purpose machines to simulate these physics-like models on a fine-grained space [89, 62] originated there. A good review of the kind of cellular automata modeling done in the early 1980's is given by Gérard Vichniac [94]. During this time, Stephen Wolfram visited the Information Mechanics Group and was stimulated by their work. In 1983 Wolfram popularized cellular automata as a simple mathematical model to investigate self-organization in statistical mechanics [95, 72]. Beyond this, no useful insights towards understanding or modelling real physical systems arose.

After visiting the MIT Information Mechanics Group in 1983 and seeing a simple discrete gas on a square lattice running on the cellular automata machine CAM-5 of Toffoli and Margolus [90, 89], Pomeau realized the potential for simulating large fluid systems and much new interest and activity in the field emerged. A race began

to theoretically prove that a hydrodynamic limit emerges from simple lattice gas rules. The intense interest was not stirred as much by the subject of hydrodynamics itself, but instead by the possibility of a simple cellular space-time model capturing such complex natural behavior in an exact way. In 1985 Wolfram completed the first hydrodynamics simulations on a triangular lattice [98] on the first Connection Machine—at that time, lattice gases were a very appropriate application for the bit oriented single instruction, multiple data Connection Machine. By 1986 Frisch, Hasslacher, and Pomeau had reported the existence of an isotropic two-dimensional lattice gas on the triangular lattice [42]. In the same year Wolfram completed the most detailed treatment of the basic theory of discrete fluids including novel symmetry considerations and introduced the Boltzmann approximation. Frisch *et al.* found the minimal lattice symmetry needed to recover isotropic flow in the continuum limit is a triangular lattice with a particle possessing six momentum states. Their model is now referred to as the FHP-model or hexagonal lattice gas model. Accompanying the seminal 1986 FHP paper was a paper by Margolus, Toffoli, and Vichniac on cellular-automata supercomputers for fluid-dynamics modeling [66]. The contribution of Margolus *et al.* was meant to complement the theoretical work of Frisch *et al.*, pointing out that with dedicated computational hardware the lattice gas models may gain an advantage over traditional methods of physical modeling.

By 1987 the lattice gas methodology was extended to model three-dimensional flows. The minimal lattice found by Frisch *et al.* [41] was the face centered hypercubic (fchc) lattice. The fchc lattice with 24-nearest neighbors is projected onto three dimensions in a simple fashion by limiting the depth of the fourth dimension of the simulation volume to one lattice link. Much effort was spent on finding optimal

collisions to minimize the viscosity of the fluid [50], however this task has proven very difficult. The reason for this difficulty is that the fchc lattice gas has 2^{24} or 16.7 million input configurations. In practice, all possible collisions are not included in a simulation because of the large demand for local memory needed to pre-store all the necessary collisional events in table look-up format—an efficient scheme for implementing complex interactions. To ease memory loads, lattice isometries are exploited to reduce the size of look-up tables [83].

The lattice gas approach has been extended to the direct simulation of the Boltzmann equation [60, 74, 69, 27], since space and time are discrete it is termed the *lattice-Boltzmann equation* [23]. Since the Boltzmann equation is an integrodifferential equation, usually a cutoff to the collision integral is made to treat the Boltzmann equation as an approximate differential equation. In the lattice gas community, typically the collision integral is reduced to a simple form introduced in 1954 by D. Bhatnager, E. Gross, and M. Krook [10]. A more descriptive title for the mesoscopic transport equation would be the *lattice-Boltzmann equation in the BGK approximation*. In place of the exactly computable microscopic dynamics of Boolean particles, one begins at the mesoscopic regime which deals with the probability of a particle occupying a given momentum state. This probability is set by a certain statistical distribution function of choice. So, the lattice Boltzmann equation is the transport equation for the single particle distribution function. The approach offers both theoretical and computational advantages. For modelling, one specifies a priori the single particle equilibrium distribution. Computationally it has the advantage of eliminating inherent noisy fluctuations in the simulation, but at the expense of discarding semi-detailed balance and information concerning particle-particle correlations.

The lattice Boltzmann equation in the BGK approximation is a unique contribution of the lattice gas community to high-performance computational physics [55]. The lattice Boltzmann equation, usually implemented within one hundred lines of code on a massively parallel processor², allows one to efficiently model complex fluids and provides a straightforward particle-based metaphor to computation. It relies on floating point calculations and therefore is suited for massively parallel machines such as Thinking Machine's Connection Machine-5 (CM-5), International Business Machines's SP-2, or Cray T3E. Essential connections between physics and computing are lost in this method. It is a finite difference method useful for the simulation of viscous fluids [68] and multiphase fluids [78]. It offers no intrinsic promise to explore essential connections between physics and computing. Therefore, lattice Boltzmann simulations are not treated in this volume.

The hope of modeling very high Reynolds number flows by lattice gas methods has not been realized, even with models that violate semi-detailed balance—lattice gas models in the Boltzmann approximation have shown considerably more success in achieving high Reynolds number flows³. The simulation of high Reynolds flow by a quantum lattice gas is investigated in volume III [103].

Areas of lattice gas research include: hydrodynamics and thermohydrodynamics [27, 35, 44, 2, 68], immiscible fluids [76, 26, 47, 46], multiphase systems [22, 4, 3, 5, 104, 45, 78, 101, 99, 79], reaction-diffusion systems [32, 58, 54], magnetohydrodynamics [24, 25, 28, 67], flow through porous media [75, 29], renormalized kinetic theory [56, 18, 51,

²See Appendix C for example of lattice-Boltzmann code written in the parallel C-Star language for the Connection Machine-5.

³Lattice Boltzmann simulations for three dimensional flows with Reynolds numbers of about 50,000 were presented in June 1993 at the International Conference on Pattern Formation and Lattice-Gas Automata sponsored by the Fields Institute, Waterloo, Canada.

19, 93, 71, 12], and quantum dynamics [84, 85, 16, 105]. A good review of the lattice gas subject, with particular emphasis on interfaces, phase transitions, and multiphase flow, has recently been presented by Rothman and Zaleski [77]. Additionally, a fairly comprehensive bibliography of the subject has been compiled [53].

Recently the first prototype of the next generation cellular automata machine, CAM-8, has been constructed [65]. The current 8-module CAM-8 prototype, with a site density of 2^{24} 16-bit sites per module, has a total of 128 million sites. A machine with one billion sites whose total space can be updated in less than a second has been designed [91].

1.3 Lattice Gas Attributes

There are several motives for studying lattice gases, some practical and some theoretical. Commonly cited motives are oriented towards computer science and issues related to massively parallel processing or reasons related to modeling physical systems with complex boundary conditions. The lattice gas' attributes usually mentioned in the literature include: 1) bit "democracy"; 2) simplicity and universality; 3) exact computability; 4) locality; and 5) unitarity.

Firstly, to quote Frisch, a lattice gas possesses "bit democracy." It was believed a decade ago that lattice gases would be efficient for physical modelling. However, it is now quite clear that lattice gases are generally very inefficient at this. In floating point calculations there exist uncontrolled round-off errors in the least significant bits. The most significant bits are weighted exponentially more than the least significant bits (because of the exponential encoding used in floating-point numbers). Consequently the value of the most significant bits determines the computational outcome, at least

under numerically stable conditions. In contrast, in lattice gases all bits have equal weight (an exception to this is the integer lattice gas that is discussed in detail in the last chapters 5 and 6 of this volume). Bit democracy usually is not as efficient vis a vis bit weighting found in standard numerical methods. In a simple lattice gas, only a single bit is used to represent a particle, whereas in molecular dynamics a few hundred bits are used (six floating-point numbers for position and momentum). Nevertheless, molecular dynamics is in most cases a much better modelling tool. The only exception to this general rule occurs at large hydrodynamic scales and for quite complex fluids. Under these circumstances, lattice gases can outstrip molecular dynamics, and lattice gases are the best modelling tool (in this area of computational physics usually no competing high level scheme exists) [15]. These issues are explored in detail in Volume II on long-range lattice gases for multiphase fluid dynamics [102].

Secondly, lattice gases possess an inherent simplicity and universality. Just as simple models in statistical mechanics, such as the Ising model, shed light on equilibrium thermodynamics and equilibrium critical phenomena, so too do lattice gas models shed light on kinetics and dynamical phenomena [104]. Moreover, its inherent simplicity gives the lattice gas pedagogical value since many properties of macroscopic systems can be predicted through analysis of simple local microscopic properties. For example, lattice gases are a simple way to understand details of fluid system properties such as the dependence of the shear viscosity on particle collision rates. Most computational fluid dynamics codes are complicated and intricate in their approximations. In contrast, lattice gases are the simplest conceptual expression of Navier-Stokes flow.

Thirdly, lattice gases are exactly computable. Lattice gases can model classical systems while keeping mass, momentum, and energy exactly conserved. Exact mod-

eling is valuable, for example, in cases where multiparticle correlations are essential to the system's behavior. Lattice gas simulations can verify theoretical predictions beyond the Boltzmann mean-field approximation of uncorrelated collisions: the phenomenon of long-time tails in the velocity autocorrelation function [1, 73, 37] has recently been observed in lattice gases [56, 18, 19].

Fourthly, like their cellular automata cousins, lattice gases are local. The combination of simplicity and locality of lattice gas rules allows—in principle—nearly ideal logic density. The highest logic density that one could physically imagine would be the atomic density of solids. There is the interesting prospect of lattice gas architectures built at such a high informational density, termed *nanoscale computing*. There is hope that in the future computation will be achieved with “quantum gates” [63, 61, 11, 49, 7]. In fact the first quantum gate has recently been implemented using nuclear magnetic resonance spectroscopy where a few nuclear spins in each molecule of a liquid sample embody quantum bits [31]. As the fundamental computational element's size reduces to nanoscale ranges its behavior is governed by quantum mechanics. This leads to the following discussion of a quantum version of a lattice gas.

Fifthly, the evolution operator for *quantum lattice gases* is unitary—a quantum lattice gas is a generalization of a classical lattice gas where quantum bits replace classical bits, see Volume III [103]. Quantum mechanics requires unitary, and hence invertible, time evolution—the microscopic reversibility of the lattice gas dynamics is important here.⁴ The ultimate type of computation would allow one to exactly

⁴Even before quantum mechanics becomes a constraint, the reversibility of lattice gas dynamics may become a significant benefit, since at very high logic densities the dissipation of heat caused by irreversible computations has already become an important engineering issue [8, 9].

represent a quantum system. In the context of computation on a discrete spacetime lattice, Feynman noticed “the possibility that there is to be an *exact* simulation, that the computer will do *exactly* the same as nature” [38]. He hoped that using computers in an exactly computable way might lead to new possibilities in our understanding of physics. Feynman introduced a brand new notion: there may exist the possibility of a quantum computer [39]. Quantum lattice gases are a realization of this.⁵ It is believed that quantum lattice gases can exhibit emergent behavior quite similar to the many-body behavior described by the Schrödinger equation of nonrelativistic quantum mechanics [84, 85, 16]. Volume III on lattice gas dynamics for quantum fluids explores some lattice based models for quantum computation. For example, it is shown that an array of quantum bits evolving by a particular local unitary evolution operator can Bose condense in close analogy with the Helium II phase of the He⁴ isotope below the λ -point [105].

1.4 Organization

This volume is the first of three volumes that treat the subject of lattice gas dynamics. This volume focuses on viscous fluid dynamics and sets a foundation for the next two volumes which deal with generalizations of the method presented here. Volume II deals with nonlocal lattice gases. Here the generalization comes about by including two-point interparticle interactions. This is an appealing alternative to molecular dynamics in that multiphase fluid behavior is simulated at hydrodynamic scales not

⁵It has been shown by Shor [81] that quantum computers, good at finding the period of periodic functions, can be used to factor large numbers, a computational task whose complexity falls into the nonpolynomial-complete algorithmic class. That is, no classical computer can effectively factor a number of arbitrarily large size, and this fact is the cornerstone upon which cryptographic algorithms are based. The prospects for building a quantum computer are just beginning to be explored [82, 34].

achievable by molecular dynamics. Volume III deals with quantum lattice gases. This new type of lattice gas is also quite appealing since it addresses the feasibility of performing quantum computation on a large collection of spin- $\frac{1}{2}$ quantum objects.

Lattice-based particle models implemented on spatially fine-grained parallel computers can represent, in a coarse-limit, interesting physical dynamics in a way that offers the computational physicist exactly computed results not easily obtained with conventional techniques implemented on conventional computers.

A self-contained review of the lattice gas subject sufficient for one to understand how to model viscous hydrodynamics is provided here. The mathematical treatment presented is carried out in an arbitrary number of dimensions. For simplicity when doing numerical verification, two-dimensional lattice gas simulations have often been implemented and tested.

The analysis of the lattice gas system is applied at three separate limits or physical regimes. The *microscopic limit* deals with the individual motions of the particles in the system. At this level a particle is nothing more than a single bit of information and everything is discrete. Next, the *mesoscopic limit* deals with the expectation value of microscopic quantities obtained by ensemble averaging in the grand canonical ensemble. The statistical mechanics treatment applies at the mesoscopic limit. Finally, the *macroscopic limit* (also referred to as the *scaling limit*) deals with emergent hydrodynamic behavior of the system. In this limit, one characterizes the dynamical behavior of the system by emergent partial differential equations of motion, one for each additive conserved quantity of the system (*viz.* mass, momentum, and energy). In the macroscopic limit everything is continuous and the system behaves like a fluid.

I address neutral, incompressible, viscous hydrodynamics and thermohydrody-

namics. Some of the material here is well known by the lattice gas community and is given as review material of the subject of lattice gases with purely local collisions. Presented is the concept of collisions and streaming and the lattice gas microdynamical transport equation. One goes from a microscopic description to a mesoscopic one by ensemble averaging. The mesoscopic equation is the lattice Boltzmann equation. The macroscopic limit is reached by performing a Chapman-Enskog expansion of the mesoscopic particle distribution function in terms of the macroscopic density and velocity variables. Although the microscopics is severely discretized, the resulting form of the macroscopic equation is a well defined partial differential equation, the Navier-Stokes equation for incompressible viscous fluids.

The theoretical description presented for a discrete lattice gas system is new. I begin by recovering the lattice gas microdynamical transport equation from Hamilton's equations. The idea of particle kinetics on a lattice embedded in continuous space is presented and some useful mathematical tools are introduced for the purpose of doing discrete calculus on the lattice. A discrete Green's function is used to formulate the interacting part of the Hamiltonian. The equations of motion for a single lattice gas particle are then cast in Hamiltonian format. The Hamiltonian for a many-body system is then obtained by summing the single particle Hamiltonian over all sites of the lattice and over all lattice directions.

All the exact numerical simulations of some new lattice gases⁶ have been carried out on the cellular automata machine (CAM-8), and in fact are the first lattice gas experiments conducted on this prototype machine.⁷ The lattice gas experiments

⁶In Volume II, focus is on novel classical lattice gases with long-range interactions as a way to model finite-temperature multiphase dynamics and molecular dynamics for solid-state modeling.

⁷A brief description of the CAM-8 architecture is given in Appendix A.

presented here are the first of their kind carried out on the new prototype machine beginning in 1992, the cellular automata machine CAM-8, the architecture built by Margolus and Toffoli [64]. Results of the simulation range from viscous hydrodynamics to multiphase systems to solid-state systems to quantum systems: (Volume I) Rayleigh-Bénard convection instability, Kelvin-Helmholtz shear instability, and Von-Karman vortex shedding instability; (Volume II) liquid-gases, spinoidal decomposition, and liquid-solid melts; and (Volume III) superfluidity and second sound.

Also presented in this volume is a treatment of a multispeed lattice gas. Sound speed versus temperature measurements for a simple hydrothermal lattice gas are given to illustrate the behavior of this lattice gas.

A novel integer lattice gas is presented [17] and a mean-field prediction for the shear viscosity is shown to agree with numerical experiment. The integer lattice gas is shown to obey fractional statistics, which is a simple closed form analytical function. The form of this fractional distribution function reduces to identically the Fermi-Dirac form in its one-particle-per-momentum-state limit and furthermore reduces to identically the Bose-Einstein form in its infinite-number-of-particles-per-momentum-state limit. A statistical mechanics treatment of the subject which has not been previously worked out for any lattice gas system is presented here.

Chapter 2

Single-Speed Lattice Gas Theory

A Boolean formulation of an exactly computable dynamical system, known as a lattice gas, is given as a discretization of classical kinetic transport of a system of identical particles. The discretization disconnects collisional scattering from kinetic transport, or *streaming*. The disjoint events are both fixed within a cellular phase space.

The lattice gas dynamics is stated in a way that is consistent with the Boltzmann equation for kinetic transport. In essence the lattice gas dynamics are a simplified form of molecular transport restricted to a cellular phase space.

In this chapter, the dynamics is described at the microscopic, mesoscopic, and then macroscopic scale. Starting with a discrete microdynamical transport equation for number variables (the particle occupations), mesoscopic equations are obtained by averaging over an ensemble of states. In this way a Boltzmann equation is obtained for the particle distributions. Next, the macroscopic equations, in particular mass continuity and the Navier-Stokes equation for viscous incompressible flow, are obtained by a Chapman-Enskog expansion. The scheme exploits the isometries of the finite-point group of a crystallographic spatial lattice to recover isotropic fluid

Table 2.1: Glossary of Model Constants

Constants	Names
ℓ	length unit
τ	time unit
m	mass unit
c	velocity unit ($\frac{\ell}{\tau}$)
D	spatial dimension
B	lattice coordination number
\hat{e}_a	unit lattice vectors
L	number of bits per channel
a	directional index (1,2,..., B)
i, j, k, l	spatial indices

Table 2.2: Glossary of Single-Speed lattice gas Variables (L=1)

Variables	Names
p	number of particles per collision
n_a	Boolean particle number variable
f_a	particle distribution function
Ω_a	collision operator
J_{ab}	Jacobian matrix
$ \alpha\rangle$	eigenkets of J
κ_α	eigenvalues of J
c_s	sound speed
p	pressure
ρ	density
v_i	velocity
Π_{ij}	momentum flux density tensor

Table 2.3: Statistical Mechanics Glossary of Variables

Variables	Names
GRAND CANONICAL ENSEMBLE	
Ξ	grand partition function
Ω	grand potential
U_m	connected correlation functions
F	distribution function
f	reduced distribution function
z	fugacity
β	inverse temperature
μ	chemical potential
P	pressure
T	temperature
S	entropy
V	volume
N	number of particles

dynamics in the macroscopic limit.

In this chapter on single-speed lattice gases, since I am concerned only with recovering viscous incompressible fluid dynamics, it is important at the outset to explain the characteristics of this flow regime. In the incompressible limit the fluid density is constant and mass continuity is equivalent to the fluid being divergenceless

$$\partial_i v_i = 0. \quad (2.1)$$

In an ideal fluid, with a nonthermal equation of state, the pressure is directly proportional to the density with the square of the sound speed the constant of proportionality

$$p = \rho c_s^2. \quad (2.2)$$

This is a *viscous fluid*. In the incompressible limit, a fluid can also be characterized by one transport coefficient, the shear viscosity, denoted $\eta(\rho)$ and for incompressible lattice gas fluids has been extensively studied [41, 83, 50, 100]. It is a density depen-

dent coefficient that determines the rate of momentum diffusion within the fluid. I do not concern myself with the other transport coefficients: there is no bulk viscosity coefficient since the flow is divergence-free, and there is no thermal conductivity, since there is not a separate energy equation. Therefore, in the continuum limit of this flow regime, momentum conservation implies the simplest form of the nonlinear Navier-Stokes equation

$$\rho \partial_t v_i + g \rho \partial_j (v_i v_j) = -\partial_i p + \eta \partial^2 v_i, \quad (2.3)$$

where the factor, g , is unity for real fluids but usually not unity in lattice gas models— g is referred to as the *Galilean prefactor*. The nonlinearity of the dynamics comes about because of the $v_i v_j$ term, the so called *convective* term, that gives rise to interesting flow instabilities (in Chapter 3, see for example the well known Kelvin-Helmholtz instability depicted in Figure 3.10 and the Von Karman instability depicted in Figure 3.11).

So the agenda is to introduce an artificially discrete microscopic dynamical system whose evolution in the continuum limit is described by a simple but nonlinear fluid equation. In this Chapter I deal only with the simplest discrete microdynamics that involves only local collisions.

The discrete nature of the lattice gas microscopic dynamics implemented on present day computers has low *spacetime resolution*. To state this another way, as a general rule, the characteristic length and time scales of a lattice gas simulation are relatively small. The exception to this rule occurs for lattice gases that model a *complex fluid*. The term complex fluid refers to any fluid where the form of its continuum dynamical equations is either uncertain or altogether unknown. Examples of complex fluids are a multiphase fluid such as a liquid-gas system, and a multispecies

fluid such as a microemulsion with two immiscible species and a dipolar surfactant. In this first part of the dissertation where I consider only viscous fluids, a gain in resolution is not obvious (later in the second part where I treat multiphase fluids, the gain in resolution will be apparent). To clarify issues, let us try to see why this is so.

There are two ways one could attempt to do hydrodynamics on a computer. The first way is to do a complete molecular dynamics treatment of a many-body system, a very low-level approach. With the largest available computers today capable of simulating the complete molecular dynamics of hundreds of millions of particles, emergent hydrodynamic behavior of the system of particles is observed. Yet the characteristic scale of the hydrodynamic flow remains extremely small, on the order of a single micron. This is far too small for most hydrodynamic problems of interest and consequently molecular dynamics is not used as a tool for hydrodynamic modeling of ideal fluids. The second way to do hydrodynamics on a computer is to directly implement the Navier-Stokes equation using either a finite-differencing scheme, a finite-element scheme, or a spectral scheme for example. With this kind of high-level approach, the characteristic hydrodynamic scale modeled can be increased to any arbitrary size so long as the Reynolds number of the simulation matches that of the fluid system of interest (and $Re < 10,000$ in 3D).

The lattice gas approach is a non-traditional way to do hydrodynamics on a computer. Here the characteristic scales achievable for ideal fluids is on the order of a single meter, a million times greater than that achievable using traditional molecular dynamics. The point is that although the resolution attainable by a lattice gas method is far smaller than that of a high level scheme, a spectral or finite element scheme for example, it is nevertheless far greater than the resolution offered by molec-

ular dynamics. Since for complex fluids one often does not even know the continuum dynamical equations, high level schemes are not even an option for modeling the system. So one would traditionally have to resort to a low-level molecular dynamics treatment and suffer a lack of system resolution. The lattice gas approach offers a way to model the continuum behavior of the system with a significant boost in resolution over that offered by molecular dynamics for systems that cannot be modeled by some high-level scheme.

The primary reason for this boost in resolution over molecular dynamics is that in the artificial microworld of the lattice gas, much microscopic detail is left out by the severe discreteness in the numerical treatment. Consequently, in a lattice gas the typical distance between particle collisions, the *mean-free path*, is only a single lattice spacing. And the typical time between particle collisions, the *mean-free time*, is only a single time step iteration. So in every computational step of the lattice gas model, every particle undergoes a collisional scattering event. In molecular dynamics this is not at all the case. For a particle to traverse the distance of a mean-free path and for the elapsed time to span the period of a mean-free time, hundreds or thousands of computational iterations are expended.

The discreteness of the artificial microscopic world also provides several menacing handicaps. Specifically, there is a lack of Galilean invariance, substantial noisy fluctuations, and a limitation to subsonic flow regimes. Over the past several years, the lattice gas community has strived to overcome these handicaps. For example, the lattice Boltzmann method recovers Galilean invariance and is essentially a noiseless method, yet it sacrifices exact computability and is plagued with numerical instabilities. I have found a new and interesting way to overcome these handicaps without

sacrificing exact computability, using an integer lattice gas [17]. This generalization of a Boolean lattice gas is discussed in Chapter 5 later in this report.

Remark:

It is an interesting fact, and perhaps inevitable, that to obtain an exactly computable representation of fluid dynamics one must resort to performing a statistical treatment over discrete number variables that locally interact according to some simple fixed sets of rules.

2.1 Microdynamics: An Exactly Computable Dynamical System

2.1.1 Preliminaries

Before introducing the basic lattice gas microdynamical transport equation, let us give some notational conventions. Consider a spatial lattice with N total sites. Particles have a unit of mass m and propagate on the lattice. The unit of length is the size of a lattice cell, ℓ , and the unit of time, τ , is the time it takes for a particle to go from one lattice site to a nearest neighboring site, so the unit propagation speed is defined by $c = \frac{\ell}{\tau}$.

The lattice vectors denoted by e_{ai} where $a = 1, 2, \dots, B$ define a Bravais lattice, where B is the lattice coordination number. I will be quite selective when choosing a vector set $\{e_{ai}\}$. The set will be a valid set only if all n -th rank tensors composed of a product of these lattice vectors are isotropic and fully symmetric under interchange of indices, see §2.1.2 below.

A particle's *momentum state* is completely specified at some time, t , by specifying its location on the lattice, x_i , and its direction, mce_{ai} , at that location. The particles

locally obey Pauli exclusion since only one particle can occupy a single momentum state at a time and are consequently Fermi-Dirac distributed. The number of configurations of momenta states per site is 2^B . The number of possible single particle momentum states available in the system is $N_{\text{total}} = BN$, so the number of system configurations¹, or phasespace points, is 2^{BN} . With P particles in the system, denote the background filling fraction, or the *reduced density*, by $d = \frac{P}{BN_{\text{total}}}$. Note that $0 \leq d \leq 1$ and for a large system d is considered a continuous variable.

The number variable, denoted by $n_a(\vec{x}, t)$, takes the value of one if a particle exists at site \vec{x} at time t in momentum state $mc\hat{e}_a$, and takes the value of zero if a particle is not present at \vec{x} at time t with momentum $mc\hat{e}_a$. As a matter of notation it should be understood that whenever a directionally dependent quantity is written, its subscripted index is taken modulo B . For example, it is understood that $n_{a+b} = n_{\text{mod}(a+b)}$. In terms of these quantities, the particle's momentum may be expressed as

$$p_{ai}(\vec{x}, t) \equiv mce_{ai}n_a(\vec{x}, t). \quad (2.4)$$

2.1.2 Isotropic Lattice Tensors

Construct an n -th rank tensor composed of a product of lattice vectors [97]

$$E^{(n)} = E_{i_1 \dots i_n} = \sum_a (e_a)_{i_1} \cdots (e_a)_{i_n}. \quad (2.5)$$

It is implied that sums over a directional index range from 1 to B , $\sum_a \equiv \sum_{a=1}^B$. All odd rank E vanish. Express $E^{(2n)}$ in terms of Kronecker deltas, $\delta_{ij} = 1$ for $i = j$ and zero otherwise. This problem of expressing the E -tensors in terms of products of Kronecker deltas can be turned into a problem of combinatoric counting.

¹For a typical lattice gas in two dimensions $B = 6$ and $N = 1,000,000$, so the number of phasespace points $2^{6,000,000}$ is quite large.

It is possible to enumerate all the possible symmetric tensors with even rank, denoted $\Delta^{(2n)}$. For $n = 1$ the second symmetric rank tensor is

$$\Delta_{ij}^{(2)} = \delta_{ij}. \quad (2.6)$$

Next, consider the $n = 2$ case, the fourth rank tensor $\Delta_{ijkl}^{(4)}$. Since the Kronecker delta is symmetric in its indices, the following four products are identical: $\delta_{ij}\delta_{kl} = \delta_{ij}\delta_{lk} = \delta_{ji}\delta_{kl} = \delta_{ji}\delta_{lk}$. The degeneracy is 2^2 . Furthermore, the order of the Kronecker deltas also doesn't matter since they commute; that is, $\delta_{ij}\delta_{kl} = \delta_{kl}\delta_{ij}$. This degeneracy is $2!$. So for $n = 2$, the total number of ways to write a fourth-rank tensor as a product of two Kronecker deltas is $2^2 2! = 8$. The total number of permutations for 4 indices is $4! = 24$. So from this counting procedure, it follows that $\Delta^{(4)}$ consists of $\frac{24}{8} = 3$ terms. Therefore, for $n = 2$ the fourth rank symmetric tensor is

$$\Delta_{ijkl}^{(4)} = \delta_{ij}\delta_{kl} + \delta_{ik}\delta_{jl} + \delta_{il}\delta_{kj}. \quad (2.7)$$

For the case where n is arbitrary, there are 2^n identical ways of writing the product of n Kronecker deltas. For each choice of indices, there are an additional $n!$ number of ways of ordering the products. Therefore, the total number of ways to write an $2n^{\text{th}}$ -rank tensor as a product of n Kronecker deltas is $2^n n! = (2n)!!$. The total number of permutations for $2n$ indices equals $(2n)!$. So from this counting procedure it follows that $\Delta^{(2n)}$ consists of a sum of $\frac{(2n)!}{(2n)!!} = (2n-1)!!$ terms. That is, for $n = 3$, $\Delta^{(6)}$ will have fifteen terms, for $n = 4$, $\Delta^{(8)}$ will have 35 terms, and so forth.

Using cartesian unit vectors, in two-dimensions for example, write

$$\Delta^{(2)} = \hat{x}\hat{x} + \hat{y}\hat{y}. \quad (2.8)$$

It follows that

$$\delta_{ij}\delta_{kl} = (\hat{x}\hat{x} + \hat{y}\hat{y})_{ij}(\hat{x}\hat{x} + \hat{y}\hat{y})_{kl} \quad (2.9)$$

$$= (\hat{x}\hat{x}\hat{x}\hat{x} + \hat{x}\hat{x}\hat{y}\hat{y} + \hat{y}\hat{y}\hat{x}\hat{x} + \hat{y}\hat{y}\hat{y}\hat{y})_{ijkl} \quad (2.10)$$

and similarly

$$\delta_{ik}\delta_{jl} = (\hat{x}\hat{x}\hat{x}\hat{x} + \hat{x}\hat{y}\hat{x}\hat{y} + \hat{y}\hat{x}\hat{y}\hat{x} + \hat{y}\hat{y}\hat{y}\hat{y})_{ikjl} \quad (2.11)$$

$$\delta_{il}\delta_{kj} = (\hat{x}\hat{x}\hat{x}\hat{x} + \hat{x}\hat{y}\hat{y}\hat{x} + \hat{y}\hat{x}\hat{x}\hat{y} + \hat{y}\hat{y}\hat{y}\hat{y})_{ilkj}. \quad (2.12)$$

Therefore, $\Delta_{ijkl}^{(4)}$ must be of the following form

$$\Delta^{(4)} = 3\hat{x}\hat{x}\hat{x}\hat{x} + 3\hat{y}\hat{y}\hat{y}\hat{y} + \hat{x}\hat{y}\hat{y}\hat{x} + \hat{y}\hat{x}\hat{x}\hat{y} + \hat{x}\hat{y}\hat{x}\hat{y} + \hat{y}\hat{x}\hat{y}\hat{x} + \hat{x}\hat{y}\hat{y}\hat{x} + \hat{y}\hat{x}\hat{x}\hat{y}. \quad (2.13)$$

Knowing that for E to be isotropic and symmetric, it must be proportional to Δ

$$E^{(2n)} = \alpha^{(2n)} \Delta^{(2n)}. \quad (2.14)$$

The constant of proportionality, $\alpha^{(2n)}$, may be obtained by taking the trace successively as follows. Since $e_{ai}e_{ai} = 1$ and $\delta_{ii} = D$, for $n = 1$ it follows that

$$\sum_a e_{ai}e_{ai} = \alpha^{(2)} \delta_{ii} \longrightarrow \alpha^{(2)} = \frac{B}{D}, \quad (2.15)$$

giving the result for the second rank tensor

$$E^{(2)} = \frac{B}{D} \delta_{ij}. \quad (2.16)$$

Since $\delta_{ijkk} = (D+2)\delta_{ij}$ and consequently $\delta_{iijj} = D(D+2)$, for $n = 2$ it follows that

$$\sum_a e_{ai}e_{ai}e_{aj}e_{aj} = \alpha^{(4)} \delta_{iijj} \longrightarrow \alpha^{(4)} = \frac{B}{D(D+2)}, \quad (2.17)$$

giving the result for the fourth rank tensor

$$E^{(4)} = \frac{B}{D(D+2)} (\delta_{ij}\delta_{kl} + \delta_{ik}\delta_{jl} + \delta_{il}\delta_{kj}). \quad (2.18)$$

Continuing this procedure, in general, the lattice tensors are

$$E^{(2n+1)} = 0 \quad (2.19)$$

$$E^{(2n)} = \frac{B}{D(D+2) \cdots (D+2n-2)} \Delta^{2n}. \quad (2.20)$$

In this chapter product tensors up to $E^{(4)}$ will be needed, but not beyond. Appropriate choices for the lattice vector sets are: $D = 2$, the triangular lattice with $B = 6$; $D = 3$, the icosahedral lattice with $B = 12$; and $D = 4$, the face-centered hypercubic lattice with $B = 24$ [97].

2.1.3 Dynamical Transport Equation

The evolution of the lattice gas is written in terms of n_a as a two-part process: a collision part and a streaming part. One therefore expresses the microscopic dynamics by writing down a collision equation and a streaming equation for the occupation variable $n_a(\vec{x}, t)$. Both of these equations are quite simple. Combining them gives the lattice gas microscopic transport equation.

If a single bit is used to encode a particle's position and momentum state (referred to as the $L = 1$ case where L is a model parameter for the number of bits per local momentum state), at every site in the lattice there are B bits and consequently 2^B possible local configurations. All these local configurations could be partitioned into mutually exclusive sets. A set of local configurations where every element of the set is a local configuration with the same value for the invariant quantities for the particular system (*i.e.* mass and momentum for a single speed lattice gas) is termed an *equivalence class* and is denoted \mathcal{EC} . A lattice gas collision operator has the property that it will cause transitions from one local configuration to another, where

the “incoming” and “outgoing” configurations are elements of the same equivalence class.

Denote a particular incoming configuration at some spacetime point (\vec{x}, t) by the set $\vec{n}(\vec{x}, t) = \{n_1(\vec{x}, t), n_2(\vec{x}, t), \dots, n_B(\vec{x}, t)\}$. After the collision step, the particles would be in a new outgoing configuration, denoted $\vec{n}'(\vec{x}, t) = \{n'_1(\vec{x}, t), n'_2(\vec{x}, t), \dots, n'_B(\vec{x}, t)\}$. The collision part of the dynamics permutes the particles locally at each site and this is written as follows

$$n'_a(\vec{x}, t) = n_a(\vec{x}, t) + \Omega_a(\vec{n}(\vec{x}, t)), \quad (2.21)$$

where Ω_a represents the collision operator and in general depends on all the particles, \vec{n} , at the site. In the streaming part of the dynamics a particle at position \vec{x} with momentum $m\vec{c}\hat{e}_a$ “hops” to its neighboring site at $\vec{x} + \ell\hat{e}_a$ and then time is incremented by τ

$$n_a(\vec{x} + \ell\hat{e}_a, t + \tau) = n'_a(\vec{x}, t). \quad (2.22)$$

Combining the collision equation (2.21) and the streaming equation (2.22) gives the lattice gas microdynamical transport equation of motion

$$n_a(\vec{x} + \ell\hat{e}_a, t + \tau) = n_a(\vec{x}, t) + \Omega_a[\vec{n}(\vec{x}, t)]. \quad (2.23)$$

In a classical lattice gas, the collision operator can only permute the particles locally on the site and so the local particle number is conserved before and after the collision. The outgoing configuration, \vec{n}' , can be chosen deterministically or probabilistically. But regardless of the collision mechanism, the set of outgoing bits $\{n'_1, n'_2, \dots, n'_B\}$

must be a permutation of the incoming bits $\{n_1, n_2, \dots, n_B\}$.²

$$n(\vec{x}, t) = \sum_a n'_a(\vec{x}, t) = \sum_a n_a(\vec{x}, t). \quad (2.24)$$

Equation (2.24) defines the local number of particles. Summing (2.23) over lattice directions then implies the following constraint on the collision operator

$$\sum_a \Omega_a = 0. \quad (2.25)$$

We may define the local momentum as

$$p_i(\vec{x}, t) = mc \sum_a e_{ai} n'_a(\vec{x}, t) = mc \sum_a e_{ai} n_a(\vec{x}, t), \quad (2.26)$$

which of course must also be conserved before and after a collision. Again, this imposes a constraint on the collision operator that for all i the following sum must vanish

$$\sum_a e_{ai} \Omega_a = 0. \quad (2.27)$$

These constraints (2.25) and (2.27) on the collision operator will allow us to obtain the proper form of the macroscopic equations of motion, in particular the mass continuity equation and the Navier-Stokes equation.³

There are several ways to allow for collisional transitions between elements of an equivalence class. It is important to categorize the possibilities because they determine the underlying nature of our artificial microworld: whether it is deterministic or statistical, whether it satisfies detailed balance or semi-detailed balance (defined below), and whether there exists a time-reversal invariance.

²For a quantum lattice gas, this restriction is lifted. The outgoing configuration is not a permutation of the incoming configuration. Instead, the outgoing configuration can be a superposition of any configurations within the respective equivalence class. This quantum generalization of a classical lattice gas is treated in Volume III [103].

³This is so only if detailed balance or semi-detailed balance is obeyed—these are defined below.

Consider a simple equivalence class with four members: $\{A, B, C, D\}$. The likelihood of all collisions can be expressed in a 4×4 matrix, called the *transition matrix*, whose element $T_{n,n'}$ gives the probability of transition for state n to state n' . In this simple example, the transition matrix is

$$T = \begin{pmatrix} T_{AA} & T_{AB} & T_{AC} & T_{AD} \\ T_{BA} & T_{BB} & T_{BC} & T_{BD} \\ T_{CA} & T_{CB} & T_{CC} & T_{CD} \\ T_{DA} & T_{DB} & T_{DC} & T_{DD} \end{pmatrix}. \quad (2.28)$$

An *energy-sector* is the set of all states with the same total energy. The statistical mechanics of a lattice gas system is worked out below, but for now it is assumed that the probability for being in a state depends on the total energy of the state. In a particular energy sector, the transition matrix must satisfy the property that the marginal probabilities all sum to unity, along both the columns and rows of the matrix. The sum along columns is the *semi-detailed balance condition*

$$\sum_n T_{n,n'} = 1, \quad (2.29)$$

and the sum along rows is the conservation of probability condition

$$\sum_{n'} T_{n,n'} = 1. \quad (2.30)$$

Note that summing over all collisions gives back the size of the equivalence class, denoted by $\|T\|$. That is,

$$\sum_{n,n' \in \mathcal{EC}} T_{n,n'} = \|T\|. \quad (2.31)$$

A *deterministic* dynamical system is one whose transition matrix components are either zero or one. The trivial deterministic transition matrix is just the identity matrix that maps all states onto themselves. There are two types of deterministic transition matrices, symmetric and non-symmetric. An example of a symmetric transition

matrix is the following

$$T = \begin{pmatrix} 0 & 1 & 0 & 0 \\ 1 & 0 & 0 & 0 \\ 0 & 0 & 0 & 1 \\ 0 & 0 & 1 & 0 \end{pmatrix} \quad (2.32)$$

where configuration $A \leftrightarrow B$ and configuration $C \leftrightarrow D$, and a non-symmetric one is

$$T = \begin{pmatrix} 0 & 1 & 0 & 0 \\ 0 & 0 & 1 & 0 \\ 1 & 0 & 0 & 0 \\ 0 & 0 & 0 & 1 \end{pmatrix} \quad (2.33)$$

where configuration $A \rightarrow B \rightarrow C \rightarrow A$ and configuration D does not make a transition. Traditionally, these two types of transition matrices are said to describe systems that obey *deterministic detailed balance* and *deterministic semi-detailed balance*, respectively.

The deterministic transition matrices are permutation matrices. One way to express a deterministic transition matrix is to specify the collision operator, Ω_a , as a polynomial in the number variables as follows

$$\Omega_a = \sum_{\{i_1, \dots, i_k\} \in \mathcal{EC}} \alpha Q_a(i_1, \dots, i_k), \quad (2.34)$$

where $\{i_1, \dots, i_k\}$ is a set of occupied particle states, $\alpha \in \{-1, 0, +1\}$ is a scalar coefficient, and where each term in the sum is written in factorized form as

$$Q_a(i_1, \dots, i_k) = \frac{n_{a+i_1}}{1 - n_{a+i_1}} \dots \frac{n_{a+i_k}}{1 - n_{a+i_k}} \prod_{j=1}^B (1 - n_{a+j}). \quad (2.35)$$

Ω_a in (2.34) is deterministic and the associated transition matrix is a permutation matrix.⁴

⁴For example, on a square lattice with $B = 4$ lattice vectors, $\hat{e}_0 = \hat{x}$, $\hat{e}_1 = \hat{y}$, $\hat{e}_2 = -\hat{x}$, and $\hat{e}_3 = -\hat{y}$, consider the collision operator in the mass two and momentum zero equivalence class. There are two elements of this equivalence class, $A \equiv \{1, 0, 1, 0\}$ and $B \equiv \{0, 1, 0, 1\}$ and the

A *statistical* dynamical system is one whose transition matrix components are fractional numbers. Again, there are two types of statistical transition matrices, those obeying *statistical detailed balance* and those obeying *statistical semi-detailed balance* depending on whether they are symmetric or non-symmetric. An example of a transition matrix obeying statistical detailed balance is the following

$$T = \begin{pmatrix} 0 & \frac{1}{2} & \frac{1}{2} & 0 \\ \frac{1}{2} & 0 & 0 & \frac{1}{2} \\ \frac{1}{2} & 0 & 0 & \frac{1}{2} \\ 0 & \frac{1}{2} & \frac{1}{2} & 0 \end{pmatrix} \quad (2.36)$$

and a statistical semi-detailed balance one is

$$T = \begin{pmatrix} 0 & \frac{1}{2} & 0 & \frac{1}{2} \\ 0 & 0 & \frac{1}{2} & \frac{1}{2} \\ \frac{1}{2} & \frac{1}{2} & 0 & 0 \\ \frac{1}{2} & 0 & \frac{1}{2} & 0 \end{pmatrix}. \quad (2.37)$$

A *uniform* statistical transition matrix obeys detailed balance and has all components

collision operator is

$$\Omega_a^{\text{square}} = Q_a(1,3) - Q_a(0,2) = n_{a+1}n_{a+3}(1-n_a)(1-n_{a+2}) - n_an_{a+2}(1-n_{a+1})(1-n_{a+3}).$$

The associated transition matrix is

$$T = \begin{pmatrix} T_{AA} & T_{AB} \\ T_{BA} & T_{BB} \end{pmatrix} = \begin{pmatrix} 0 & 1 \\ 1 & 0 \end{pmatrix}.$$

To see this explicitly write out the collision equation (2.21)

$$n'_a = n_a + n_{a+1}n_{a+3}(1-n_a)(1-n_{a+2}) - n_an_{a+2}(1-n_{a+1})(1-n_{a+3}),$$

and supposing $\vec{n} = \{1, 0, 1, 0\}$, then the above equation generates the following outgoing configuration, $\vec{n}' = \{0, 1, 0, 1\}$, and vice versa. For $a = 0$, we have

$$n'_0 = n_0 + n_1n_3(1-n_0)(1-n_2) - n_0n_2(1-n_1)(1-n_3) = 0,$$

since $n_0 = 1$, $n_1 = 0$, $n_2 = 1$, and $n_3 = 0$. So Ω_0 causes $n_0 = 1$ to flip to value 0. Similarly, for $a = 1, 2, 3$ all the bits are flipped and the outgoing configuration is $n'_0 = 0$, $n'_1 = 1$, $n'_2 = 0$, and $n'_3 = 1$.

equal to the inverse of the size of the equivalence class: $T_{n,n'} = \frac{1}{\|T\|}$. For example

$$T = \begin{pmatrix} \frac{1}{4} & \frac{1}{4} & \frac{1}{4} & \frac{1}{4} \\ \frac{1}{4} & \frac{1}{4} & \frac{1}{4} & \frac{1}{4} \\ \frac{1}{4} & \frac{1}{4} & \frac{1}{4} & \frac{1}{4} \\ \frac{1}{4} & \frac{1}{4} & \frac{1}{4} & \frac{1}{4} \end{pmatrix}. \quad (2.38)$$

When implementing a statistical lattice gas on a computer it is often simplest to just take the transition matrix to be uniform. Even if the equivalence class is particularly large, a uniform sampling algorithm is all that is required. On the CAM-8, a table lookup method is used to implement the uniform sampling within an equivalence class (i.e. a random offset is added to a pointer to the base address of a block of memory that holds all the elements of a particular equivalence class, see (E.4) in Appendix E for more details).⁵

Remark:

In the exactly computed lattice gas systems, information is preserved and the physical kinetics is strictly microscopically reversible. Nevertheless in the continuum limit there emerges dissipative behavior, that is, viscous damping. That there can be viscous damping at the macroscopic scale and also time-reversal invariance at the microscopic scale is a manifestation of a well-known aspect of classical statistical mechanics. There exist determinism and reversibility in the microscopic physics while simultaneously there exist dissipation and increasing entropy (viz. second law of thermodynamics) in

⁵If one chooses all the components equaling the inverse of the size of the equivalence class minus one: $T_{n,n'} = \frac{1}{\|T\|-1}$, then all the diagonal components are zero. For example,

$$T = \begin{pmatrix} 0 & \frac{1}{3} & \frac{1}{3} & \frac{1}{3} \\ \frac{1}{3} & 0 & \frac{1}{3} & \frac{1}{3} \\ \frac{1}{3} & \frac{1}{3} & 0 & \frac{1}{3} \\ \frac{1}{3} & \frac{1}{3} & \frac{1}{3} & 0 \end{pmatrix}. \quad (2.39)$$

This simple transition matrix still satisfies detailed balance and allows for a slight reduction in viscosity. Yet it is more difficult to implement than a uniform statistical transition matrix.

the macroscopics physics.

2.1.4 Embedding in a Continuum

It is necessary to define a calculus of functional quantities that have definite values on the lattice sites x_i . Toward this end, consider the lattice described earlier in §2.1.2 embedded in a continuous space. It is possible to do this by interpreting x_i as a position coordinate in the continuum.

Let $A_{\vec{x}}$ denote a lattice-based quantity; that is, it is an array of values. It is possible to construct a continuous field $A(\vec{x}, t)$ defined over all spacetime such that $A(\vec{x}, t)|_{\vec{x} \text{ on lattice}} = A_{\vec{x}, t}$. For example, $A(\vec{x}, t)$ may be envisioned as an interpolated spline function of the discrete set $A_{\vec{x}, t}$. The concept of the change in the quantity $\delta A_{\vec{x}, t} = A_{\vec{x}+\ell\hat{e}, t} - A_{\vec{x}, t}$ with respect to a change in the vector $\delta x_{ai} = \ell e_{ai}$ is related to a spatial derivative of $A(\vec{x}, t)$ as follows

$$\frac{\delta A_{\vec{x}, t}}{\delta x_{ai}} \leftrightarrow \left. \frac{\partial A(\vec{x}, t)}{\partial x_i} \right|_{\text{on lattice}}, \quad (2.40)$$

and the concept of the change in the quantity $\delta A_{\vec{x}, t} = A_{\vec{x}, t+\tau} - A_{\vec{x}, t}$ with respect to a change in one time step $\delta t = \tau$ is related to a temporal derivative of $A(\vec{x}, t)$ as follows

$$\frac{\delta A_{\vec{x}, t}}{\delta t} \leftrightarrow \left. \frac{\partial A(\vec{x}, t)}{\partial t} \right|_{\text{on lattice}}. \quad (2.41)$$

Throughout the rest of this dissertation, Leibniz differential notation is used on lattice-based quantities with this understanding. The *scaling limit* is defined as that limit where the correspondence relations (2.40) and (2.41) become physically realizable. In the scaling limit, a series expansions in powers of the smallness ε (*viz.* Knudsen number or Mach number) is taken in a fashion whereby *diffusive ordering* holds for the differentials $\delta t \sim \varepsilon^2$ and $\delta x \sim \varepsilon$.

The smallest unit of phase space volume (the single particle phase space volume) is denoted by $h^D \sim \delta p^D \delta x^D$. Note that in terms of the fundamental units ($\delta p = mc$ and $\delta x = \ell$), the “Planck constant” for the lattice gas is

$$h \sim m \frac{\ell^2}{\tau}. \quad (2.42)$$

Then in analogy to the connection between the counting of states in classical statistical mechanics and quantum statistical mechanics (see Appendix F), the following identity holds in the scaling limit where the total phase space volume of the system is much larger than the unit phase space volume h^D

$$\sum_x \sum_a \leftrightarrow \frac{1}{h^D} \int d^D x \int d^D p. \quad (2.43)$$

This can be partitioned into the sum over spatial sites and the sum over momentum directions, given by the following integrals

$$\sum_x \leftrightarrow \frac{1}{\ell^D} \int d^D x \quad (2.44)$$

$$\sum_a \leftrightarrow \frac{1}{(mc)^D} \int d^D p, \quad (2.45)$$

respectively. Note that the sum over all sites (2.44) is in fact the volume of the lattice, denoted as V .

2.1.5 Hamiltonian

The Hamiltonian is the sum of the kinetic energy and the potential energy of interaction

$$H(\vec{x}, \vec{p}) = T(\vec{p}) + U(\vec{x}), \quad (2.46)$$

where \vec{x} and \vec{p} are the position and momentum respectively, in the generalized coordinates. The particle's kinetic energy is

$$T(\vec{p}) \equiv c_i p_i, \quad (2.47)$$

Where c_i is the fundamental propagation speed for the system and p_i is the particle's momentum vector. To be explicit, since the particle is on the lattice, in channel a say, its kinetic energy can be written as

$$T_a \equiv c e_{ai} p_{ai} = m c^2 e_{ai} e_{ai} n_a(\vec{x}), \quad (2.48)$$

where (2.4) has been inserted in the R.H.S. of the above expression. In (2.48) there is an implied sum over the spatial index i but there is no implied summation over the directional index a . This convention is used throughout this dissertation. We will see a posteriori that (2.48) leads to the correct lattice gas transport equation.⁶ Note that in (2.48), unimodularity of the occupation variable ($n_a^2 = n_a$) is not required. Therefore, (2.48) is a suitable definition of the kinetic energy for the case where the maximum number of particles occupying a particular momentum state may exceed one ($L > 1$). This is the situation treated in Chapter 5 on integer lattice gases. But for now, we focus on the Boolean case ($L = 1$).

The potential energy at x_i due to all other particles in the system can be straightforwardly expressed in terms of the discrete Green's function of Poisson's equation

⁶Note that if the kinetic energy had the alternate form

$$T = \frac{p^2}{2m},$$

then (2.56) would be off by a factor of n_a since in this case the result would be

$$\dot{x}_i = c_{ai} n_a(\vec{x}).$$

This would lead to an incorrect nonlinear form for the lattice gas transport equation.

$g(\vec{x}, \vec{x}')$ (see §B.3 in Appendix B)

$$U_a(\vec{x}) \equiv -\frac{mc}{\tau} \sum_{x'} g(\vec{x}, \vec{x}') e_{ai} \frac{\partial \Omega_a(\vec{x}')}{\partial x'_i}, \quad (2.49)$$

where there is an implied summation over the spatial index i and no summation over the directional index a . The validity of the form of (2.49) will be determined a posteriori in that the correct microscopic lattice gas transport equation is obtained thereby. Therefore the single particle lattice gas Hamiltonian,

$$H_a = E_a n_a(\vec{x}) - \frac{mc}{\tau} \sum_{x'} g(\vec{x}, \vec{x}') e_{ai} \frac{\partial \Omega_a(\vec{x}')}{\partial x'_i}, \quad (2.50)$$

where $E_a \equiv mc^2 \hat{e}_a^2$, is taken here as an ansatz.

The Jacobian of the collision operator is defined as

$$J_{ab} \equiv \frac{\partial \Omega_a}{\partial n_b}. \quad (2.51)$$

The collisional part of the Hamiltonian (2.50) can be written in terms of J after using the chain rule $\partial \Omega / \partial x' = (\partial \Omega / \partial n)(\partial n / \partial x')$ to give

$$H_a = E_a n_a(\vec{x}) - \frac{mc}{\tau} \sum_{x'} \sum_b g(\vec{x}, \vec{x}') e_{ai} J_{ab} \frac{\partial n_b}{\partial x'_i} \quad (2.52)$$

In this form, the Hamiltonian is written as an explicit function of the occupation variable and its gradient, $H = H(n, \nabla n)$.

2.1.6 Hamilton's Equations

Hamilton's first equation in continuum form is

$$\frac{\partial H}{\partial p_i} = \dot{x}_i. \quad (2.53)$$

A dot above a quantity indicates the total time derivative of that quantity. The lattice-based form of Hamilton's first equation may be written

$$\left. \frac{\partial H}{\partial p_i} \right|_{\text{on lattice}} = \dot{x}_i|_{\text{on lattice}}.$$

It will be a matter of convention to write this more simply as

$$\dot{x}_i = \frac{\partial H_a}{\partial p_{ai}}, \quad (2.54)$$

where the R.H.S. is assumed to be a Kaehler derivative.⁷ Note the R.H.S. of (2.54) explicitly depends on the directional index a whereas the L.H.S. does not. At first glance this may seem confusing. Yet there is actually no inconsistency in the indices with the understanding that an *on lattice* derivative (*i.e.* $\frac{d\vec{x}}{dt}$) generates a change along one of the lattice directions. Kaehler differentiating (2.48) with respect to the momentum (2.4) gives

$$\frac{\partial T_a}{\partial p_{ai}} = ce_{ai}. \quad (2.55)$$

Equating (2.54) and (2.55), Hamilton's first equation reduces to

$$\dot{x}_i = ce_{ai}. \quad (2.56)$$

This is consistent with particle kinetics on a lattice since $\delta x_i = \ell e_{ai}$ and $\delta t = \tau$.

Hamilton's second equation in continuum form is

$$-\frac{\partial H}{\partial x_i} = \dot{p}_i. \quad (2.57)$$

The lattice-based form of Hamilton's second equation may be written

$$-\frac{\partial U_a}{\partial x_i} = \dot{p}_{ai}, \quad (2.58)$$

⁷Consider some polynomial function in the discrete number variable. A Kaehler derivative of this function with respect to the number variable is the polynomial function that would be obtained if the number variable were continuous. As an example where $n \in \{0, 1\}$, the Kaehler derivative of the polynomial function $f(n) = n^k$ is defined as follows $\frac{\partial f(n)}{\partial n} \equiv kn^{k-1}$, where k is some integer.

since the spatial gradient of the kinetic energy vanishes because T_a depends only on p_i . The scaling limit derivative of (2.49) with respect to the position coordinate is

$$\frac{\partial U_a}{\partial x_i} = -\frac{mc}{\tau} \sum_{x'} \frac{\partial g(\vec{x}, \vec{x}')}{\partial x_i} e_{ai} \frac{\partial \Omega_a(\vec{x}')}{\partial x'_i}. \quad (2.59)$$

Using the reflection symmetry identity (B.15), it is possible to do a discrete version of integration by parts according to (B.9), see §B.2 in Appendix B. Then we have

$$\frac{\partial U_a}{\partial x_i} = \frac{mc}{\tau} \sum_{x'} \frac{\partial g(\vec{x}, \vec{x}')}{\partial x'_i} e_{ai} \frac{\partial \Omega_a(\vec{x}')}{\partial x'_i} \quad (2.60)$$

$$= -\frac{mc}{\tau} \sum_{x'} \frac{\partial^2 g(\vec{x}, \vec{x}')}{\partial x'^2_i} e_{ai} \Omega_a(\vec{x}') \quad (2.61)$$

$$= -\frac{mc}{\tau} \sum_{x'} \delta_{xx'} e_{ai} \Omega_a(\vec{x}') \quad (2.62)$$

$$\rightarrow \frac{\partial U_a}{\partial x_i} = -\frac{mc}{\tau} e_{ai} \Omega_a(\vec{x}). \quad (2.63)$$

This result for the gradient of the potential energy can be obtained from (2.59) in another way. Differentiate (2.59) with respect to the position vector again

$$\frac{\partial^2 U_a}{\partial x_i^2} = -\frac{mc}{\tau} \sum_{x'} \frac{\partial^2 g(\vec{x}, \vec{x}')}{\partial x_i^2} e_{ai} \frac{\partial \Omega_a(\vec{x}')}{\partial x'_i} \quad (2.64)$$

$$= -\frac{mc}{\tau} \sum_{x'} \delta_{xx'} e_{ai} \frac{\partial \Omega_a(\vec{x}')}{\partial x'_i} \quad (2.65)$$

$$\rightarrow \frac{\partial^2 U_a}{\partial x_i^2} = -\frac{mc}{\tau} e_{ai} \frac{\partial \Omega_a(\vec{x})}{\partial x_i} \quad (2.66)$$

Integrating this last result over all space and taking the constant of integration to be zero gives identically (2.63).

Equating (2.58) and (2.63), Hamilton's second equation reduces to

$$\dot{p}_{ai} = \frac{mc}{\tau} e_{ai} \Omega_a(\vec{x}) \quad (2.67)$$

The second Hamilton equation (2.67) is also consistent with particle kinetics on a lattice, where the discrete moment change is $\delta p_i = mce_{ai}\Omega_a(\vec{x})$ in the time interval

$\delta t = \tau$. In fact, (2.67) is just the usual lattice gas transport equation in disguise.

Let's see why this is so.

Using (2.4), write (2.67) as follows

$$\frac{d}{dt} [m c e_{ai} n_a(\vec{x})] = \frac{m c}{\tau} e_{ai} \Omega_a(\vec{x}). \quad (2.68)$$

Since the lattice vectors are constants, this reduces to the simpler expression

$$\frac{d}{dt} [n_a(\vec{x})] = \frac{1}{\tau} \Omega_a(\vec{x}). \quad (2.69)$$

Using Hamilton's first equation, (2.56), the total time derivative can be written as

$$\begin{aligned} \frac{d}{dt} &= \frac{\partial}{\partial t} + \dot{x}_i \frac{\partial}{\partial x_i} \\ &= \frac{\partial}{\partial t} + c e_{ai} \frac{\partial}{\partial x_i}. \end{aligned}$$

Inserting this into (2.69) to replace the total time derivative gives

$$\left(\tau \frac{\partial}{\partial t} + \ell e_{ai} \frac{\partial}{\partial x_i} \right) n_a(\vec{x}) = \Omega_a(\vec{x}). \quad (2.70)$$

This is just a Taylor expansion (to the first order in the smallness) of the lattice gas microdynamical transport equation (2.23)

$$n_a(\vec{x} + \ell \hat{e}_a, t + \tau) = n_a(\vec{x}, t) + \Omega_a(\vec{x}).$$

This proves that Hamilton's second equation is the well known lattice gas transport equation. Therefore, the ansatz for the lattice Hamilton (2.50) is appropriate for particle kinetics on a lattice.

Because the lattice gas dynamics is partitioned into distinct streaming (2.22) and colliding events (2.21) that occur in sequence, there is an instantaneous switch between kinetic energy and potential energy. That is, the particles do not move and collide simultaneously. This has an important consequence when analyzing the behavior of the lattice gas system from a statistical mechanical point of view.

Table 2.4: Statistical Ensembles Obtained by Successive Legendre Transformations. The grand canonical ensemble is used here for lattice gas calculations.

Energy	Set	Thermodynamics	Ensemble
INTERNAL ENERGY	(S, V, N)	$dU = TdS - pdV + \mu dN$	
ENTHALPY	(S, P, N)	$dH = TdS + VdP + \mu dN$	
GIBBS FREE ENERGY	(T, P, N)	$dG = -SdT + VdP + \mu dN$	
HELMHOLTZ FREE ENERGY	(T, V, N)	$dA = -SdT - PdV + \mu dN$	Canonical
GRAND POTENTIAL	(T, V, μ)	$d\Omega = -SdT - PdV - Nd\mu$	Grand Canonical

2.2 Mesoscopic Equilibrium: A Statistical Mechanics Treatment

Let $\{n\}$ represent the set of all accessible states in the grand canonical ensemble for the lattice gas system. Let E_n and m_n denote the total energy (kinetic plus potential) and the total mass, respectively, of the system. Then in the grand canonical ensemble, the *grand partition function* is defined as the the Boltzmann weights summed over all accessible states

$$\Xi \equiv \sum_{\{n\}} e^{-\beta(E_n - \mu m_n)}. \quad (2.71)$$

In (2.71), β is the *inverse of the thermal energy*, which is Boltzmann's constant times the system temperature ($\beta \equiv \frac{1}{k_B T}$). Also, μ is the *chemical potential*. The mesoscopic expectation value of a quantity O is obtained in the grand canonical ensemble by the following recipe

$$\langle O \rangle \equiv \frac{1}{\Xi} \sum_{\{n\}} e^{-\beta(E_n - \mu m_n)} O(n). \quad (2.72)$$

The grand potential, which has units of energy, is defined as

$$\Omega \equiv -\frac{1}{\beta} \log \Xi. \quad (2.73)$$

If Ω can be calculated, all thermodynamic properties of the lattice gas system can be calculated in turn. In particular, I am interested in calculating the equilibrium particle distribution function and eventually the pressure, P , of the lattice gas system using (2.73).

Let N denote the expected number of particles in a system with volume V when the system is at fixed temperature and chemical potential

$$N \equiv \frac{1}{\Xi} \sum_{\{n\}} m_n e^{-\beta(E_n - \mu m_n)}. \quad (2.74)$$

Since, the pressure is a function of the system temperature, T , and density, $\rho \equiv \frac{N}{V}$, it will be necessary to calculate N also using (2.73). By inspection of (2.71), an expression for N can be immediately written in terms of the grand potential

$$N = - \left(\frac{\partial \Omega}{\partial \mu} \right)_{\beta, V}. \quad (2.75)$$

To obtain a similar expression for the pressure as a derivative of the grand potential, it is necessary to first obtain the thermodynamics relation for the grand potential in the grand canonical ensemble. In this ensemble, the expected energy is the product of the pressure times the volume

$$E \equiv \frac{1}{\Xi} \sum_{\{n\}} E_n e^{-\beta(E_n - \mu m_n)}. \quad (2.76)$$

Again by inspection of (2.71), it follows that

$$E - \mu N = - \left(\beta \frac{\partial \Omega}{\partial \mu} \right)_{\mu} \quad (2.77)$$

$$= \Omega + \beta \left(\frac{\partial \Omega}{\partial \beta} \right)_{\mu} \quad (2.78)$$

$$= \Omega - T \left(\frac{\partial \Omega}{\partial T} \right)_{\mu}. \quad (2.79)$$

Therefore, solving for the grand potential gives the following thermodynamic relation

$$\Omega = E - TS - \mu N, \quad (2.80)$$

where the equilibrium *entropy* denoted by S is defined as

$$S \equiv - \left(\frac{\partial \Omega}{\partial T} \right)_{\mu, V}. \quad (2.81)$$

From (2.80), the equilibrium pressure is

$$P = - \left(\frac{\partial \Omega}{\partial V} \right)_{\beta, \mu}, \quad (2.82)$$

where $dE = -PdV$ and

$$d\Omega = -PdV - SdT - Nd\mu. \quad (2.83)$$

In this section I will derive the grand partition function in the grand canonical ensemble. There are three constraints one must consider to do the counting of states correctly. These constraints are energy conservation, mass conservation, and momentum conservation. Because of the partitioning of the particle dynamics into disjoint streaming and colliding events, the interacting part of the Hamiltonian is not needed to compute the total energy of the system and may be dropped altogether. Consequently, the grand partition function of the locally interacting lattice gas can be written in closed analytical form [17].

The total energy of a lattice gas system is obtained by counting all the occupations and only the free part of the Hamiltonian is needed

$$H_o \equiv \sum_{\vec{x}a} E_a n_a(\vec{x}), \quad (2.84)$$

where E_a is the energy of the a^{th} momentum state. This intuitively follows from the partitioning of the microscopic transport equation into two distinct phases: streaming and collision. If the total energy is counted in the streaming phase, (2.84) is appropriate as there is no long-range interaction manifesting potential energy. In §?? on long-range lattice gases where the system does possess potential energy, it is rigorously shown that as the interaction range approaches zero the potential energy contribution to the total energy vanishes for small Knudsen numbers. Note that the double sum appearing in shorthand in (2.84) simply means $\sum_{xa} = \sum_{x=1}^V \sum_{a=1}^B$. The total mass density and momentum density for the integer lattice gas system are respectively

$$\rho_{\text{tot}} \equiv \sum_{xa} m n_a(\vec{x}), \quad (2.85)$$

and

$$\rho_{\text{tot}} V_i \equiv \sum_{xa} m c_{ai} n_a(\vec{x}). \quad (2.86)$$

These serve as constraints on the system as it equilibrates towards high entropy states. Following (2.71), the grand partition function is

$$\Xi \equiv \sum_{\{n\}} e^{-\beta(H_0 - \mu \rho_{\text{tot}}) + \rho_{\text{tot}} V_i \alpha_i}, \quad (2.87)$$

where $\sum_{\{n\}}$ represents a sum over all possible configurations of the occupation variables.

Inserting (2.84), (2.85), and (2.86) into (2.87), the grand partition function becomes

$$\Xi = \sum_{\{n\}} \prod_{xa} e^{-\beta(E_a n_a - \mu m n_a) + \alpha_i m c_{ai} n_a}. \quad (2.88)$$

Notice that all the exponents in (2.88) are first-order linear in n_a . So it is convenient

to define the fugacity as

$$z_a \equiv z_{0a} e^{\alpha_i m c e_{ai}}, \quad (2.89)$$

where

$$z_{0a} \equiv e^{-\beta(E_a - \mu m)}. \quad (2.90)$$

Then the grand partition function is compactly written as

$$\Xi = \sum_{\{n\}} \prod_{a} z_a^{n_a}. \quad (2.91)$$

In this case the grand partition function can be straightforwardly calculated. To begin with, one may derive, in the usual fashion of the statistical mechanics for system of fermionic particles, the grand partition function as follows

$$\Xi = \prod_{a} \sum_{n=0}^1 z_a^n \quad (2.92)$$

$$= \prod_{a} (1 + z_a) \quad (2.93)$$

$$\longrightarrow \log \Xi = \sum_{a} \log(1 + z_a) \quad (2.94)$$

Since $\partial z_a / \partial \beta = -E_a z_a$, then

$$-\frac{\partial \log \Xi}{\partial \beta} = \sum_{a} \frac{z_a}{1 + z_a} E_a. \quad (2.95)$$

The expected energy is then

$$\langle E \rangle \equiv -\frac{\partial \log \Xi}{\partial \beta} = \sum_{a} F_1(z) E_a, \quad (2.96)$$

where the Fermi-Dirac distribution is immediately identified

$$F_1(z_a) = \frac{1}{z_a^{-1} + 1}. \quad (2.97)$$

2.3 Mesodynamics: A Mean-Field Treatment

To theoretically analyze the lattice gas dynamics, it is convenient to work in the Boltzmann limit where a field point is obtained by an ensemble average over the number variables. Define the particle distribution function, $f_a \equiv \langle n_a \rangle$, resulting from an ensemble of initial conditions and the neglect of correlations, with the average taken over the ensemble.

If all the particles entering a site in the lattice are uncorrelated at all times, then the particle occupancies are considered randomized by *Boltzmann molecular chaos* (this is called the *Stosszahlansatz*). Define the *mean-field collision operator* as the ensemble average of the microscopic collision operator, $\Omega_a^{\text{mf}} \equiv \langle \Omega_a \rangle$. Using the Boltzmann molecular chaos assumption, the mesoscopic collision operator is considerably simplified. So neglecting all two-point and higher order correlations between particle occupancies, the mean-field collision operator is constructed in a fashion identical to its counterpart (2.34) in the microscopic limit. Ω_a^{mf} , as a polynomial in the particle distribution variables as follows

$$\Omega_a^{\text{mf}} = \sum_{\{i_1, \dots, i_k\} \in \mathcal{EC}} \alpha \langle Q_a(i_1, \dots, i_k) \rangle, \quad (2.98)$$

where $\{i_1, \dots, i_k\}$ is a set of occupied particle states and $\alpha \in \{-1, 0, +1\}$ is a scalar coefficient and where each term in the sum is written in the mean-field limit in factorized form as

$$\langle Q_a(i_1, \dots, i_k) \rangle = \frac{f_{a+i_1}}{1-f_{a+i_1}} \dots \frac{f_{a+i_k}}{1-f_{a+i_k}} \prod_{j=1}^B (1-f_{a+j}). \quad (2.99)$$

Ω_a^{mf} in (2.98) is probabilistic. Further discussion about the mesoscopic collision operation, in particular its dependence on the transition matrix, is given below in §2.3.2.

In the mean-field limit, f_a still satisfies a collision and streaming equation corresponding to (2.21) and (2.22)

$$f'_a(\vec{x}, t) = f_a(\vec{x}, t) + \Omega_a^{mf}(\vec{f}(\vec{x}, t)), \quad (2.100)$$

and

$$f_a(\vec{x} + \ell \hat{e}_a, t + \tau) = f'_a(\vec{x}, t). \quad (2.101)$$

By ensemble-averaging all terms in the microscopic transport equation (2.23), then obtain the mesoscopic transport equation

$$f_a(\vec{x} + \ell \hat{e}_a, t + \tau) = f_a(\vec{x}, t) + \Omega_a^{mf}[\vec{f}(\vec{x}, t)], \quad (2.102)$$

that appears identical in form to (2.23).

The actual particle distribution is composed as a series expansion in powers of $\varepsilon \sim \delta x \sim \sqrt{\delta t}$

$$f_a = f_a^{(0)} + \varepsilon f_a^{(1)} + \mathcal{O}(\varepsilon^2). \quad (2.103)$$

This is termed *diffusive ordering* when $\delta t \propto (\delta x)^2$, well known for random walk processes. Taylor expanding the L.H.S. of (2.102) to only first order in time but to second order in space, one obtains the lattice Boltzmann equation

$$\partial_t f_a(\vec{x}, t) + c e_{ai} \partial_i f_a(\vec{x}, t) + \frac{\ell^2}{2\tau} e_{ai} e_{aj} \partial_i \partial_j f_a(\vec{x}, t) + \mathcal{O}(\varepsilon^3) = \frac{1}{\tau} \Omega_a^{mf}[\vec{f}(\vec{x}, t)]. \quad (2.104)$$

where (2.104) has been expanded to second order in ε .

Write the particle number density, momentum density, and momentum flux density in terms of the single-particle distribution function as follows

$$m \sum_a f_a(\vec{x}, t) = \rho(\vec{x}, t) \quad (2.105)$$

$$mc \sum_a e_{ai} f_a(\vec{x}, t) = \rho(\vec{x}, t) v_i(\vec{x}, t) \quad (2.106)$$

$$mc^2 \sum_a e_{ai} e_{aj} f_a(\vec{x}, t) = \Pi_{ij}(\vec{x}, t). \quad (2.107)$$

Note that for a uniform filling of states, $f_a = d$ for all directions, then

$$\rho(\vec{x}, t) = mBd \quad (2.108)$$

$$v_i(\vec{x}, t) = 0 \quad (2.109)$$

$$\Pi_{ij}(\vec{x}, t) = \rho c_s^2 \delta_{ij}, \quad (2.110)$$

where $c_s \equiv \frac{c}{\sqrt{D}}$. This is expected since when $v_i = 0$, the momentum flux density tensor is diagonal and scales with the pressure ($\Pi_{ij} = p\delta_{ij}$) and for an ideal gas $p = \rho c_s^2$ and c_s is the sound speed in the fluid.

The general form of the single particle distribution function, appropriate for single speed lattice gases, is a Fermi-Dirac distribution (2.97) and is a function of the sum of scalar collision invariants, $\alpha + \beta e_{ai} v_i$, having the following form

$$f_a = \frac{1}{1 + e^{\alpha + \beta e_{ai} v_i}}. \quad (2.111)$$

Fundamentally, this arises because the individual digital bits used to represent particles satisfy the Pauli exclusion principle. By Taylor expanding (2.111) about $\vec{v} = 0$ to fourth order in the velocity and equating the zeroth, first, and second moments of f_a to (2.105), (2.106), and (2.107) respectively, the parameters α and β are determined.

To provide a kind of roadmap for the remainder of this chapter, I now give the Mach number expansion of the inviscid part of the lattice gas distribution function

$$(f_a^{eq})_{LGA}^{ideal} = \frac{n}{B} + \frac{nD}{cB} e_{ai} v_i + g \frac{nD(D+2)}{2c^2 B} e_{ai} e_{aj} v_i v_j - g \frac{n(D+2)}{2c^2 B} v^2 + \mathcal{O}(v^3), \quad (2.112)$$

where the Galilean prefactor is

$$g \equiv \frac{D}{D+2} \frac{1-2d}{1-d}. \quad (2.113)$$

The procedures for carrying out this expansion are given in §2.4.1 and in Appendix D. It is important to check all the moments of this distribution to see if it gives us what is expected. That is, using $\rho = mn$ for the density and $c_s = \frac{c}{\sqrt{D}}$ for the sound speed, the moments of lattice gas distribution are

$$m \sum_a (f_a^{eq})_{LGA}^{ideal} = \rho \quad (2.114)$$

$$mc \sum_a e_{ai} (f_a^{eq})_{LGA}^{ideal} = \rho v_i \quad (2.115)$$

$$mc^2 \sum_a e_{ai} e_{aj} (f_a^{eq})_{LGA}^{ideal} = \rho c_s^2 (1 - g \frac{v^2}{c^2}) \delta_{ij} + g \rho v_i v_j. \quad (2.116)$$

The form of the ideal part of the momentum flux density tensor should be [57]

$$\Pi_{ij}^{ideal} = p \delta_{ij} + \rho v_i v_j. \quad (2.117)$$

There are two problems encountered here; however I will show that they are related. Firstly, the single-speed lattice gas almost produces the correct form for the momentum flux density tensor, except that the diagonal part of Π_{ij} appears to have a spurious dependence on the square of the velocity field,

$$p = \frac{\rho}{D} (c^2 - g v^2). \quad (2.118)$$

Secondly, the prefactor g arises as an artifact of the discreteness of the number variables that breaks Galilean invariance.

2.3.1 Interpreting the Form of the Lattice Gas Pressure

We find that an apparent problem encountered in a single-speed lattice gas of the pressure (2.118) depending on the square of the velocity field is actually a consequence of a degeneracy between mass and kinetic energy. Since there is only a single speed

species of particle, all particles carry a single unit of mass and also a single unit of kinetic energy, so counting the total mass of the system is equivalent to counting the total kinetic energy of the system. We will see in Chapter 4 that given a multispeed lattice gas, where mass and kinetic energy are not degenerate, this form of the pressure (2.118) is actually physically proper. In fact, it is easy to see why. The reason is that in a classical hydrothermal gas, the pressure is

$$p = (\gamma - 1)(nE - \frac{1}{2}\rho v^2) \quad (2.119)$$

where $n = Bd$ is the number density per site, γ is the ratio of the specific heat at constant pressure to the specific heat at constant volume (that is $\gamma = C_p/C_v$), E is the kinetic energy per particle, and $\gamma - 1 = \frac{2}{D}$. For a single speed lattice gas, the kinetic energy carried per particle is $E = \frac{1}{2}mc^2$ and (2.119) becomes

$$p = \frac{\rho}{D}(c^2 - v^2). \quad (2.120)$$

Except for the g -factor, this is identical to the expression for the pressure that was obtained for a single speed lattice gas (2.118).

Remark:

The lattice gas' pressure dependence on the bulk flow velocity (2.118) is similar to that which occurs in a natural hydrofluid (2.120). That is, $p_{\text{LGA}} = p_{\text{classical}}$ provided $g = 1$. However, in a $L = 1$ lattice gas the g -factor does not equal unity. So finding a way to have $g = 1$ fixes everything.

I have focused much attention on restoring Galilean invariance to the lattice gas dynamics. It can be repaired in several ways.

The first way to solve this problem is well known in the lattice gas community. Working directly in the Boltzmann limit and using only symmetry arguments, it is possible to directly set the g -factor to unity by starting with the mesoscopic transport equation (2.102) and specifying a non-Fermi-Dirac single particle distribution function at the outset (see §2.3.4 and §D.2). The lattice Boltzmann equation method is described later in this chapter. Yet, as mentioned in the introduction to this dissertation, the lattice Boltzmann equation method is a finite differencing scheme and suffers from numerical instabilities due to its lack of detailed balance or semi-detailed balance in the BGK collision operator.

The second way recently found to solve this problem of a lack of Galilean invariance in a single speed lattice involves using a finite integer to encode a momentum state instead of using only a single bit to encode that state. This type of lattice gas is called an *integer lattice gas*. The integer lattice gas is more robust than the lattice Boltzmann equation because the integer lattice gas collisions obey detailed balance. I devote a full chapter to the integer lattice gas method (see Chapter 5). Some interesting insights connecting physics and computation are gained from the integer lattice gas method, particularly when the integer lattice gas is analyzed from a statistical mechanics viewpoint.

The third way to solve this problem is to use appropriately chosen long-range interactions. A small nonlocal attractive force between the particles can restore Galilean invariance in the macroscopic limit. This alternative is discussed in volume II [102].

2.3.2 Collision Operator in the Mesoscopic Limit

It will be essential to express the collision operator (2.34) in the mesoscopic limit. Denote the input and output configuration of a collision by s and s' at some point in time. With the individual momentum states within a configuration denoted by $n_a(x, t)$ where $a = 1 \dots B$, the probability of a particular input configuration with p particles and $B - p$ holes is the product of $f_a(x, t)$ and $[1 - f_a(x, t)]$ is

$$P_s = \prod_a f_a^{n_a} (1 - f_a)^{1-n_a}. \quad (2.121)$$

It is understood that $P_s = P_s(x, t)$ and $f_a = f_a(x, t)$ so for convenience we leave off the explicit spacetime dependence of the mesoscopic variables. The particle distribution can be obtained from the inverse of (2.121) by a weighted sum over all the incoming configurations, s ,

$$f_a = \sum_s n_a P_s. \quad (2.122)$$

Let $T_{s,s'}$ denote the collision probability for a transition from configuration s to s' . It will be identical to the transition matrix for the microscopic dynamics. Because of detailed balance, T is symmetric and all the marginal probabilities must sum to one: $\sum_s T_{s,s'} = \sum_{s'} T_{s,s'} = 1$. We can rewrite the sum over input configurations in (2.122) as a sum over collisions, denoted by $\sum_C \equiv \sum_s \sum_{s'}$, by inserting one into the sum

$$f_a = \sum_s n_a \sum_{s'} T_{s,s'} P_s = \sum_C n_a T P_s. \quad (2.123)$$

The particle distribution (2.122) can also be obtained by summing over the outgoing configurations, s' ,

$$f_a = \sum_{s'} n'_a P_{s'} = \sum_C n'_a T P_s \quad (2.124)$$

since $P_{s'} = \sum_s T_{s,s'} P_s$.

Subtracting (2.123) from (2.124) and since $\Omega_a^{\text{mf}} = f'_a - f_a$, it follows that

$$\Omega_a^{\text{mf}} = \sum_C (n'_a - n_a) T P_s \quad (2.125)$$

or more explicitly

$$\Omega_a^{\text{mf}} = \sum_C (n'_a - n_a) T \prod_b f_b^{n_b} (1 - f_b)^{1-n_b}. \quad (2.126)$$

A quite interesting consequence of the Boolean nature of lattice gases is that it is possible to logically rewrite (2.126) noting that $f_b^{n_b} (1 - f_b)^{1-n_b} = 1 - n_b - f_b + 2n_b f_b$ so as to reduce the mean-field collision operator to the following form

$$\Omega_a^{\text{mf}} = \sum_C (n'_a - n_a) T \prod_b (1 - n_b - f_b + 2n_b f_b). \quad (2.127)$$

This form of the collision operator will be very useful in several derivations below.

2.3.3 Jacobian of the Collision Operator

In this section consider the eigensystem of the Jacobian of the mean-field collision operator

$$J_{ab} \equiv \frac{\partial \Omega_a^{\text{mf}}}{\partial f_b}. \quad (2.128)$$

The Jacobian is important because it appears in the first relevant term of a Taylor expansion of the collision operator about the equilibrium distribution, denoted $f^{(0)}$ or f^{eq} . Expanding the distribution function about its equilibrium value, f^{eq}

$$f_a = f_a^{\text{eq}} + \epsilon f_a^{(1)} + \mathcal{O}(\epsilon^2) \quad (2.129)$$

so, to first order in the smallness, the collision operator is

$$\Omega_a^{\text{mf}}(f) = \Omega_a^{\text{mf}}(f^{\text{eq}}) + \sum_b \left[\frac{\partial \Omega_a^{\text{mf}}}{\partial f_b} \right]_{f=f^{\text{eq}}} (f_b - f_b^{\text{eq}}) + \mathcal{O}(\epsilon^2) \quad (2.130)$$

or

$$\Omega_a^{\text{mf}}(f) = \sum_b J_{ab}(f_b - f_b^{\text{eq}}) + \mathcal{O}(\epsilon^2). \quad (2.131)$$

$\Omega_a^{\text{mf}}(f^{\text{eq}})$ must vanish since the particle distribution is non-changing under equilibrium conditions. So in this approximation one can also write

$$\Omega_a^{\text{mf}}(f) = J_{ab}(f^{(0)})f_b^{(1)} + \mathcal{O}(\epsilon^2), \quad (2.132)$$

We can substitute this form of the mean-field collision operator (2.131) into the mesoscopic transport equation (2.102)

$$f_a(x + \ell c_a, t + \tau) = f_a(x, t) + \sum_b J_{ab}(f_b - f_b^{\text{eq}}). \quad (2.133)$$

2.3.4 BGK Approximation

It is worthwhile to consider the simplest form of the dynamical transport equation for the particle distribution function (2.133) above. The simplest ansatz for the Jacobian is to choose it to be a diagonal matrix [28]

$$J_{ab}^{\text{BGK}} = -\frac{\tau}{\mathcal{T}}\delta_{ab}, \quad (2.134)$$

where \mathcal{T} is the characteristic relaxation time for a point in the system to reach local equilibrium. This form was introduced in 1954 by D. Bhatnager, Eugene Gross, and M. Krook [10]. So the collision operator in the BGK approximation is simply

$$\Omega_a^{\text{BGK}}(f) = -\frac{\tau}{\mathcal{T}}(f_a - f_a^{\text{eq}}), \quad (2.135)$$

and is proportional to the difference of the distribution function and its equilibrium value. Although it is not explicitly clear that the BGK collision operator allows for any mixing between particle directions, (2.135) does implicitly include collisional

mixing because the equilibrium distribution itself depends on the local density and flow velocity, $f_a^{eq} = f_a^{eq}(\rho, v_i)$,

$$\rho = m \sum_a f_a \quad (2.136)$$

and

$$v_i = c \frac{\sum_a e_{ai} f_a}{\sum_a f_a}, \quad (2.137)$$

which in turn do depend on all particle directions.

Substituting (2.134) into (2.133) gives us the lattice Boltzmann equation in the BGK approximation

$$f_a(\vec{x} + \ell \hat{e}_a, t + \tau) = f_a(\vec{x}, t) - \frac{\tau}{T} (f_a(\vec{x}, t) - f_a^{eq}(\vec{x}, t)). \quad (2.138)$$

When thought of as a local computing rule, clearly (2.138) provides a quite straightforward way to evolve the mesoscopic particle dynamics on a parallel computer. All that one need specify is a simple algebraic form of f_a^{eq} . In §D.2 symmetry arguments are used to determine the form of f_a^{eq} that allows us to recover ideal fluid dynamics. So primarily for reasons of simplicity, suitability to parallel computing, and as a way to bypass all microscopic detail (particularly noisy fluctuations), (2.138) has gained much popularity within the lattice gas research community. This mesoscopic modeling approach is customarily referred to as the *lattice Boltzmann equation* method.

2.3.5 Eigensystem of the Jacobian of the Collision Operator

The eigenvalues of the Jacobian of the collision operator can be calculated and the number of these that vanish must equal the number of invariant quantities in the lattice gas dynamics in the Boltzmann limit. For a single speed lattice gas with no rest particles, because of the isosymmetry of the collisions, the Jacobian matrix is

circulant and therefore its elements can be specified by the difference of their indices, $J_{ab} = J_{a-b}$. This property of the Jacobian simplifies the solution of the eigenvalue equation

$$\sum_b J_{a-b} \xi_b^\alpha = \lambda^\alpha \xi_a^\alpha, \quad (2.139)$$

with eigenvectors ξ^α and eigenvalues λ^α where $\alpha = 1, \dots, B$. Make the ansatz that the eigenvectors have the following form

$$\xi_a^\alpha = e^{2\pi i a \alpha / B}. \quad (2.140)$$

Then inserting (2.140) into (2.139) and taking $m = a - b$, gives

$$\lambda^\alpha = \sum_m J_m e^{2\pi i m \alpha / B}. \quad (2.141)$$

Remark:

In (2.141) it is immediately evident how the eigenvalues are set by the components of the collision matrix. The eigenvalues completely determine the fluid's emergent behavior. In this way, the details of the microscopic collisions affect the magnitude of transport coefficients. It is possible to go beyond the Boltzmann limit, and consider the effect of correlations in the microscopic system [12]. It is then possible to develop a formal expression for a renormalized J . Then various approximations to the exact expression are made to obtain improved estimates of the transport coefficients of the system. In practice this has been done for only very simple lattice gases.

For convenience, Dirac bracket notation is used in this section. Let $|\alpha\rangle$ be an eigenket of J and κ_α the associated eigenvalue so that

$$J |\alpha\rangle = \kappa_\alpha |\alpha\rangle \quad (2.142)$$

where orthonormality holds, $\langle \alpha | \beta \rangle = \delta_{\alpha\beta}$ for $(\alpha, \beta) = 1, \dots, B$; and closure holds, $\sum_{\alpha} |\alpha\rangle\langle\alpha| = \hat{1}$. I introduce a *direction-eigenket*, $|a\rangle$, where as usual $a = 1, \dots, B$. Then an eigenvector of J in the *direction representation* is $\langle a | \alpha \rangle$.

For a single speed lattice gas with no rest particles J is circulant because of the isometry of the collisions. Therefore its elements can be specified by the difference of their indices, $J_{ab} = J_{b-a}$. Because of this the matrix element of J reduces to

$$\langle a | J | b \rangle = \langle J | b - a \rangle, \quad (2.143)$$

that really defines the eigenket $|J\rangle$.

Remark:

The collision operator is a matrix, J . One can define an eigenket $|J\rangle$ that is a single row of J . Since J is circulant, one can therefore completely specify it by $|J\rangle$.

The eigenvectors in the direction representation satisfy

$$\langle a | \alpha \rangle = e^{2\pi i a \alpha / B}. \quad (2.144)$$

An alternate way of expressing this property of the eigenvectors is

$$\langle \alpha | a \rangle \langle b | \alpha \rangle = \langle b - a | \alpha \rangle. \quad (2.145)$$

These properties of the Jacobian's eigenkets and eigenvalues simplify the solution of the eigensystem. Manipulating (2.142), it is possible to express κ_{α} as

$$\begin{aligned} \kappa_{\alpha} &= \langle \alpha | J | \alpha \rangle \\ &= \langle \alpha | a \rangle \langle a | J | b \rangle \langle b | \alpha \rangle \\ &= \langle a | J | b \rangle \langle \alpha | a \rangle \langle b | \alpha \rangle \\ &= \langle J | b - a \rangle \langle b - a | \alpha \rangle \\ &= \langle J | \alpha \rangle = \sum_a J_a \exp\left(i \frac{2\pi}{B} a \alpha\right). \end{aligned} \quad (2.146)$$

Now there are two types of degeneracies that are encountered. First of all, there will be as many zero eigenvalues as there are conserved quantities in the lattice gas dynamics. This is easily seen by inserting (2.132) in the mesoscopic collision equation (2.100)

$$|f'\rangle = |f\rangle + J |f^{(1)}\rangle. \quad (2.147)$$

Using (2.142), write

$$J = \sum_{\alpha} \kappa_{\alpha} |\alpha\rangle\langle\alpha|. \quad (2.148)$$

so

$$|f'\rangle = |f\rangle + \sum_{\alpha} \kappa_{\alpha} |\alpha\rangle\langle\alpha|f^{(1)}\rangle. \quad (2.149)$$

Clearly, all the scalars $\langle\alpha|f^{(1)}\rangle$ for which $\kappa_{\alpha} = 0$ have no effect on the dynamics and so are the conserved quantities of the system. This set of eigenvectors with degenerate eigenvalue of zero span is called the *hydrodynamic* space, \mathcal{H} . The remaining eigenvectors span what is called the *kinetic* space, \mathcal{K} . However within \mathcal{K} there exists the *viscous* subspace, $\mathcal{V} \subset \mathcal{K}$ characterized by the degenerate eigenvalue κ_{η} . Therefore J can be explicitly written as a linear combination over eigenvectors in the kinetic space

$$J = \sum_{\alpha \in \mathcal{K}} \kappa_{\alpha} |\alpha\rangle\langle\alpha|. \quad (2.150)$$

Its inverse, now well defined, is then just

$$J^{-1} = \sum_{\alpha \in \mathcal{K}} \frac{1}{\kappa_{\alpha}} |\alpha\rangle\langle\alpha|. \quad (2.151)$$

This can be separated into a viscous part and a nonviscous part as

$$J^{-1} = \frac{1}{\kappa_{\eta}} \sum_{\alpha \in \mathcal{V}} |\alpha\rangle\langle\alpha| + \sum_{\alpha \in \mathcal{K} \setminus \mathcal{V}} \frac{1}{\kappa_{\alpha}} |\alpha\rangle\langle\alpha|. \quad (2.152)$$

2.3.6 Collision Set Formulation of J

The convenient form of the collision operator given in (2.127) allows us to directly calculate the Jacobian, $J_{ab} = \frac{\partial \Omega_a}{\partial f_b}$, as

$$J_{ab} = \sum_C (n'_a - n_a)(2n_b - 1)T \prod_{c \neq b} f_c^{n_c} (1 - f_c)^{1-n_c}. \quad (2.153)$$

We rewrite (2.153) as follows

$$J_{ab} = \sum_C (n'_a - n_a)T \frac{(2n_b - 1)}{f_b^{n_b} (1 - f_b)^{1-n_b}} \prod_c f_c^{n_c} (1 - f_c)^{1-n_c} \quad (2.154)$$

We can simplify this expression by taking $f_a \rightarrow d$ and by noting that since d is a constant the terms in the product become

$$\prod_a d^{n_a} (1 - d)^{1-n_a} = d^p (1 - d)^{B-p}, \quad (2.155)$$

where p denotes the number of particles in a particular collision event. This leads to

$$J_{ab} = \sum_C (n'_a - n_a)T d^{p-1} (1 - d)^{B-p-1} (2n_b - 1) d^{1-n_b} (1 - d)^{n_b}. \quad (2.156)$$

Noting that $d^{1-n_b} (1 - d)^{n_b} = (1 - 2d)n_b + d$ and using the unimodularity of the number variable, $n_b^2 = n_b$, this further simplifies to

$$J_{ab} = \sum_C (n'_a - n_a)T d^{p-1} (1 - d)^{B-p-1} (n_b - d). \quad (2.157)$$

By the symmetry of the collision probability $T(s, s')$ the last term vanishes

$$\sum_C (n'_a - n_a)T d^{p-1} (1 - d)^{B-p-1} (-d) = 0, \quad (2.158)$$

so (2.157) reduces to the simple form

$$J_{ab} = \sum_C (n'_a - n_a) n_b T d^{p-1} (1 - d)^{B-p-1}. \quad (2.159)$$

The remarkable property of (2.159) is that one can use it to determine the components of J_{ab} even for complicated situations where J is not circulant. It is a very important formula. I will use it to calculate the shear viscosity transport coefficient.

2.4 Bridging the Meso and Macroscales: Chapman-Enskog Expansions

Three methods are given to derive the single particle distribution function and the ideal part of the momentum flux density tensor. The first two derivations of the single particle distribution function given here are similar to that given by Wolfram [97]. The first method uses the Fermi-Dirac distribution that is appropriate to a lattice gas system. The second method uses a symmetry argument that is appropriate in the mean-field limit. In this case, a non-Fermi-Dirac distribution is found and used to find the form of the single-particle equilibrium distribution f^{eq} in the lattice Boltzmann equation approach that leads to the exact recovery of the Navier-Stokes equation, but sacrifices exact computability. The third method actually uses an expansion of the fugacity and is the most direct and straightforward method. A generalization of this case allows us to specify a non-Fermi-Dirac distribution used in the integer lattice gas that also leads to the exact recovery of the Navier-Stokes equation while retaining exact computability.

2.4.1 Mach Number Expansion of the Fugacity

For a single-speed lattice gas, the equilibrium probability for finding a particle in momentum state mce_{ai} at position \vec{x} and at time t is given by a Fermi-Dirac distribution

$$f_a^{(0)} = \frac{1}{1 + z_a^{-1}} \equiv F_1(z_a), \quad (2.160)$$

where the *fugacity* is defined as

$$z_a = \exp [m(\alpha^p + c\alpha_i^u e_{ai})]. \quad (2.161)$$

Note that α^ρ and α_i^u are functions of $\rho(\vec{x}, t)$ and $v_i(\vec{x}, t)$, as will be shown below. It is straightforward to do a Taylor expansion of the fugacity about $z^o = e^{m\alpha^\rho}$, the subsonic limit expansion

$$z_a = z^o \left(1 + m c \alpha_i^u e_{ai} + \frac{1}{2} m^2 c^2 \alpha_i^u \alpha_j^u e_{ai} e_{aj} + \dots \right). \quad (2.162)$$

Inserting the deviation of the fugacity $\delta z \equiv z_a - z^o$ into a Taylor expansion of $f_a^{(0)}$ about z^o then gives

$$\begin{aligned} f_a^{(0)} &= F_1(z^o) + F_1'(z^o) \delta z + \frac{1}{2} F_1''(z^o) \delta z^2 + \dots \\ &= F_1(z^o) + \left[z F_1' \right]_{z=z^o} m c \alpha_i^u e_{ai} + \\ &\quad \frac{1}{2} \left[z F_1' + z^2 F_1'' \right]_{z=z^o} m^2 c^2 \alpha_i^u \alpha_j^u e_{ai} e_{aj} + \\ &\quad \mathcal{O}(c^3) \end{aligned} \quad (2.163)$$

$$(2.164)$$

Inserting (2.164) into the first moment (2.105) and second moment (2.106) of $f_a^{(0)}$ gives the following expressions for the particle density

$$\rho = m B F_1(z^o) + \frac{m^3 c^2 B}{2D} \left[z F_1' + z^2 F_1'' \right]_{z=z^o} (\alpha^u)^2 \quad (2.165)$$

and the momentum density

$$\rho v_i = \frac{m^2 c^2 B}{D} \left[z F_1' \right]_{z=z^o} \alpha_i^u, \quad (2.166)$$

respectively. Manipulating (2.165) and (2.166) allows us to solve for α_i^u and then $F_1(z^o)$

$$F_1(z^o) = d - \frac{D d^2 v^2}{2c^2} \left[\frac{z F_1' + z^2 F_1''}{(z F_1')^2} \right]_{z=z^o}, \quad (2.167)$$

where the reduced density is defined as $d \equiv \frac{\rho}{mB}$. Therefore, express the equilibrium particle distribution as an expansion in ρ and v_i by inserting (2.166) and (2.167) into

(2.164) to obtain the desired result

$$f_a^{(0)} = d \left(1 + \frac{D}{c} e_{ai} v_i + g \frac{D(D+2)}{2c^2} Q_{aij} v_i v_j \right) + \mathcal{O}(v^3), \quad (2.168)$$

where

$$Q_{aij} \equiv e_{ai} e_{aj} - \frac{\delta_{ij}}{D} \quad (2.169)$$

and the Galilean prefactor is

$$g = d \frac{D}{D+2} \left[\frac{z F_1' + z^2 F_1''}{(z F_1')^2} \right]_{z=z^o}. \quad (2.170)$$

As a consistency check, write g solely in terms of d to see if the usual result is obtained. First note that since $F_1(z) = \frac{z}{z+1}$, the expression in brackets in (2.170) reduces to $\frac{1}{z^o} - z^o$. A plot of the fractional occupation versus the fugacity is given in Figure 2.1. Then noting that $z^o = F_1^{-1}(d) = \frac{d}{1-d}$, the expected result (D.12) is obtained for a single speed lattice gas: $g(d) = \frac{D}{D+2} \frac{1-2d}{1-d}$ given in Appendix D. The Galilean prefactor, $g(d)$, is plotted versus the fractional occupation in Figure 2.2.

In the Appendix D.1, a Chapman-Enskog expansion is carried out to second order in the velocity for the equilibrium distribution (D.11). So far in this section an identical result (2.168) has been obtained. Now it is possible to determine a correction to the particle distribution function accounting for spatial variations of the velocity field. From (2.100) and (2.101) write the mean field collision operator as

$$\Omega_a^{\text{mf}}(f) = f_a' - f_a = \ell e_{ai} \partial_i f_a^{(0)} + \mathcal{O}(\epsilon^2) \quad (2.171)$$

the so called propagation equation. Multiplying (2.132) by J_{ab}^{-1} and inserting (2.171) for $\Omega_a(f)$ gives the first correction to the equilibrium distribution function

$$f_a^{(1)} = \ell J_{ab}^{-1}(f^{(0)}) e_{bi} \partial_i f_b^{(0)}. \quad (2.172)$$

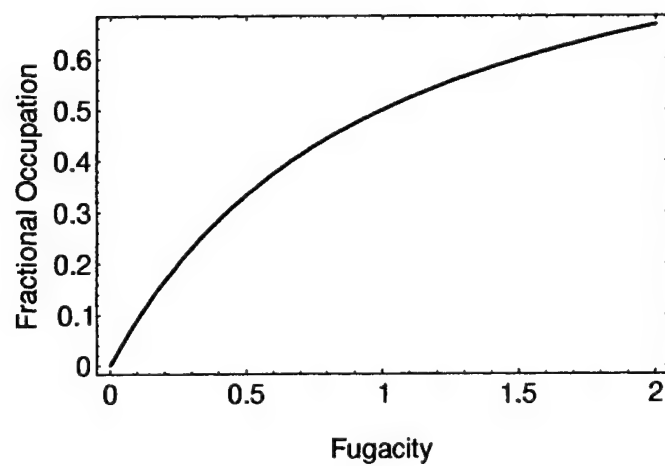


Figure 2.1: Fractional occupation versus fugacity for a classical lattice gas, $L = 1$.

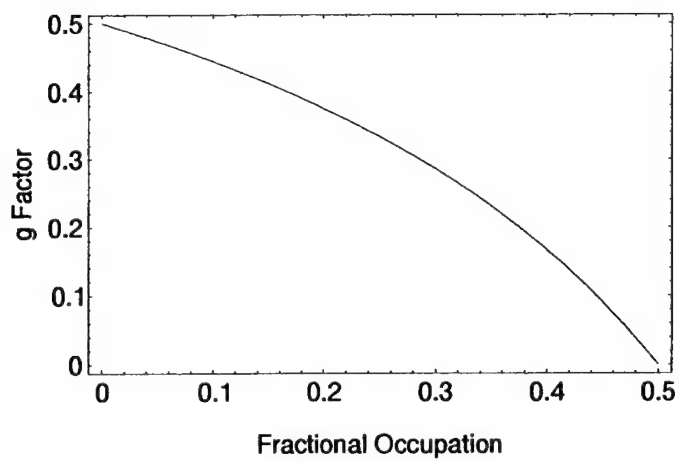


Figure 2.2: Galilean prefactor versus fractional occupation for a classical lattice gas, $L = 1$ in $D = 2$ dimensions.

Therefore, since $f_a = f_a^{(0)} + f_a^{(1)}$, using (2.172) it follows that

$$f_a = [\delta_{ab} + \ell J_{ab}^{-1}(f^{(0)})e_{bi}\partial_i] f_b^{(0)}. \quad (2.173)$$

And finally, insert the expression for $f_a^{(0)}$ from (2.168) this into (2.173) to obtain the form of the corrected distribution

$$f_a = d[1 + \frac{D}{c}e_{ai}v_i + g\frac{D(D+2)}{2c^2}Q_{aij}v_iv_j + \tau D J_{ab}^{-1}e_{bi}e_{bj}\partial_iv_j] + \mathcal{O}(v^3). \quad (2.174)$$

2.4.2 J Theorem

To proceed it is first necessary to simplify the term $\tau D J_{ab}^{-1}e_{bi}e_{bj}\partial_iv_j$ in the above expression (2.174) for the particle distribution by relying on a piece of physical intuition. Clearly this term will contribute solely to the shear viscosity of the macroscopic fluid. The inverse of the Jacobian is defined only over the kinetic modes of the system (that is, it cannot depend on the hydrodynamic modes since the hydrodynamic eigenvalues are zero and so J^{-1} is singular here). Moreover, because of isometry of collisions and consequent lack of preference in direction for momentum diffusion, there must exist a subspace of those kinetic eigenvectors having a degenerate eigenvalue and that contribute positively to the shear viscosity. We have termed this subspace the viscous subspace, \mathcal{V} . Moreover, since one observes that the projection of the tensor $|e_ie_j\rangle$ onto the space spanned by the kinetic eigenvectors is actually totally contained in \mathcal{V} , I state the following theorem

Theorem 1 *The ket $|e_ie_j\rangle$ formed from the dyadic $e_{ai}e_{aj}$ is an eigenket of the matrix inverse of the Jacobian of the collision operator J^{-1} , with eigenvalue $\frac{1}{\sum_{ab} J_{ab}(\hat{e}_a \cdot \hat{e}_b)^2}$, for an incompressible fluid. That is, if $\partial_iv_i = 0$, the following eigenequation holds*

$$J^{-1} |e_ie_j\rangle = \frac{B}{\sum_{ab} J_{ab}(\hat{e}_a \cdot \hat{e}_b)^2} |e_ie_j\rangle \quad (2.175)$$

in the kinetic subspace where the inverse Jacobian is not singular.

PROOF:

We begin by separating J^{-1} into its viscous part and a nonviscous part according to (2.152)

$$J^{-1} = \frac{1}{\kappa_\eta} \sum_{\alpha \in \mathcal{V}} |\alpha\rangle\langle\alpha| + \sum_{\alpha \in \mathcal{K} \ominus \mathcal{V}} \frac{1}{\kappa_\alpha} |\alpha\rangle\langle\alpha|.$$

In general the set of second rank lattice dyadics $|e_i e_j\rangle$ for $(i, j) = 1, \dots, D$ have the property that their projection resides in the space $\mathcal{H} + \mathcal{V}$, so that one may write

$$|e_i e_j\rangle = \sum_{\alpha \in \mathcal{H}} |\alpha\rangle\langle\alpha| e_i e_j + \sum_{\alpha \in \mathcal{V}} |\alpha\rangle\langle\alpha| e_i e_j. \quad (2.176)$$

Consequently one can determine $\langle e_i e_j | J^{-1} | e_i e_j \rangle$ directly by applying (2.176) from the left and right onto (2.152)

$$\langle e_i e_j | J^{-1} | e_i e_j \rangle = \frac{1}{\kappa_\eta} \sum_{\alpha \in \mathcal{V}} \langle e_i e_j | \alpha \rangle \langle \alpha | e_i e_j \rangle. \quad (2.177)$$

We can simplify the R.H.S. of this expression. First, sum over all eigenkets, and rearrange terms as follows

$$\langle e_i e_j | J^{-1} | e_i e_j \rangle = \frac{1}{\kappa_\eta} \sum_{ab} e_{ai} e_{aj} e_{bi} e_{bj} \sum_{\alpha} \xi_a^\alpha \xi_b^\alpha, \quad (2.178)$$

Now because of closure of the eigenkets, $\sum_{\alpha} \xi_a^\alpha \xi_b^\alpha = \delta_{ab}$ and using the identity for the product of four lattice vectors (2.18), it follows that

$$\langle e_i e_j | J^{-1} | e_i e_j \rangle = \frac{1}{\kappa_\eta} \frac{B}{D(D+2)} \Delta_{ijij}^{(4)}, \quad (2.179)$$

Since $\Delta_{ijij} = D(D+2)$, it is immediately clear that

$$\langle e_i e_j | J^{-1} | e_i e_j \rangle = \frac{B}{\kappa_\eta}. \quad (2.180)$$

We can similarly separate J into its viscous part and a nonviscous part

$$J = \kappa_\eta \sum_{\alpha \in \mathcal{V}} |\alpha\rangle\langle\alpha| + \sum_{\alpha \in \mathcal{K} \setminus \mathcal{V}} \kappa_\alpha |\alpha\rangle\langle\alpha|,$$

and determine $\langle e_k e_l | J | e_k e_l \rangle$ directly by applying (2.176) from the left and right onto (2.4.2)

$$\langle e_k e_l | J | e_k e_l \rangle = \kappa_\eta \sum_{\alpha \in \mathcal{V}} \langle e_k e_l | \alpha \rangle \langle \alpha | e_k e_l \rangle. \quad (2.181)$$

Now since the lattice vectors e_{ai} are all of unit length, and because of closure of the eigenkets $|\alpha\rangle$, in a similar fashion it follows that

$$\langle e_i e_j | J | e_i e_j \rangle = \kappa_\eta B. \quad (2.182)$$

Multiplying (2.180) and (2.182) gives

$$\langle e_k e_l | J | e_k e_l \rangle \langle e_i e_j | J^{-1} | e_i e_j \rangle = B^2, \quad (2.183)$$

which upon rearranging terms implies

$$J^{-1} | e_i e_j \rangle = \frac{B}{\langle e_k e_l | J | e_k e_l \rangle} | e_i e_j \rangle. \quad (2.184)$$

This completes the proof of Theorem 2.175. **QED** \square

Defining the eigenvalue

$$\lambda \equiv \frac{-\ell B}{\sum_{ab} J_{ab} (\hat{e}_a \cdot \hat{e}_b)^2} = \frac{-\ell}{B} \sum_{ab} J_{ab}^{-1} (\hat{e}_a \cdot \hat{e}_b)^2, \quad (2.185)$$

it is possible to write the J -theorem as

$$J^{-1} | e_i e_j \rangle = -\frac{\lambda}{\ell} | e_i e_j \rangle. \quad (2.186)$$

Using this theorem by substituting (2.186) into the corrected distribution function (2.174) of the previous section gives us the simplification

$$f_a = d[1 + \frac{D}{c} e_{ai} v_i + g \frac{D(D+2)}{2c^2} Q_{aij} v_i v_j - \frac{D}{c} \lambda e_{ai} e_{aj} \partial_i v_j] + \mathcal{O}(v^3). \quad (2.187)$$

We have relations for λ in terms of κ_η

$$\lambda = \frac{-\ell B}{\kappa_\eta \sum_{\alpha \in \mathcal{V}} \langle e_i e_j | \alpha \rangle \langle \alpha | e_i e_j \rangle} = \frac{-\ell}{B \kappa_\eta} \sum_{\alpha \in \mathcal{V}} \langle e_i e_j | \alpha \rangle \langle \alpha | e_i e_j \rangle. \quad (2.188)$$

This method of determining λ is most direct, but it relies on knowing the viscous eigenvalue, κ_η , and the associated viscous eigenvectors of J . When J is circulant this is readily known, so (2.188) would be quite convenient. However, in more complicated lattice gases, such as a multispeed lattice gas or a finite-integer lattice with a rest channel, J is not circulant. Moreover, since the size of J is quite large for these systems, the eigenvalue problem cannot be generally solved (for instance, a multispeed fchc lattice gas would have at least $24+24+1=49$ bits, so J would be a 49×49 matrix). Therefore, a more practical way of determining λ for more complex systems is needed. This is accomplished as follows.

Inserting (2.159) into the R.H.S., we immediately obtain

$$\lambda = \frac{-\ell B}{\sum_C T d^{p-1} (1-d)^{B-p-1} \sum_{ab} (n'_a - n_a) n_b (\hat{e}_a \cdot \hat{e}_b)^2}. \quad (2.189)$$

and now λ is computed solely with a supplied collision set. Note if J is not circulant and it is not straightforward to solve for its eigenvalues and eigenvectors, (2.189) still gives us a direct way to determine λ and so it is an important result. The benefit of this way to find λ is that it provides a new generalizable way to determine the viscosity of a lattice gas, generalizable to an integer lattice gas for example.

2.5 Macrodynamics

The macroscopic equations of motion are then determined from mass conservation (continuity equation)

$$\partial_t \rho + \partial_i (\rho v_i) = 0 \quad (2.190)$$

and momentum conservation (Euler's equation)

$$\partial_t(\rho v_i) + \partial_j \Pi_{ij} = 0. \quad (2.191)$$

Note that in the incompressible limit where the density is constant, $\partial_t \rho = 0$, so there is divergence-free flow.

Now following Landau and Lifshitz [57], the momentum flux density tensor is written in standard form as

$$mc^2 \sum_a e_{ai} e_{aj} f_a = p \delta_{ij} + \rho v_i v_j - \sigma'_{ij} \quad (2.192)$$

where in (2.192) the first two terms represent the ideal part of the momentum flux density tensor and $\sigma'_{ij} = \eta(\partial_i v_j - \partial_j v_i)$ is the viscous stress tensor. Alternatively the momentum flux density tensor may be written

$$\Pi_{ij} = mc^2 \sum_a e_{ai} e_{aj} f_a = -\sigma_{ij} + \rho v_i v_j, \quad (2.193)$$

where σ_{ij} is the pressure stress tensor

$$\sigma_{ij} = -p \delta_{ij} + \eta (\partial_i v_j - \partial_j v_i). \quad (2.194)$$

Given a non-divergent flow ($\partial_j v_j = 0$) appropriate to the incompressible fluid limit, it is possible to write

$$\Pi_{ij} = p \delta_{ij} + \rho v_i v_j + \eta \partial_j v_i. \quad (2.195)$$

Substituting (2.195) into Euler's equation (2.191), gives us the Navier-Stokes equation for a viscous fluid

$$\rho (\partial_t v_i + v_j \partial_j v_i) = -\partial_i p + \eta \partial^2 v_i. \quad (2.196)$$

In this section I calculate a general expression for the transport coefficient for momentum diffusion within a lattice gas in the continuum limit, that is, the shear viscosity,

η , for a single speed lattice gas on a Bravais lattice. Two different forms are presented. We use our new J -theorem (2.175) to calculate the shear viscosity quite directly. The method is readily generalizable to the calculation of the shear viscosity of more complex lattice gas systems, such as an integer lattice gas. In fact, this has been the motivation to find a new way to calculate this transport coefficient, since the shear viscosity of an integer lattice gas has recently been observed, by exact numerical computations, to be lower than in a traditional lattice gas.

The first form given for the shear viscosity is

$$\eta = \rho \frac{\ell^2}{\tau} \frac{1}{(D+2)} \left(-\frac{1}{B} \langle e_i e_j | J^{-1} | e_i e_j \rangle - \frac{1}{2} \right). \quad (2.197)$$

This expression for η , though simpler, is similar to the expression for the shear viscosity given recently by Boghosian and Taylor [13] in 1995. This method is quite practical for a single speed lattice gas with no rest particles because J is circulant owing to the isometry of the collisions.

The second form given for the shear viscosity is

$$\eta = \rho \frac{\ell^2}{\tau} \frac{1}{(D+2)} \left(-\frac{B}{\langle e_i e_j | J | e_i e_j \rangle} - \frac{1}{2} \right). \quad (2.198)$$

This form directly leads to an expression for the shear viscosity given by Hénon [50] in 1990 for a D-dimensional lattice gas.

In any lattice gas simulation, one typically obtains a realization of the macroscopic dynamical variables by block averaging in both space and time over the microscopic variables. In this way, for example, a momentum map can be produced so that the dynamic evolution the the fluid can be monitored. The size of the coarse grain block affects the resolution with which one can observe the system but does not at all

affect the underlying dynamics. If too small a coarse grain block size is used, more fluctuations in the macroscopic variables occur.

2.5.1 Derivation of the Continuum Equations

For each additive conserved quantity of the microdynamics, there exists a macroscopic variable that is expressed as a moment of the mesoscopic particle distribution function. The associated macroscopic variable is a field with a value at every space-time point of the continuum and the evolution of this field is governed by a particular dynamical partial differential equation that in turn is obtained by taking moments of the mesoscopic Boltzmann equation. Since by construction one knows the form of the conserved quantities in terms of the mesoscopic distribution function, and since one knows the mesoscopic Boltzmann equation to second order in $\epsilon \sim \delta x^2 \sim \delta t$ for the lattice gas system, it is a straightforward procedure to derive the continuum equations of motion.

We are now ready to determine the macroscopic equations of motion using the lattice Boltzmann equation (2.104) and the corrected distribution function (2.187) along with definitions for mass density (2.105) and momentum density (2.106). Since $\sum_a \Omega_a^{\text{mf}} = 0$, the zeroth moment of (2.104) is

$$\partial_t m \sum_a f_a + \partial_i m c \sum_a e_{ai} f_a + \frac{\ell^2}{2\tau} \partial_i \partial_j \sum_a e_{ai} e_{aj} f_a = 0. \quad (2.199)$$

This reduces to mass continuity

$$\partial_t \rho + \partial_i \rho v_i + \mathcal{O}(v^2) = 0, \quad (2.200)$$

which in the incompressible limit (ρ constant) implies divergence-free flow ($\partial_i v_i = 0$).

Since $\sum_a e_{ai} \Omega_a^{\text{mf}} = 0$ too, the first moment of (2.104) is

$$\partial_t mc \sum_a e_{ai} f_a + \partial_j mc^2 \sum_a e_{ai} e_{aj} f_a + \frac{\ell^2}{2\tau} \partial_j \partial_k mc \sum_a e_{ai} e_{aj} e_{ak} f_a = 0. \quad (2.201)$$

This reduces to Euler's equation

$$\rho \partial_t v_i + \partial_j \Pi_{ij} = 0, \quad (2.202)$$

where the momentum flux density is

$$\Pi_{ij} = p \delta_{ij} + g \rho v_i v_j - \frac{\rho c \lambda}{D+2} \partial_j v_i + \frac{\ell^2}{2\tau} \frac{\rho}{(D+2)} \partial_j v_i \quad (2.203)$$

or

$$\Pi_{ij} = p \delta_{ij} + g \rho v_i v_j - \frac{\rho c}{D+2} \left(\lambda - \frac{\ell}{2} \right) \partial_j v_i. \quad (2.204)$$

The shift in λ is a constant negative contribution to the shear viscosity by a lattice effect. With sound speed $c_s \equiv \frac{c}{\sqrt{D}}$, identify the pressure as

$$p = \rho c_s^2 \left(1 - g \frac{v^2}{c^2} \right). \quad (2.205)$$

Finally, inserting (2.204) into Euler's equation (2.202), the Navier-Stokes equation for viscous incompressible flow emerges

$$\rho \partial_t v_i + g \rho \partial_j (v_i v_j) = -\partial_i p + \eta \partial^2 v_i \quad (2.206)$$

with shear viscosity

$$\eta = \frac{\rho c}{(D+2)} \left(\lambda - \frac{\ell}{2} \right). \quad (2.207)$$

Since it is known how to determine the value of λ , using (2.188) or (2.189), the shear viscosity of a lattice gas is completely determined as well.

2.5.2 Recalculating the Shear Viscosity Transport Coefficient

The derivation presented here is based on one originally given by H  non [50] for a D-dimensional lattice gas and it will confirm the result obtained in the previous section.

In the Chapman-Enskog expansion above, one essentially decomposes the particle distribution function into two parts: $f_a = f^{(0)} + f^{(1)}$. Here it is decomposed into two different parts, its background value plus its deviation from the background: $f_a = d + \delta f_a$. With this decomposition the collision operator (2.126) becomes

$$\Omega_a = \sum_C (n'_a - n_a) T \prod_b (d + \delta f_b)^{n_b} (1 - d - \delta f_b)^{1-n_b}. \quad (2.208)$$

Since δf is small, use the following binomial expansions (exact since n_a is Boolean)

$$(d + \delta f_a)^{n_a} = d^{n_a} + n_a d^{n_a-1} \delta f_a \quad (2.209)$$

$$[(1 - d) - \delta f_a]^{1-n_a} = (1 - d)^{1-n_a} - (1 - n_a)(1 - d)^{-n_a} \delta f_a \quad (2.210)$$

which gives us

$$\Omega_a = \sum_C (n'_a - n_a) T \prod_b d^{n_b} (1 - d)^{1-n_b} \left[1 + \frac{n_b - d}{d(1 - d)} \delta f_b \right]. \quad (2.211)$$

Thus, we obtain

$$\Omega_a = \sum_C (n'_a - n_a) T d^p (1 - d)^{B-p} \left[1 + \sum_b \frac{n_b - d}{d(1 - d)} \delta f_b \right], \quad (2.212)$$

where the following approximation holds provided all $x_i \ll 1$

$$\prod_i [1 + x_i] \simeq 1 + \sum_i x_i. \quad (2.213)$$

By the symmetry of the collision probability $T(s, s')$ the first term vanishes

$$\sum_C (n'_a - n_a) T d^p (1-d)^{B-p} = 0$$

and the last term also vanishes since $\sum_a \delta f_a = 0$, so we arrive at the fundamental collision equation for δf_a

$$\Omega_a = \sum_C (n'_a - n_a) T d^{p-1} (1-d)^{B-p-1} \sum_b n_b \delta f_b. \quad (2.214)$$

Now, using the corrected distribution (2.174) and our ansatz (2.175), one can write an expression for the deviation of the particle distribution function⁸

$$\delta f_a = \frac{D}{c} e_{ai} v_i - \frac{d\lambda D}{c} e_{ai} e_{aj} \partial_i v_j + \mathcal{O}(v^2). \quad (2.215)$$

Inserting (2.215) into (2.214) and only keeping terms linear in the velocity gives

$$\Omega_a^{\text{collision}} = -\frac{d\lambda D}{c} \sum_C (n'_a - n_a) T d^{p-1} (1-d)^{B-p-1} \sum_b n_b e_{bi} e_{bj} \partial_i v_j. \quad (2.216)$$

Now from the propagation equation (2.171) it follows

$$\Omega_a^{\text{propagation}} = \ell e_{ai} \partial_i f_a^{(0)} = \frac{d\ell D}{c} e_{ai} e_{aj} \partial_i v_j. \quad (2.217)$$

Equating our two expressions for the collision operator, $\Omega_a^{\text{collision}} = \Omega_a^{\text{propagation}}$, it is possible to solve for λ

$$\lambda = \frac{-\ell}{\sum_C (n'_a - n_a) T d^{p-1} (1-d)^{B-p-1} \sum_b n_b (\hat{e}_a \cdot \hat{e}_b)^2}. \quad (2.218)$$

Note that the denominator of (2.218) depends on the index a . Since the spatial lattice is isotropic, it does not matter which direction is used; any particular direction can be chosen without loss of generality. However, to make the connection with our previous

⁸Note that $\sum_a \delta f_a$ does indeed vanish since the flow is divergenceless, $\partial_i v_i = 0$.

expression for λ , we sum over all lattice vectors. Therefore, it is preferable to write this as

$$\lambda = \frac{-\ell B}{\sum_C \sum_a (n'_a - n_a) T d^{p-1} (1-d)^{B-p-1} \sum_b n_b (\hat{e}_a \cdot \hat{e}_b)^2}. \quad (2.219)$$

This result is exactly (2.189) found directly in §2.4.2 and provides a good consistency check.

Inserting (2.219) into (2.207), we get the shear viscosity of a single-speed lattice gas is expressed explicitly in terms of the particle occupation number variables

$$\eta = \frac{\rho \ell c}{D+2} \left(\frac{B}{\sum_{nn'} d^{p-1} (1-d)^{B-p-1} T(n, n') \sum_{ab} (n_a - n'_a) n_b (\hat{e}_a \cdot \hat{e}_b)^2} - \frac{1}{2} \right) \quad (2.220)$$

where $T(n, n')$ is the probability of a collision with n incoming and n' outgoing configurations. This is the most generally useful expression for this transport coefficient.

2.5.3 Variation of Viscosity Minima with Lattice Coordination Number

Three cases are presented for the kinematic viscosity versus reduced density for two-dimensional systems with $B = 4$, $B = 6$, and $B = 8$ number of momentum states. No solutions exist for odd B . All possible collisions are included by finding all permutations of the input configurations that conserve momentum. Therefore the collisions are particle-hole symmetric and the minimum value of the kinematic viscosity occurs at half filling: $\nu_{B=4}(0.5) = 0.125$, $\nu_{B=6}(0.5) = 0.0972$, and $\nu_{B=8}(0.5) = 0.0908$. The kinematic viscosities are

$$\nu_{B=4}(d) = \frac{1}{4} \left(\frac{1}{4\tilde{d}d} - \frac{1}{2} \right) \quad (2.221)$$

$$\nu_{B=6}(d) = \frac{1}{4} \left(\frac{1}{3\tilde{d}^3d + 12\tilde{d}^2d^2 + 3\tilde{d}d^3} - \frac{1}{2} \right) \quad (2.222)$$

$$\nu_{B=8}(d) = \frac{1}{4} \left(\frac{1}{2(\frac{4}{3}\tilde{d}^5d + 8\tilde{d}^4d^2 + \frac{92}{5}\tilde{d}^3d^3 + 8\tilde{d}^2d^4 + \frac{4}{3}\tilde{d}d^5)} - \frac{1}{2} \right), \quad (2.223)$$

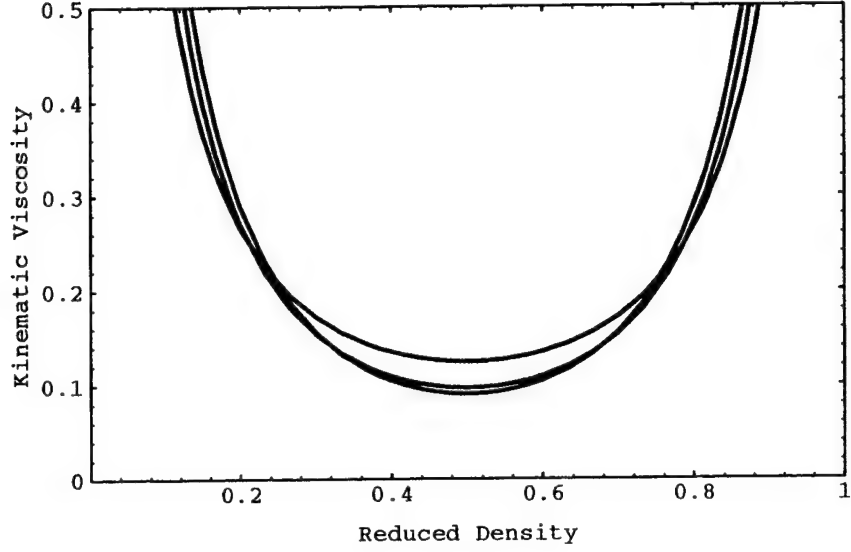


Figure 2.3: Kinematic shear viscosity, $\nu(d)$, versus reduced density, $d = n/B$, for two-dimensional lattice gases with $B=4, 6$, and 8 momentum states. Viscosity decreases with increasing B .

where the reduced hole density is $\hat{d} \equiv 1 - d$. Plots of these results are overlayed in Figure 2.3. Calculations have been done for up to $B = 12$ but no significant decrease in the viscosity is observed.

Chapter 3

The Simplest Lattice-Gas ($L=1$)

3.1 Introduction

The discovery that a very simple discrete model, the Frisch, Hasslacher, and Pomeau (FHP) lattice gas model [42], using only six bits of memory at each point in space reproduces hydrodynamics in its macroscopic limit has stimulated many investigations of the subject of discrete kinetic equations. This subject, broadly termed lattice gas methods, has to date expanded its scope beyond incompressible hydrodynamics to thermodynamics, multiphase phenomena, magnetohydrodynamics, reaction-diffusion systems, and seems to be continuing its growth. Given the conceptual importance of a simple lattice gas model with its ability to simulate so much, the FHP lattice gas is presented here. The FHP lattice gas has three invariants: the total mass and the two components of momentum.

It is well known that symmetric 3-body collisions must be included along with the FHP model's even and odd chirality 2-body collisions to achieve the correct macroscopic limit. However, the fact that both even and odd 2-body collision possibilities are present dictates that when a 2-body collision occurs, a coin toss must also occur to determine the outgoing state. This coin toss does not make the FHP model

irreversible. Clearly if the model is constrained to have a definite chirality, say for example 2-body collisions generated by $\frac{\pi}{3}$ rotations are retained while $\frac{2\pi}{3}$ collisions are discarded, then the lattice gas would be strictly reversible. But does this additional constraint of a fixed chirality engender any spurious invariants? The answer is it does not.

When introduced to the hexagonal lattice gas model for the first time, one inevitably asks the following question: Why does the discrete dynamics fail to reproduce the correct continuum hydrodynamic limit when implemented on a square lattice? One finds that four momentum states are insufficient by noting that the derivation in chapter 2 of the correct form of the Navier-Stokes equation (2.206) relied on the expansion of the momentum flux density tensor in terms of the isotropic tensor $E^{(2n)}$. Each isotropic tensor itself could be expanded in products of two-dimensional Kronecker deltas (2.20). In particular for $D = 2$,

$$\begin{aligned} E^{(4)} &= \frac{B}{8} (\delta_{ij}\delta_{kl} + \delta_{ik}\delta_{jl} + \delta_{il}\delta_{kj}) \\ &= \frac{B}{8} (3\hat{x}\hat{x}\hat{x}\hat{x} + 3\hat{y}\hat{y}\hat{y}\hat{y} + \hat{x}\hat{y}\hat{y}\hat{x} + \hat{y}\hat{x}\hat{x}\hat{y} + \hat{x}\hat{y}\hat{x}\hat{y} + \hat{y}\hat{x}\hat{y}\hat{x} + \hat{x}\hat{y}\hat{y}\hat{x} + \hat{y}\hat{x}\hat{x}\hat{y}). \end{aligned}$$

Refer to §2.1.2 to see why this is so. For the square lattice case, $B = 4$, the lattice vectors are orthogonal and $E^{(4)}$ cannot be decomposed into two-dimensional Kronecker deltas. Instead

$$E_{ijkl}^4|_{B=4} \propto \delta_{ijkl} = \hat{x}\hat{x}\hat{x}\hat{x} + \hat{y}\hat{y}\hat{y}\hat{y}$$

where δ_{ijkl} is a four-dimensional Kronecker delta [97] illustrating the lack of isotropy of the momentum flux density on a square lattice gas. Since $B = 5$ is not space filling, the next possible choice is $B = 6$ or the hexagonal lattice gas system.

3.2 Using the Tools of the Trade

3.2.1 Triangular Lattice

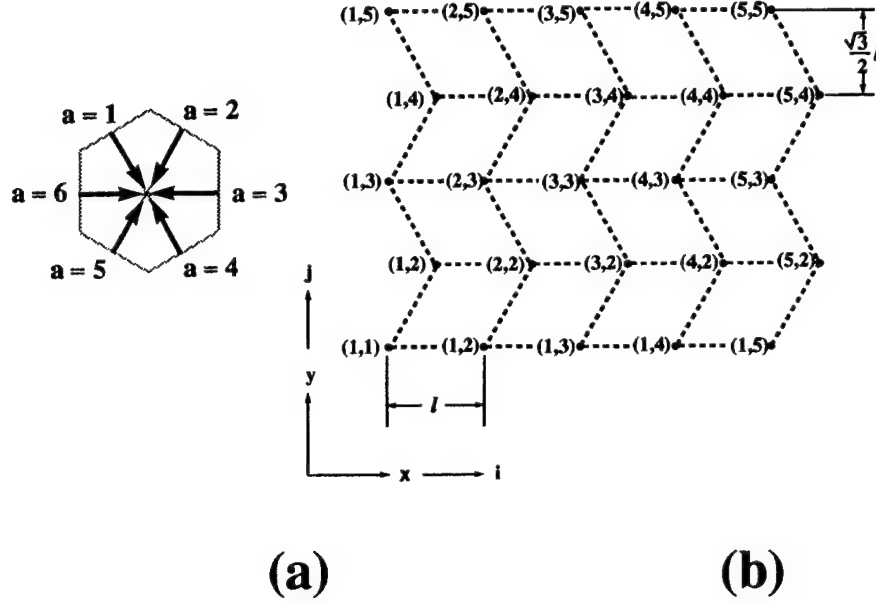


Figure 3.1: Triangular Lattice Convention: (a) Lattice vector label convention; (b) Triangular lattice convention with lattice directions $a = 3$ up and $a = 6$ down. Coordinates above the lattice nodes are (i, j) memory array indices.

In a triangular lattice there are six vectors, enumerated in this section by the convention

$$\hat{e}_a = \left(\cos \frac{\pi a}{3}, -\sin \frac{\pi a}{3} \right), \quad (3.1)$$

where $a = 1, 2, \dots, 6$. The spatial coordinates of the lattice sites may be expressed as follows

$$\mathbf{x}_{ij} = \left(i - \frac{1}{2}(j \bmod 2), \frac{\sqrt{3}}{2}j \right) \quad (3.2)$$

where i and j are rectilinear indices that specify the data memory array location used

to store the lattice gas site data.

Let $s = (j \bmod 2)(r \bmod 2)$. Given a particle at site (i, j) , it may be shifted r lattice units away to a remote site (i', j') by the mapping

$$(i', j')_1 = \left(i + \frac{r+1}{2} - s, j - r\right) \quad (3.3)$$

$$(i', j')_2 = \left(i - \frac{r}{2} - s, j - r\right) \quad (3.4)$$

$$(i', j')_3 = (i - r, j) \quad (3.5)$$

$$(i', j')_4 = \left(i - \frac{r}{2} - s, j + r\right) \quad (3.6)$$

$$(i', j')_5 = \left(i + \frac{r+1}{2} - s, j + r\right) \quad (3.7)$$

$$(i', j')_6 = (i + r, j) \quad (3.8)$$

where $(i', j')_a$ denotes the shifted site, that is, $(i, j) \rightarrow (i', j')$ with a shift along vector $\vec{r} = r\hat{e}_a$ and where division by 2 is considered integer division.

These streaming relations are useful for implementing a lattice gas in a structured language such as the C-language. An implementation on the connection machine CM-5 in the C-language and DPEAC uses these relations for all address computations [106]. In these streaming relations, the modulus operator is base 2 because a two-dimensional triangular lattice embedded into a square three-dimensional mesh is pleated.

The simplest way to see this embedding is to define $z = (j \bmod 2)$. Therefore the third dimension along the z-axis is narrow, only one lattice distance wide. Half of the lattice sites are at $z = 0$ and the other half are at $z = 1$. This divides the triangular lattice into two sublattices that are referred to as *pleat 0* and *pleat 1*. Table 3.1 lists the components of the data translation vectors, or kicks, for each stream direction, $a = 1, 2, \dots, 6$, for both pleats. This kick table was used for a CAMForth

Table 3.1: Streaming for 2D Hex Lattice Embedded a into 3D Mesh

Direction	x	y	z
PLEAT 0			
1	0	0	1
2	0	-1	1
3	0	-1	0
4	1	-1	1
5	1	0	1
6	0	1	0
PLEAT 1			
1	-1	1	-1
2	-1	0	-1
3	0	-1	0
4	0	0	-1
5	0	1	-1
6	0	1	0

implementation on the CAM-8 and a C* implementation on the CM-5 [106]. This is equivalent to our general streaming relations for the case when $r = 1$. The usefulness of this kind of embedding is that if the data for any one of the sublattices is rendered for display, it can be drawn in simple raster form and fluid structures will appear correctly, *e.g.* a sound pulse will appear circular.

In a triangular lattice there are six lattice vectors enumerated by

$$\hat{e}_a = \left(\cos \frac{\pi a}{3}, \sin \frac{\pi a}{3} \right), \quad (3.9)$$

or explicitly

$$\begin{aligned} \hat{e}_1 &= \left(\frac{1}{2}, \frac{\sqrt{3}}{2} \right) \\ \hat{e}_2 &= \left(-\frac{1}{2}, \frac{\sqrt{3}}{2} \right) \\ \hat{e}_3 &= (-1, 0) \end{aligned}$$

$$\begin{aligned}
\hat{e}_4 &= \left(-\frac{1}{2}, -\frac{\sqrt{3}}{2}\right) \\
\hat{e}_5 &= \left(\frac{1}{2}, -\frac{\sqrt{3}}{2}\right) \\
\hat{e}_6 &= (1, 0).
\end{aligned}$$

We therefore have the following two *lattice kets*

$$\begin{aligned}
|e_x\rangle &= \frac{1}{2}[1, -1, -2, -1, 1, 2] \\
|e_y\rangle &= \frac{\sqrt{3}}{2}[1, 1, 0, -1, -1, 0]
\end{aligned}$$

We will need the following ket obtained by multiplying e_x and e_y component by component

$$|e_x e_y\rangle = \frac{\sqrt{3}}{4}[1, -1, 0, -1, 1, 0]. \quad (3.10)$$

Similarly

$$|e_x e_x\rangle = \frac{\sqrt{1}}{4}[1, 1, 4, 1, 1, 4] \quad (3.11)$$

$$|e_y e_y\rangle = \frac{\sqrt{3}}{4}[1, 1, 0, 1, 1, 0]. \quad (3.12)$$

At this point, without any specification of the collision set or any knowledge of the collision operator, one can still write down the eigenvectors of the Jacobian of the collision operator. Using (2.144) the eigenkets are

$$|\alpha\rangle = [\epsilon^\alpha, (-\epsilon^*)^\alpha, (-1)^\alpha, (-\epsilon)^\alpha, (\epsilon^*)^\alpha, 1] \quad (3.13)$$

or explicitly

$$|1\rangle = [\epsilon, -\epsilon^*, -1, -\epsilon, \epsilon^*, 1]$$

$$|2\rangle = [-\epsilon^*, -\epsilon, 1, -\epsilon^*, -\epsilon, 1]$$

$$\begin{aligned}
|3\rangle &= [-1, 1, -1, 1, -1, 1] \\
|4\rangle &= [-\varepsilon, -\varepsilon^*, 1, -\varepsilon, -\varepsilon^*, 1] \\
|5\rangle &= [\varepsilon^*, -\varepsilon, -1, -\varepsilon^*, \varepsilon, 1] \\
|6\rangle &= [1, 1, 1, 1, 1, 1],
\end{aligned}$$

where $\varepsilon \equiv \exp(i\frac{\pi}{3})$ and $\varepsilon^* \equiv \exp(-i\frac{\pi}{3})$. For later convenience in computing the eigenvalues, define a new set of eigenkets as follows

$$\begin{aligned}
|1'\rangle &= |6\rangle \\
|2'\rangle &= \frac{1}{i\sqrt{3}}(|1\rangle - |5\rangle) \\
|3'\rangle &= |1\rangle + |5\rangle \\
|4'\rangle &= |2\rangle - |4\rangle \\
|5'\rangle &= \frac{1}{i\sqrt{3}}(|2\rangle + |4\rangle) \\
|6'\rangle &= |3\rangle,
\end{aligned}$$

or explicitly

$$\begin{aligned}
|1'\rangle &= [1, 1, 1, 1, 1, 1] = |e_x e_x\rangle + |e_y e_y\rangle \\
|2'\rangle &= [1, 1, 0, -1, -1, 0] = \frac{2}{\sqrt{3}} |e_y\rangle \\
|3'\rangle &= [1, -1, -2, -1, 1, 2] = 2 |e_x\rangle \\
|4'\rangle &= [1, 1, -2, 1, 1, -2] = 2(|e_y e_y\rangle - |e_x e_x\rangle) \\
|5'\rangle &= [1, -1, 0, 1, -1, 0] = \frac{4}{\sqrt{3}} |e_x e_y\rangle \\
|6'\rangle &= [-1, 1, -1, 1, -1, 1].
\end{aligned}$$

To satisfy normality one must have

$$\begin{aligned}
\langle 1' | &= \frac{1}{6} | 6 \rangle^\dagger \\
\langle 2' | &= \frac{1}{i4\sqrt{3}} (| 1 \rangle^\dagger - | 5 \rangle^\dagger) \\
\langle 3' | &= \frac{1}{12} (| 1 \rangle^\dagger + | 5 \rangle^\dagger) \\
\langle 4' | &= \frac{1}{12} (| 2 \rangle^\dagger - | 4 \rangle^\dagger) \\
\langle 5' | &= \frac{1}{i4\sqrt{3}} (| 2 \rangle^\dagger + | 4 \rangle^\dagger) \\
\langle 6' | &= \frac{1}{6} | 3 \rangle^\dagger,
\end{aligned}$$

where the dagger indicates column form.

3.2.2 Mean-Field Calculation of the Shear Viscosity

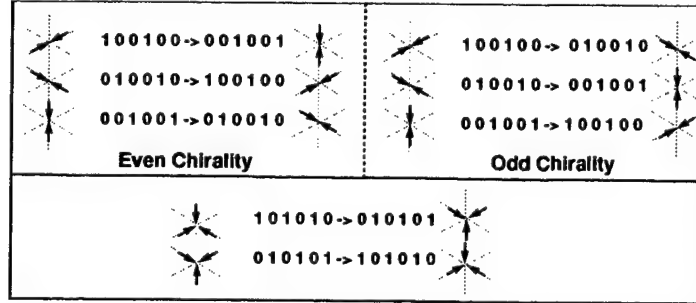


Figure 3.2: Enumeration of FHP 2-body collisions, even and odd chirality, and 3-body collisions.

The possible two-body collisions are illustrated in Figure 3.2, the blocks labeled even and odd chirality, and also in Figure 3.6, which has three particles on-site but with only two of the three particles undergoing a collision. This is referred to as 2-body collisions with a spectator particle. The original FHP-model [42] did not include collisions with spectators and instead included the two possible 3-body collisions, as

illustrated in Figure 3.2. For two-dimensional flow, there are three invariants, the mass, and two components of the momentum. With only the 2-body collisions in Figure 3.2, there is an additional invariant: the difference in the particle number along each of the three lattice directions give three conserved momenta instead of two. The 3-body collisions in Figure 3.2 are included in the FHP-model to remove this spurious invariant. Consequently, the collisions enumerated in Figure 3.2 are a sufficient set to produce hydrodynamic behavior in the continuum limit. The associated collision operator for the FHP-model is

$$\Omega_a^{\text{FHP}} = \frac{1}{2}Q_a(1,4) + \frac{1}{2}Q_a(2,5) - Q_a(3,6) + Q_a(1,3,5) - Q_a(2,4,6). \quad (3.14)$$

Writing this out explicitly

$$\begin{aligned} \Omega_{a=1}^{\text{FHP}} = & \frac{1}{2}f_2f_5(1-f_1)(1-f_3)(1-f_4)(1-f_6) + \\ & \frac{1}{2}f_3f_6(1-f_1)(1-f_2)(1-f_4)(1-f_5) - \\ & f_1f_4(1-f_2)(1-f_3)(1-f_5)(1-f_6) + \\ & f_2f_4f_6(1-f_1)(1-f_3)(1-f_5) - \\ & f_1f_3f_5(1-f_2)(1-f_4)(1-f_6). \end{aligned}$$

Consider the following input collision set, denoted f ,

$$\begin{aligned} f = & \{ \{1,0,0,1,0,0\}, \{0,1,0,0,1,0\}, \{0,0,1,0,0,1\}, \\ & \{1,0,1,0,1,0\}, \{0,1,0,1,0,1\} \}. \end{aligned} \quad (3.15)$$

Then the output collision set, denoted by f' , can be computed by using (3.14), the collision operator

$$\begin{aligned}
f' &= f + \Omega \\
&= \left\{ \left\{ 0, \frac{1}{2}, \frac{1}{2}, 0, \frac{1}{2}, \frac{1}{2} \right\}, \left\{ \frac{1}{2}, 0, \frac{1}{2}, \frac{1}{2}, 0, \frac{1}{2} \right\}, \right. \\
&\quad \left. \left\{ \frac{1}{2}, \frac{1}{2}, 0, \frac{1}{2}, \frac{1}{2}, 0 \right\}, \{0, 1, 0, 1, 0, 1\}, \{1, 0, 1, 0, 1, 0\} \right\}
\end{aligned} \tag{3.16}$$

Now, to completely specify the collision set, $\{f, f'\}$, one can use formula (2.159) to compute the Jacobian's elements

$$\begin{aligned}
|J\rangle &= \left[-d(1-d)^2, \frac{1}{2}d(1+d)(1-d)^2, \right. \\
&\quad \frac{1}{2}d(1-3d)(1-d)^2, \frac{1}{2}d(1-2d)(1-d)^2, \\
&\quad \left. \frac{1}{2}d(1-3d)(1-d)^2, \frac{1}{2}d(1+d)(1-d)^2 \right]
\end{aligned} \tag{3.17}$$

From (2.141) it immediately follows that the eigenvalues of J are

$$\begin{aligned}
\langle J | 1' \rangle &= 0 \\
\langle J | 2' \rangle &= 0 \\
\langle J | 3' \rangle &= 0 \\
\langle J | 4' \rangle &= -3d(1-d)^3 \\
\langle J | 5' \rangle &= -3d(1-d)^3 \\
\langle J | 6' \rangle &= 6d^2(1-d)^2.
\end{aligned}$$

Note that $\langle J | 1' \rangle$ corresponds to mass conservation, $\langle J | 2' \rangle$ to y-momentum conservation, and $\langle J | 3' \rangle$ to x-momentum conservation. The degenerate viscous eigenvalue

$\kappa_\eta = -3d(1-d)^3$ is immediately identified. Therefore, according to (2.188) and using (3.10), it follows that

$$\begin{aligned}\lambda &= \frac{1}{3d(1-d)^3} \sum_{\alpha \in \{4', 5'\}} \langle e_x e_y | \alpha \rangle \langle \alpha | e_x e_y \rangle \\ &= \frac{1}{4d(1-d)^3}.\end{aligned}$$

Finally, according to (2.207), the result is obtained

$$\eta^{\text{FHP}} = \rho \frac{\ell^2}{\tau} \left(\frac{1}{12d(1-d)^3} - \frac{1}{8} \right). \quad (3.18)$$

3.2.3 An Example of a Deterministic Lattice-Gas

When implementing a lattice gas on a parallel computer it is most convenient to use deterministic updating rules. This is important for several reasons. First, using deterministic rules, the lattice gas is strictly reversible, and can possess a time-reversal invariance with respect to a parity operation on the momentum states. Therefore, such a lattice gas mimics the time reversal invariance characterizing natural physical laws of motion. The reversibility allows one to run the gas dynamics forward to some state and then back to its initial state. As a practical matter, this is a good way to check if the local rules are coded correctly. Second, the generation of random numbers typically takes time and using random bits increases the number of states that the rule must deal with. For these reasons deterministic local rules are preferred. Two-dimensional lattice gas collisions can be categorized by their even or odd chirality. Using even chirality collisions on even time steps and odd chirality collisions on odd time steps eliminates the need for the random coin toss used in the FHP model. The collision operator that produces deterministic 2-body and 3-body symmetric collisions

is the following

$$\Omega_a = Q_a(1,4) - Q_a(0,3) + Q_a(1,3,5) - Q_a(0,2,4), \quad (3.19)$$

which is written in expanded form as

$$\begin{aligned} \Omega_1 = & f_3 f_6 (1 - f_1) (1 - f_2) (1 - f_4) (1 - f_5) - \\ & f_1 f_4 (1 - f_2) (1 - f_3) (1 - f_5) (1 - f_6) + \\ & f_2 f_4 f_6 (1 - f_1) (1 - f_3) (1 - f_5) - \\ & f_1 f_3 f_5 (1 - f_2) (1 - f_4) (1 - f_6) \end{aligned} \quad (3.20)$$

Consider the following input collision set, denoted f ,

$$\begin{aligned} f = & \{ \{1,0,0,1,0,0\}, \{0,1,0,0,1,0\}, \{0,0,1,0,0,1\}, \\ & \{1,0,1,0,1,0\}, \{0,1,0,1,0,1\} \}. \end{aligned} \quad (3.21)$$

Then the output collision set, denoted by f' , can be computed by using (3.19), the collision operator

$$\begin{aligned} f' = & f + \Omega \\ = & \{ \{0,1,0,0,1,0\}, \{0,0,1,0,0,1\}, \{1,0,0,1,0,0\}, \\ & \{0,1,0,1,0,1\}, \{1,0,1,0,1,0\} \} \end{aligned} \quad (3.22)$$

Using (2.159) the Jacobian may be calculated

$$J = [-d(1-d)^2, d^2(1-d)^2, d(1-2d)(1-d)^2, \\ -d(1-2d)(1-d)^2, -d^2(1-d)^2, d(1-d)^2] \quad (3.23)$$

Using (2.141), the eigenvalues of J may be directly calculated

$$\begin{aligned} \langle J | 1' \rangle &= 0 \\ \langle J | 2' \rangle &= 0 \\ \langle J | 3' \rangle &= 0 \\ \langle J | 4' \rangle &= -6d(1-d)^3 \\ \langle J | 5' \rangle &= -2d(1-d)^3 \\ \langle J | 6' \rangle &= 6d^2(1-d)^2. \end{aligned}$$

There are only three zero eigenvalues, so this chiral lattice gas model possesses only three invariants with eigenvectors corresponding to the total mass and the two components of momentum. Using

$$\lambda = \sum_{\alpha \in \{4', 5'\}} \frac{-\ell}{\kappa_\alpha} \langle e_i e_j | \alpha \rangle \langle \alpha | e_i e_j \rangle. \quad (3.24)$$

it becomes

$$\begin{aligned} \lambda &= \frac{\ell}{6d(1-d)^3} \langle e_x e_y | 4' \rangle \langle 4' | e_x e_y \rangle + \frac{\ell}{2d(1-d)^3} \langle e_x e_y | 5' \rangle \langle 5' | e_x e_y \rangle \\ &= \frac{3\ell}{8d(1-d)^3}. \end{aligned}$$

Finally, according to (2.207), chiral shear viscosity is

$$\eta^{\text{chiral}} = \rho \frac{\ell^2}{\tau} \left(\frac{3}{32d(1-d)^3} - \frac{1}{8} \right). \quad (3.25)$$

So by this example of a two dimensional lattice gas on a triangular lattice, the viscosity of a chiral lattice gas is slightly higher than that for a nonchiral or nondeterministic gas; compare (3.18) with (3.25).

It is interesting that although the chirality of its collisions is definite, no spurious invariants appear in the Boltzmann limit and, particularly, that this lattice gas is reversible. So this chiral lattice gas is even simpler than the FHP model and requires no random coin tosses. The methodology of successively switching between left and right-handed collision tables is therefore justified, at least in the Boltzmann limit. Switching between left and right-handed collision tables is done on the CAM-8 since there is no additional time or memory cost (per module) incurred in using multiple tables because of the double buffering of the lookup tables [64]. The observation that a fixed chirality lattice gas model can have the correct macroscopic limit is interesting. More importantly, in the case of the three-dimensional face-centered hypercubic (fchc) lattice [41], this observation may help to reduce the number of collisions. There are 24 nearest neighbors in fchc, so a full collision table has $2^{24} = 16\text{mega}$ entries. For parallel computers such as the CAM-8, implementing such a large collision table is inefficient. Compression of the fchc collision table has been explored[83]. Fixing the fchc collision table chirality may allow additional compression.

3.2.4 An Example of a Spurious Invariant

The FHP-model without 3-body collisions is a good example of a lattice gas with an unwanted spurious invariant. The collision operator in this case is

$$\Omega_a^{2\text{-body}} = \frac{1}{2}Q_a(1,4) + \frac{1}{2}Q_a(2,5) - Q_a(3,6).$$

Writing this out explicitly we have

$$\begin{aligned}\Omega_{a=1}^{2\text{-body}} &= \frac{1}{2}f_2f_5(1-f_1)(1-f_3)(1-f_4)(1-f_6) + \\ &\quad \frac{1}{2}f_3f_6(1-f_1)(1-f_2)(1-f_4)(1-f_5) - \\ &\quad f_1f_4(1-f_2)(1-f_3)(1-f_5)(1-f_6).\end{aligned}$$

Consider the following input collision set, denoted f ,

$$f = \{\{1, 0, 0, 1, 0, 0\}, \{0, 1, 0, 0, 1, 0\}, \{0, 0, 1, 0, 0, 1\}\}. \quad (3.26)$$

Then the output collision set, denoted by f' , can be computed by using (3.14), the collision operator

$$\begin{aligned}f' &= f + \Omega \\ &= \left\{ \left\{0, \frac{1}{2}, \frac{1}{2}, 0, \frac{1}{2}, \frac{1}{2}\right\}, \left\{\frac{1}{2}, 0, \frac{1}{2}, \frac{1}{2}, 0, \frac{1}{2}\right\}, \left\{\frac{1}{2}, \frac{1}{2}, 0, \frac{1}{2}, \frac{1}{2}, 0\right\} \right\}\end{aligned}$$

Using formula (2.159) gives the Jacobian's elements as

$$\begin{aligned}|J\rangle &= \left[-d(1-d)^3, \frac{1}{2}d(1-d)^3, \right. \\ &\quad \left. \frac{1}{2}d(1-d)^3, -d(1-d)^3, \right. \\ &\quad \left. \frac{1}{2}d(1-d)^3, \frac{1}{2}d(1-d)^3 \right] \quad (3.27)\end{aligned}$$

Now, using (2.141) we get the eigenvalues of J

$$\langle J | 1' \rangle = 0$$

$$\langle J | 2' \rangle = 0$$

$$\langle J | 3' \rangle = 0$$

$$\langle J | 4' \rangle = -3d(1-d)^3$$

$$\langle J | 5' \rangle = -3d(1-d)^3$$

$$\langle J | 6' \rangle = 0.$$

There are four zero eigenvalues, one too many, so as is known, a lattice gas on a triangular lattice without 3-body collisions is insufficient for recovering correct hydrodynamic behavior in the macroscopic limit.

3.3 Some Numerical Fluid Experiments

3.3.1 Measurement of Shear Viscosity

Method 1: Forced Parabolic Profile

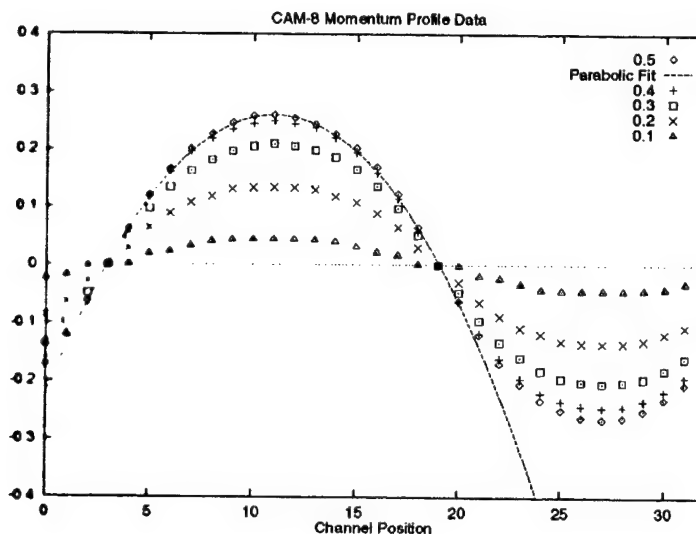


Figure 3.3: Momentum profiles for Poiseuille flow for filling fractions $d=0.1$ to $d=0.5$ for a FHP gas with particle-hole symmetric collisions. Parabolic fit shown for half-filling result.

To numerically measure the shear viscosity of a lattice gas I will consider a system with toroidal boundary conditions and square-wave forcing. This is a flow condition known as Poiseuille flow [33]. This method has been previously applied to lattice gases by Kadanoff et. al. [52]. We give a derivation of a theoretical expression for the shear viscosity in §2.5 and §2.5.2. The numerical measurements allow us to check the

consistency of our work. This numerical technique will be very valuable for measuring the shear viscosity of complicated fluids: for examples, a thermodynamic system described later in this volume or a multiphase system described later in Volume II [102]. An interesting question is whether this method will work well for a multiphase fluid near its critical point.

Let us consider flow in a channel of half-width W and length L . For Poiseuille flow under steady-state conditions with uniform forcing only along the length of the channel, the Navier-Stokes equation (2.196) reduces to a simple form

$$\eta \frac{d^2 v}{dz^2} = \mathcal{F} \quad (3.28)$$

where by denoting the total amount of forcing in each half of the channel as $p_{\mathcal{F}}$, then it follows

$$\mathcal{F} = \frac{p_{\mathcal{F}}}{\tau W L}. \quad (3.29)$$

The solution of (3.28) is a parabolic velocity profile

$$v(z) = \frac{p_{\mathcal{F}}}{\tau W L \eta} (Wz - z^2), \quad (3.30)$$

where $0 \leq z \leq W$ ranges over half the channel—the profile in the other half of the channel is a symmetric image. The maximum velocity occurs at $\frac{W}{2}$, so (3.30) reduces to

$$v_{max}|_{z=\frac{W}{2}} = \frac{p_{\mathcal{F}} W}{4\tau L \eta}. \quad (3.31)$$

Letting $g_{max} = \rho u_{max}$ denote the maximum momentum density in the Poiseuille profile, and since the kinematic viscosity $\nu = \frac{\eta}{\rho}$, the result is

$$\nu = \frac{p_{\mathcal{F}} W}{4\tau L g_{max}}. \quad (3.32)$$

When simulating the square wave forcing in the channel, one measures the maximum momentum occurring at the peak of the profile, p_{max} , by averaging along the entire length of the channel to improve the statistics. The momentum density, g_{max} , is then directly computable by

$$g_{max} = \frac{p_{max}}{A_{hex}}, \quad (3.33)$$

where the unit area of a lattice cell is $A_{hex} = \frac{\sqrt{3}}{2} \ell^2$. In terms of p_{max} the kinematic viscosity becomes

$$\nu = \frac{1}{4} \frac{p_{\mathcal{F}}}{p_{max}} \frac{\sqrt{3}W}{2L} \frac{\ell^2}{\tau}. \quad (3.34)$$

It is useful to express the kinematic viscosity in term of the number of lattice sites. Let L_i and L_j denote the number of lattice sites along the width and length of the system, respectively. Then $W = \frac{L_i}{2}$ and the length is reduced to $L = \frac{\sqrt{3}L_j}{2}$ because of a triangular lattice (see Figure 3.1). Then our final expression for the kinematic viscosity becomes

$$\nu = \frac{1}{8} \frac{p_{\mathcal{F}}}{p_{max}} \frac{L_i}{L_j} \frac{\ell^2}{\tau}. \quad (3.35)$$

The dimensions of (3.35) are explicitly written in terms of the spacetime lattice-constants: $\frac{\ell^2}{\tau}$.

Measurements were performed on the CAM-8 for a hexagonal lattice gas with particle-hole symmetric rules. Poiseuille momentum profiles for this system are obtained by forcing along the length of the channel (see Figure 3.3). The profile for the system at several densities from 10 percent to 50 percent filling are plotted. The profile is parabolic. The peak momentum value decreases with decreasing density and the mean free path increases. This in turn causes momentum diffusion to increase. The simulation data are plotted in Figure 3.4 over the theoretical curve of the shear viscosity (2.207) where λ is calculated with the method given in §2.4.2 applied to

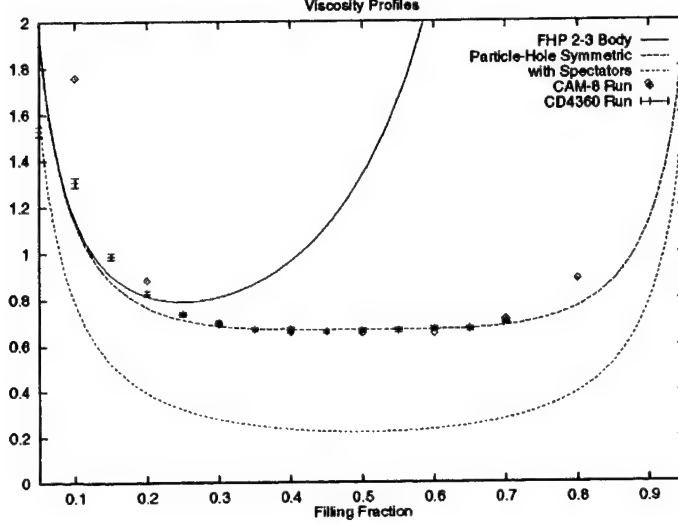


Figure 3.4: Viscosity profiles obtained by Poiseuille flow measurements. Theoretical curves plotted for FHP 2 and 3-body collisions, particle-hole symmetric collisions, and collisions with spectator particles. Simulation data from CAM-8 and CD4360 compared with particle-hole symmetric case.

an FHP lattice gas with particle-hole symmetric collisions. For low densities, a systematic error is observed in the comparison of the simulation data to the theoretical value. This is caused by the finite size of the lattice. Otherwise the agreement of simulation and theory is excellent as demonstrated in Figure 3.4.

It is worth noting that when performing this type of measurement on a parallel SIMD computer one cannot know in advance the exact number of forcing sites causing a change in the lattice gas momentum. This is because a bit plane must be used to store a mask for forcing. Any lattice site under a mask point may or may not be able to be forced. We may write the forcing operator as follows

$$\hat{\mathcal{F}}(\vec{x}) = \frac{\delta p_{\alpha\beta}}{\tau} \hat{a}_{\alpha}^{\dagger} \hat{a}_{\beta} \quad (3.36)$$

which acts on site \vec{x} and rotates a particle from momentum state β to α and where $\delta p_{\alpha\beta}/mc = \frac{1}{2}, \frac{\sqrt{3}}{2}, 1, \sqrt{3}$, depending on the value of α and β . The direction of the

forcing is $\hat{e}_\beta - \hat{e}_\alpha$. If there were not a particle present in state β or there already was a particle present in state α , $\hat{\mathcal{F}}(\vec{x})$ will have no effect on the system.

Method 2: Decay of Sinusoidal Profile

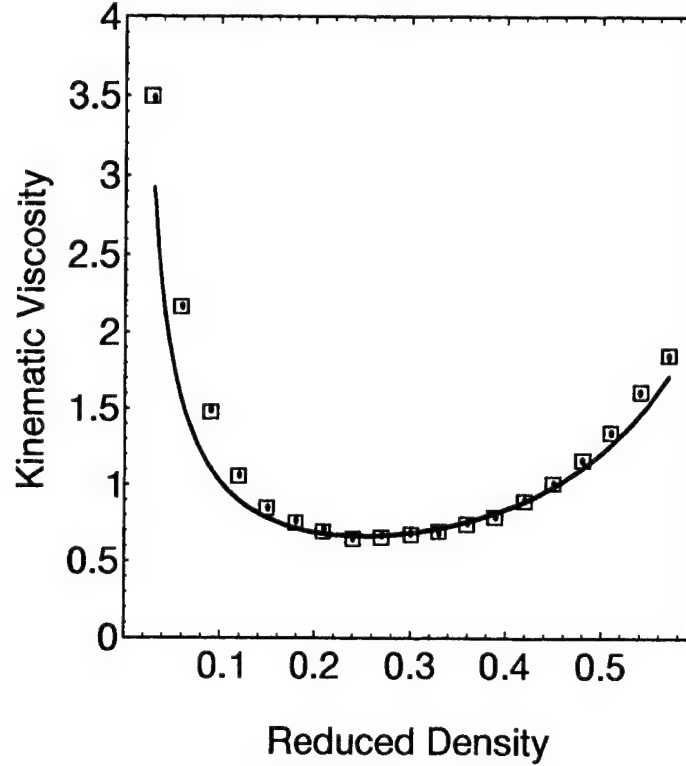


Figure 3.5: Kinematic viscosity versus density obtained by measuring the rate of exponential damping of a sinusoidal velocity perturbation. The theoretical mean-field prediction and numerical data are plotted for an FHP lattice gas with 2 and 3-body collisions on a two dimensional triangular lattice. Simulation runs were done on the CAM-8 on a 512×512 periodic space.

Given a sinusoidal perturbation of wavelength λ of a fluid one can straightforwardly measure the time for relaxation to an equilibrium state where the fluid is at rest. The relevant part of the Navier-Stokes equation is the time dependent term and

the momentum diffusion term

$$(\partial_t - \nu \partial_x^2) p_x = 0. \quad (3.37)$$

This has the solution

$$p_x = p_o \sin kx e^{-k^2 \nu t}. \quad (3.38)$$

Therefore, the decay rate, $k^2 \nu$, can be measured to determine ν since $k = \frac{2\pi}{\lambda}$ is known. This method is easier to implement on the CAM-8 than the square-wave forcing method, since no forcing bits or rules are required and it is easy to generate an initial random fluid pattern with a sinusoidal perturbation. Very good agreement is found between the mean-field theoretical prediction of the kinematic shear viscosity and the numerical data shown in Figure 3.5 taken on the CAM-8 for the FHP lattice gas.

In practice, one would like to include all allowable collisions since this reduces the shear viscosity. Therefore, one may also include 4-body collisions, as illustrated in Figure 3.7. A plot of the lattice gas shear viscosity is given in Figure 3.8 where the decrease in the shear viscosity is observed according to the mean-field prediction. The highest curve of Figure 3.4 is the theoretical value obtained using (2.207) for the FHP-model with 2 and 3-body collisions. The middle curve, which is slightly lower, is the value obtained with the addition of 4-body collisions. The fact that it is symmetric about one-half filling is due to particle-hole symmetry in the collision rules. The lowest viscosity curve is obtained by using all possible collisions, including 2-body collisions with a spectator particle present. In (3.3.1) I discuss the numerical measurements made for the simple hexagonal lattice gas and its comparison to the theoretical results.

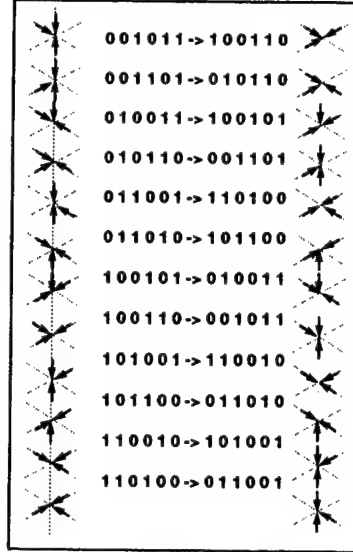


Figure 3.6: Enumeration of 2-body collisions with a spectator particle.

3.3.2 Superposition of Sound Pulses

To illustrate the macroscopic behavior of the triangular lattice gas it is sufficient to perform a simple experiment. Consider a system with toroidal boundary conditions that is initially randomly populated with particles at some particular filling fraction. The total initial momentum in the system is zero. Then extract all the particles in two

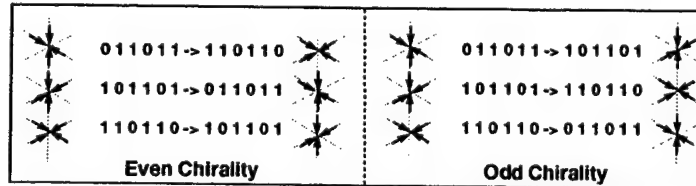


Figure 3.7: Enumeration of 4-body collisions, even and odd chirality, which are particle-hole symmetric with the 2-body collisions.

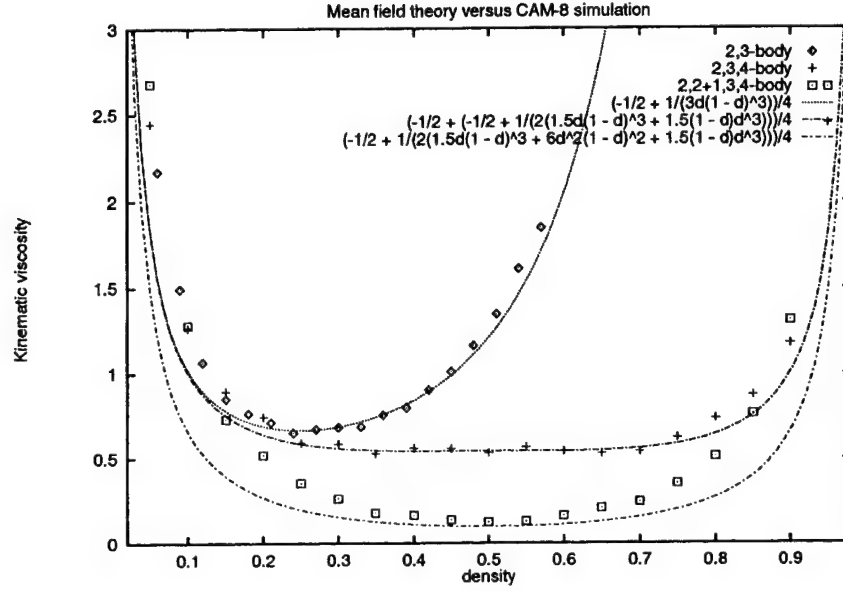


Figure 3.8: Viscosity profiles obtained by measuring the rate of exponential damping of a sinusoidal velocity perturbation. Theoretical curves and numerical data plotted for a hexagonal lattice gas with 2 and 3-body collisions, particle-hole symmetric collisions, and collisions with spectator particles. Simulation data are from the CAM-8.

adjacent small square regions near the middle of the system. That is, initially there are two small evacuated regions near the center of the system. Think of the initial conditions as a pond at rest into which are simultaneously tossed two square stones which, as they fall into the fluid and drop past the surface, remove two square regions of the fluid. Figure (3.9) depicts the resulting pressure waves that are produced. After 96 time steps the circular shape of a sound wave is clearly apparent. After 256 timesteps the two sound pulses produced interfere with one another and the superposition of sound modes is demonstrated. The simple example of the stones in a pond experiment was first done for the HPP-model on a square lattice [66].

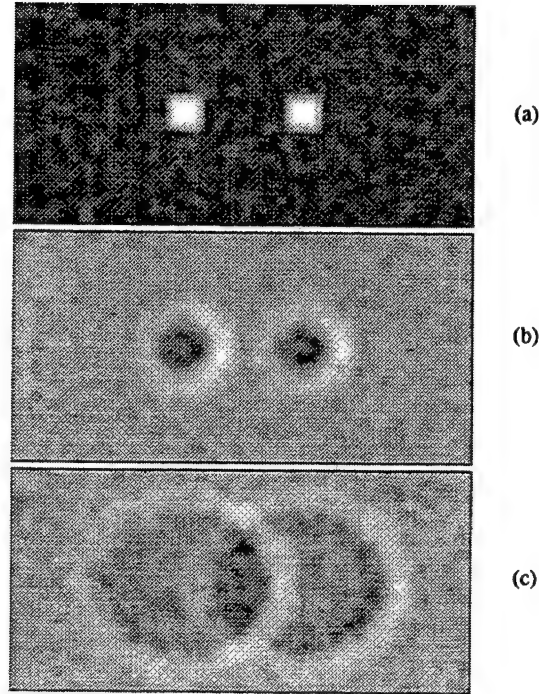


Figure 3.9: Illustration of sound mode and superposition in an FHP lattice gas. (a) Initial pattern with two square regions removed (i.e. two stones in a pond), (b) circular sound wave forms after 96 time steps, and (c) superposition observed after 256 timesteps. Sound speed is c/\sqrt{D} , where c is the speed of a single lattice gas particle and $D = 2$ in this case. Simulation carried out on a 1024×512 -lattice.

The simulation of the interference patterns of sound wave is straightforward to model with the lattice gas methodology, even if complex boundary conditions and density gradients are imposed.

3.3.3 Kelvin-Helmholtz Instability on the CAM-8

Another well known fluid instability is the Kelvin-Helmholtz shear instability. Figure 3.10 shows a simulation of a shear instability on a hexagonal lattice 4096×2048 in size with toroidal boundary conditions. The initial conditions for the simulation

are very uniform. A gas density is chosen, in this case approximately $\frac{1}{7}$ filling, and two horizontal regions are set with uniform, but opposing flow directions. That is, the majority of the fluid, the background region, is set with a uniform flow velocity of approximately $0.4 c_s$ (Mach 0.4) flowing to the right. A narrow stripe 256 sites wide is set in the center of the space flowing to the left at $-0.4 c_s$. No sinusoidal perturbation is given to the counter-flow narrow stripe region as in previous lattice gas simulations[80]. No external forcing is applied during the simulation run. The only perturbation is caused by minor fluctuations produced by the random number generator when producing a uniform fluid density. After approximately 10,000 time steps, the narrow horizontal center stripe forms a sinusoidal pattern. The sinusoid grows and eventually breaks into several counter-rotating vortices, and the two flow regions begin to substantially mix. Figure 3.10 shows the state of the fluid initially and then at 10,000 and 30,000 time steps. By $t = 30,000$, the formation of a wave is apparent, typical of the Kelvin-Helmholtz instability. Eventually, after 400,000 time steps, the fluid attains a uniform flow to the right after the system has equilibrated, exactly conserving the momentum in the initial configuration.

3.3.4 Von Karman Streets on the CAM-8

Figure 3.11 shows successive snapshots of a CAM-8 simulation of vortex shedding from a flat plate from the initial state to time step 20,000 on a hexagonal lattice 4096×2048 in size. The boundary conditions are effectively toroidal. A momentum map, overlaid on a vorticity map, is computed with a Galilean shift of 25 percent of the mean flow. Clockwise vorticity is shaded red and counter-clockwise vorticity is shaded blue. A flat plate obstacle is placed in a channel of fluid with a flow directed

towards the right of the figure. The fluid flow is forced to the right at each time step in a “forcing strip” at the right end of the channel. The effect of sound waves and other disturbances that propagate around the torus do not significantly alter the flow behavior.

The flow is started from a random distribution of particles at the appropriate density with a net velocity close to that of the steady state flow. Since this is not a true equilibrium starting condition, some transient behavior appears in the form of a sound pulse that propagates down the channel. This pulse is absorbed by the forcing strip. After 2000 time steps the system is equilibrated with no transient phenomena visible. This equilibration time is very short compared with the time necessary for vortex development. The toroidal boundary conditions are sufficient to produce vortex shedding phenomena, however the simulation’s elapsed time cannot exceed 20,000 time steps. To run the simulation to long times, a cylindrical boundary condition appears to work extremely well [106].

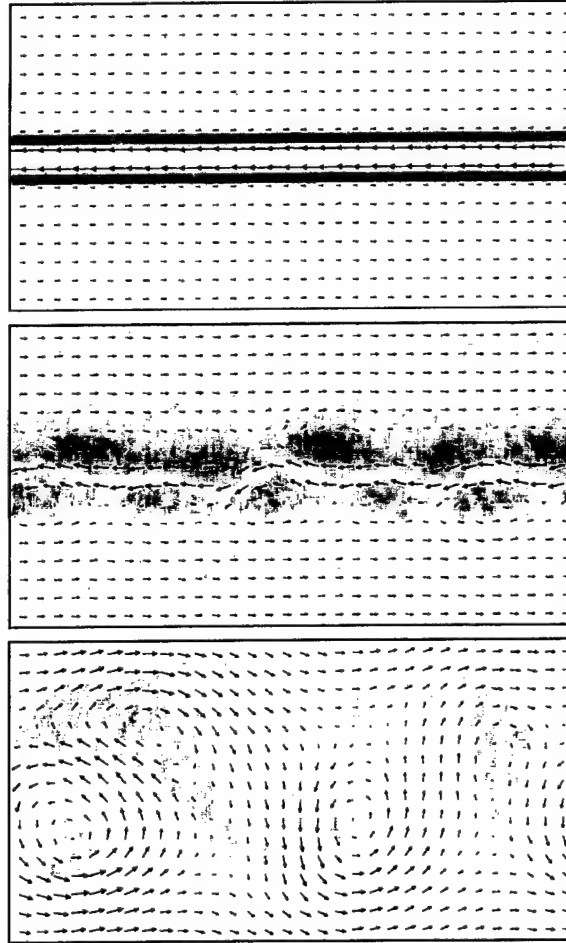


Figure 3.10: Two-speed CAM-8 experiment: Vorticity and momentum map of two-dimensional shear instability. Lattice size of 4096×2048 with toroidal boundary conditions. Spacetime averaging over 128×128 blocks for 50 time steps. FHP collisions with spectators and a rest particle. Data presented at 0, 10000, and 30000 time steps. $Re \sim 1000$.

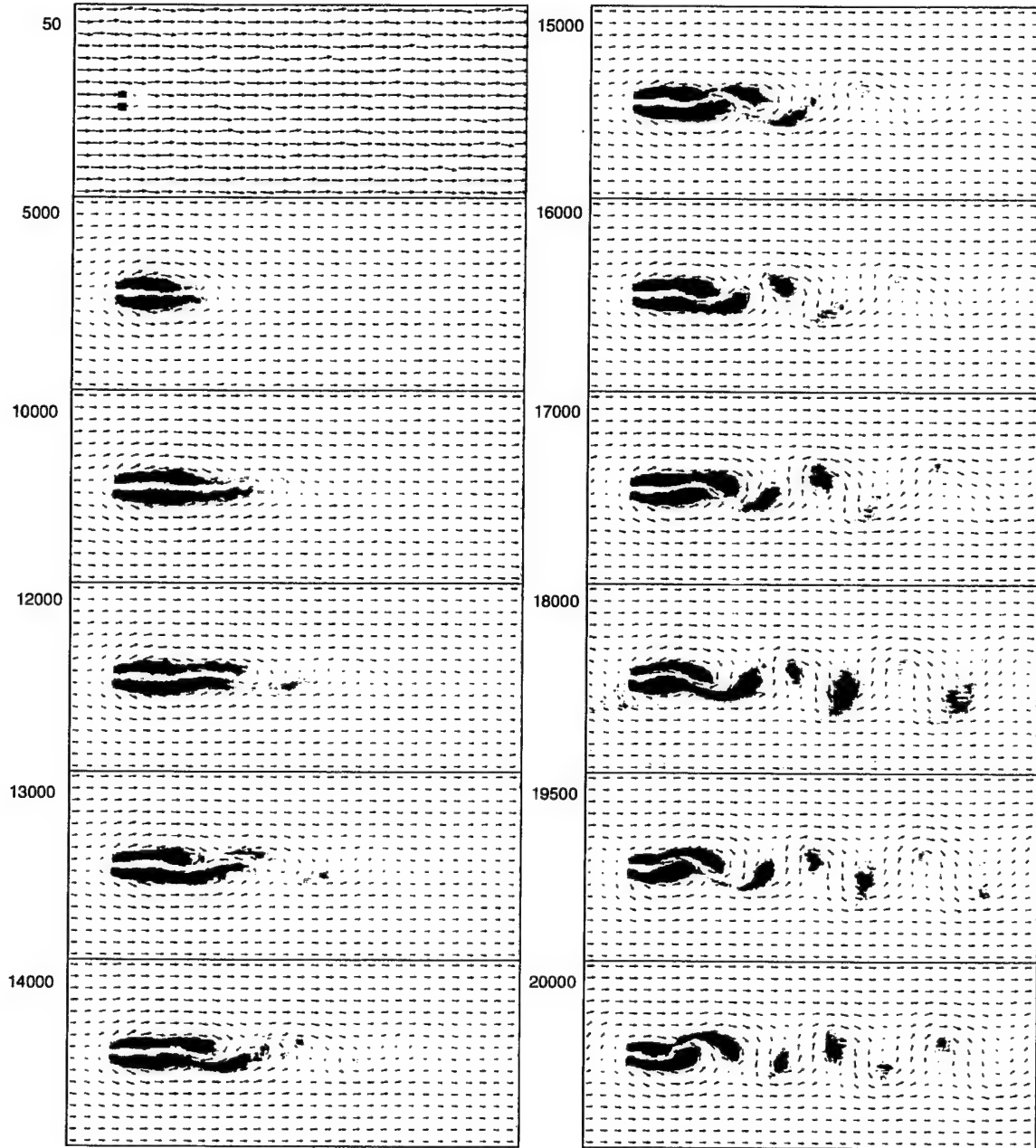


Figure 3.11: Two-speed CAM-8 simulation: momentum and vorticity plot of Von Karman Streets for a lattice size of 4096×2048 . Time Average: 50. Spatial Average: 64×64 (momentum), 16×16 (vorticity). Mass Density Fraction= $1/7$. Data presented at indicated time steps. At rest at $t = 0$, $v = 0$, and accelerating to $v = 0.3c$ at $t = 20,000$. Diameter of cylindrical obstacle: $d = 256$. Critical Reynolds number for vortex shedding, $Re = 42$ occurs at approximately $t = 10,000$. Maximum Reynolds number achieved in simulation is: $Re \sim 250$. Red indicates clockwise vorticity and blue counter clockwise vorticity.

Chapter 4

Multispeed Lattice-Gas

A simple generalization of the FHP single-speed collision rules leads to emergent behavior similar to that which occurs in hydrothermal fluids in nature. The simple generalization is to allow particles to have several speeds that are integral multiples of the fundamental unit speed, $v = nc = n\ell/\tau$. Such a lattice gas system is referred to as a *multispeed lattice gas*. Multispeed lattice gases for the recovery of the classical thermohydrodynamic fluid equations have been investigated by several researchers, Chen *et al.* [27], Teixeira [86], and Ernst and Das [36].

Following Chen [27], I have implemented a two-speed model with a rest particle. This models a thermohydrodynamic system. This kind of lattice gas was first introduced in 1987 by Burges and Zaleski [20] in the context of multispecies particles. Their goal was the study of lattice gases that model buoyant mixtures. In essence, their model was two coupled single-speed hexagonal gases with a rest particle. They succeeded in achieving a convective instability in their lattice gas driven by a concentration gradient in the species populations. However, they did not succeed in developing an equation of motion for this system. It was not until 1991 that the equation of motion for this system was derived. This was done by the lattice gas

Table 4.1: Multispeed Lattice-Gas Glossary of Variables

Variables	Names
LATTICE CONSTANTS	
ℓ	length unit
τ	time unit
m	mass unit
c	velocity unit ($\frac{\ell}{\tau}$)
D	spatial dimension
GAS CONSTANTS	
c_s	sound speed
η	shear viscosity
ν	kinematic viscosity ($\frac{\eta}{\rho}$)
MULTISPEED MODEL	
σ	particle speed index
B_σ	number of momentum states/speed
c_σ	particle speeds
\vec{e}_a^σ	lattice vectors/speed
n_σ	number density/speed
d_σ	reduced density/speed
f_a^σ	distribution function/speed
q_i	heat flux
P_{ij}	pressure tensor
E	total energy

group at Los Alamos [27]. The important step made by Shiyi Chen and coworkers was to interpret the coupled system as a single species gas but having two speeds.

Grosfils, Boon and Lallemand have introduced a three-speed thermohydrodynamic gas with speeds 1, $\sqrt{3}$, 2 and a rest particle [44]. With this 19-bit model, efficient collisional mixing can occur with all particles having the same unit mass. Since the particles may now carry different units of energy, in addition to the equation of continuity and Euler's equation, in this system we have an energy transport equation.

4.1 Summary of Physical Assumptions

- Discrete Spacetime (equivalently: cellular phase space)
- Isotropic spatial lattice

$$\sum_a e_{ai}^\sigma = 0 \quad (4.1)$$

$$\sum_a e_{ai}^\sigma e_{aj}^\sigma = \frac{B_\sigma}{D} \frac{c_a^2}{c^2} \delta_{ij} \quad (4.2)$$

$$\sum_a e_{ai}^\sigma e_{aj}^\sigma e_{ak}^\sigma = 0 \quad (4.3)$$

$$\sum_a e_{ai}^\sigma e_{aj}^\sigma e_{ak}^\sigma e_{al}^\sigma = \frac{B_\sigma}{D(D+2)} \frac{c_a^4}{c^4} (\delta_{ij}\delta_{kl} + \delta_{ik}\delta_{jl} + \delta_{il}\delta_{jk}) \quad (4.4)$$

- Mass, momentum, and energy conservation

$$\rho = m \sum_{a,\sigma} f_a^\sigma \quad (4.5)$$

$$\rho v_i = mc \sum_{a,\sigma} e_{ai}^\sigma f_a^\sigma \quad (4.6)$$

$$nE = \frac{1}{2} mc^2 \sum_{a,\sigma} (e_a^\sigma)^2 f_a^\sigma \quad (4.7)$$

- Particles are Fermi-Dirac distributed

$$f_a^\sigma = \frac{1}{1 + \exp(\alpha^\rho + \alpha^v e_{ai}^\sigma v_i + \beta E_\sigma)} \quad (4.8)$$

- Equilibrium Dynamical Equation

$$\partial_t f_a^\sigma + c e_{ai}^\sigma \partial_i f_a^\sigma = 0. \quad (4.9)$$

Note that all these physical assumptions are not independent; however it is convenient to use these as our starting point.

4.2 Microdynamics: An Exactly Computable Thermodynamical System

The evolution of the multispeed lattice gas is written in terms of n_a^σ as a two-part process: a collision part and a streaming part. The collision part permutes the particles locally at each site.

$$n_a^{\sigma'}(\vec{x}, t) = n_a^\sigma(\vec{x}, t) + \Omega_a^\sigma[\vec{n}(\vec{x}, t)], \quad (4.10)$$

where Ω_a^σ represents the collision operator and in general depends on all the particle momenta and energy states, denoted by \vec{n} , at the site. In the streaming part of the evolution the particle at position \vec{x} “hops” to its nearest neighbor (or next nearest neighbor and so forth) at $\vec{x} + \ell e_a^\sigma$, and then time is incremented by τ

$$n_a(\vec{x} + \ell e_a^\sigma, t + \tau) = n_a^{\sigma'}(\vec{x}, t). \quad (4.11)$$

Note that the set $\{e_a^\sigma\}$ are not in general unit vectors. And for each speed σ , the set of vectors $\{e_a^\sigma\}$ for $a = 1, \dots, B_\sigma$ specifies an isotropic lattice. Therefore, the usual

lattice tensor identities hold for each lattice gas speed

$$E_{\sigma}^{(2n+1)} = 0 \quad (4.12)$$

$$E_{\sigma}^{(2n)} = \frac{B_{\sigma}}{D(D+2) \cdots (D+2n-2)} \frac{c_{\sigma}^{2n}}{c^{2n}} \Delta^{2n}. \quad (4.13)$$

where $c_{\sigma} = \sigma c$ is the speed of a particle in the σ^{th} -energy level. Equations (4.12) and (4.13) impose a more stringent restriction on the choice of lattice geometry than is absolutely necessary. However, this restriction simplifies the calculations.

Combining the collision equation (4.10) and the streaming equation (4.11) gives the multispeed lattice gas microdynamical transport equation of motion

$$n_a^{\sigma}(\vec{x} + \ell \vec{e}_a^{\sigma}, t + \tau) = n_a^{\sigma}(\vec{x}, t) + \Omega_a^{\sigma}[\vec{n}(\vec{x}, t)]. \quad (4.14)$$

For each speed $\sigma = 0, 1, \dots, M$, (7.1) is identical in form to the classical lattice gas described by (2.23). The essential difference in the present case is that the set of M lattice gas transport equations (7.1) are coupled by *energy mixing collisions* implicitly contained in Ω_a^{σ} . Without such energy mixing collisions, the lattice gas system described by (7.1) could not give rise to an equipartition theorem for the multiple energy level occupations.

4.3 Statistical Mechanics of a Multispeed Lattice Gas System

The multispeed lattice gas Hamiltonian is

$$H = \sum_{x=1}^V \sum_{a=1}^B \sum_{\sigma=1}^M E_a^{\sigma} n_a^{\sigma}(x), \quad (4.15)$$

where there are a total of V spatial sites in the lattice, B momenta directions, and M momenta magnitudes. Note that in this form of the Hamiltonian, the occupation

variable is Boolean: $n_a^\sigma \in \{0, 1\}$. The “kinetic” energy of a particle moving in direction a in the σ^{th} -energy level is

$$E_a^\sigma = \frac{1}{2}mc_\sigma^2 = \frac{1}{2}mc(\vec{e}_a^\sigma)^2. \quad (4.16)$$

The total mass density is

$$\rho_{\text{total}} = \sum_{x a \sigma} m n_a^\sigma(x) \quad (4.17)$$

and the total momentum density is

$$\rho_{\text{total}} V_i = \sum_{x a \sigma} m c e_{ai}^\sigma n_a^\sigma(x). \quad (4.18)$$

The *grand partition function* for a multispeed lattice gas system with N particles is defined as

$$\Xi = \sum_{\{n\}} \exp [-\beta H + \mu \rho_{\text{total}} + \rho_{\text{total}} V_i \alpha_i]. \quad (4.19)$$

The sum is over all configurations of particle occupations in the grand canonical ensemble. This configurational set is denoted by $\{n\}$, and μ is the *chemical potential*. Inserting (4.15), (4.17), and (4.18) into (4.19) gives

$$\Xi = \sum_{\{n\}} \exp \left[-\beta \sum_{x a \sigma} E_a^\sigma n_a^\sigma(x) + \mu \sum_{x a \sigma} m n_a^\sigma(x) + \alpha_i \sum_{x a \sigma} m c e_{ai}^\sigma n_a^\sigma(x) \right] \quad (4.20)$$

$$= \sum_{\{n\}} \prod_{x a \sigma} \exp [-\beta E_a^\sigma + \mu m + \alpha_i m c e_{ai}^\sigma]^{n_a^\sigma(x)} \quad (4.21)$$

Define the fugacity as

$$z_a^\sigma = \exp [-\beta E_a^\sigma + \mu m + \alpha_i m c e_{ai}^\sigma]. \quad (4.22)$$

Note that z_a^σ is not dependent on \vec{x} . The grand partition function simplifies to

$$\Xi = \sum_{\{n\}} \prod_{x a \sigma} (z_a^\sigma)^{n_a^\sigma(x)}. \quad (4.23)$$

Now it is possible to interchange the sum over configurations $\{n\}$ with the product over the coordinates (x, a, σ) ; that is, $\sum_{\{n\}} \prod_{x a \sigma} \rightarrow \prod_{x a \sigma} \sum_n$. What are the limits of the sum over n after this interchange? The answer is that the sum must now count from $n = 0, \dots, 2^{N_{\max}} - 1$, where N_{\max} is the maximum number of particles that can occupy a *channel*. In the present construction, the channel is defined as (x, a, σ) . There can be at most a single particle per channel according to the Hamiltonian (4.15), so $N_{\max} = 1$. Furthermore, upon interchanging the sum with the product, the exponent of the fugacity becomes just a number independent of x , a , and σ . That is, we are summing over all possible powers of the fugacity. Therefore, (4.23) can be rewritten as

$$\Xi = \prod_{x a \sigma} \sum_{n=0}^{2^1-1} (z_a^\sigma)^n \quad (4.24)$$

$$= \prod_{x a \sigma} (1 + z_a^\sigma) \quad (4.25)$$

$$= \prod_{a \sigma} (1 + z_a^\sigma)^V. \quad (4.26)$$

The last line follows from the fact that z_a^σ is independent of \vec{x} . The *grand potential*, denoted Ω , is defined as the logarithm of the grand partition function, so that

$$\Omega = \log \Xi \quad (4.27)$$

$$= V \sum_{a \sigma} \log (1 + z_a^\sigma). \quad (4.28)$$

The particle number density per site, denoted f , is defined as

$$f(z) \equiv \frac{z}{V} \frac{\partial}{\partial z} \log \Xi(z), \quad (4.29)$$

so for the multispeed lattice gas system, the number density is

$$f = \sum_{a \sigma} \frac{z_a^\sigma}{1 + z_a^\sigma}. \quad (4.30)$$

Since $f = \sum_{a\sigma} f_a^\sigma$, the particle distribution per direction a and per energy level σ is the Fermi-Dirac function

$$f_a^\sigma = \frac{1}{(z_a^\sigma)^{-1} + 1}. \quad (4.31)$$

Therefore, each bit of the multispeed lattice gas obeys the Pauli exclusion principle as expected.

4.4 Obtaining the Macroscopic Equations of Motion from the Fermi-Dirac Distribution Function

In this section I generalize the calculation done in §D.1 where the single-speed Fermi-Dirac distribution function is expanded in powers of the bulk flow velocity. The distribution must be written as a function of the sum of scalar collision invariants that now includes an energy term, $\alpha^\rho + \alpha^v e_{ai}^\sigma v_i + \beta E_\sigma$, implying the following form

$$f_a^\sigma = \frac{1}{1 + \exp(\alpha^\rho + \alpha^v e_{ai}^\sigma v_i + \beta E_\sigma)}. \quad (4.32)$$

Expand the α^ρ , α^v , and β as follows

$$\alpha^\rho = \alpha_0^\rho + \frac{1}{2} \alpha_2^\rho v^2 + \mathcal{O}(v^4) \quad (4.33)$$

$$\alpha^v = \alpha_1^v + \frac{1}{2} \alpha_3^v v^2 + \mathcal{O}(v^4) \quad (4.34)$$

$$\beta = \beta_0 + \frac{1}{2} \beta_2 v^2 + \mathcal{O}(v^4). \quad (4.35)$$

Using the identities (2.19) and (2.20), an expansion to fourth order of (4.32) about zero velocity is the following

$$\begin{aligned}
f_a^\sigma &= d_\sigma \\
&-d_\sigma(1-d_\sigma)\alpha_1^v e_{ai}^\sigma \frac{v_i}{c} \\
&-\frac{1}{2}d_\sigma(1-d_\sigma)(\alpha_2^p + \beta_2 \frac{E_\sigma}{K_B T}) \frac{v^2}{c^2} \\
&+\frac{1}{2}d_\sigma(1-d_\sigma)(1-2d_\sigma)(\alpha_1^v)^2 e_{ai}^\sigma e_{aj}^\sigma \frac{v_i v_j}{c^2} \\
&-\frac{1}{2}d_\sigma(1-d_\sigma)\alpha_3^v e_{ai}^\sigma \frac{v_i v^2}{c^3} \\
&+\frac{1}{2}d_\sigma(1-d_\sigma)(1-2d_\sigma)\alpha_1^v (\alpha_2^p + \beta_2 \frac{E_\sigma}{K_B T}) e_{ai}^\sigma \frac{v_i v^2}{c^3} \\
&-\frac{1}{6}d_\sigma(1-d_\sigma)(1-6d_\sigma+6d_\sigma^2)(\alpha_1^v)^3 e_{ai}^\sigma e_{aj}^\sigma e_{ak}^\sigma \frac{v_i v_j v_k}{c^3} \\
&+O(v^4)
\end{aligned} \tag{4.36}$$

where $d_\sigma = f_a^\sigma|_{v=0}$ and $E_\sigma = \frac{1}{2} \sum_a (e_a^\sigma)^2 d_\sigma$. The macroscopic dynamics depend on the following dynamical variables.

Particle number density:

$$m \sum_{a,\sigma} f_a^\sigma = \rho, \tag{4.37}$$

Momentum density:

$$mc \sum_{a,\sigma} e_{ai}^\sigma f_a^\sigma = \rho v_i, \tag{4.38}$$

Momentum density flux tensor:

$$mc^2 \sum_{a,\sigma} e_{ai}^\sigma e_{aj}^\sigma f_a^\sigma = \Pi_{ij}. \tag{4.39}$$

Total energy density, half the trace of the momentum flux tensor:

$$nE = \frac{1}{2} \hat{\Pi}_{ii}. \tag{4.40}$$

Pressure tensor, \hat{P} :

$$\hat{P}_{ij} = m \sum_{a,\sigma} f_a^\sigma (ce_{ai}^\sigma - v_i) (ce_{aj}^\sigma - v_j). \quad (4.41)$$

Heat flux, \mathbf{q} :

$$q_i = m \sum_{a,\sigma} f_a^\sigma (ce_{aj}^\sigma - v_j)^2 (ce_{ai}^\sigma - v_i). \quad (4.42)$$

In equilibrium in the mesoscopic limit, the dynamical transport equation is

$$\partial_t f_a^\sigma + ce_{ai}^\sigma \partial_i f_a^\sigma = 0. \quad (4.43)$$

Equation (4.43) implies three conservation equations. To obtain these equations, the identities for isotropic lattice vectors (2.20) and (2.19) are necessary. Using (4.37) and (4.38) in (4.43) gives continuity (mass conservation):

$$\partial_t \rho + \partial_i (\rho v_i) = 0. \quad (4.44)$$

Using (4.38) and (4.39) in (4.43) gives the Navier-Stokes equation (momentum conservation):

$$\partial_t (\rho v_i) + \partial_j (\rho g v_i v_j) = -\partial_i p + \eta \partial^2 v_i. \quad (4.45)$$

where

$$p = (\gamma - 1)(nE - \frac{1}{2}\rho g v^2) \quad (4.46)$$

and $\gamma = \frac{C_p}{C_v}$ or $\gamma - 1 = \frac{2}{D}$. To derive the heat equation, take the second moment of (4.43)

$$\partial_t (nE) + c \partial_j \left[\sum_{a\sigma} m c_\sigma^2 e_{aj}^\sigma f_a^\sigma \right] = 0. \quad (4.47)$$

The term in square brackets can be determined by expanding the heat flux (4.42)

$$q_j = c \sum_{a\sigma} m c_\sigma^2 e_{aj}^\sigma f_a^\sigma - 2v_i \Pi_{ij} - 2\rho v_i^2 v_j - v_j nE. \quad (4.48)$$

Now the pressure tensor (4.41) reduces to

$$P_{ij} = \Pi_{ij} - \rho v_i v_j \quad (4.49)$$

so we have

$$c \sum_{a\sigma} m c_\sigma^2 e_{aj}^\sigma f_a^\sigma = q_j + 2v_i P_{ij} + v_j n E. \quad (4.50)$$

Substituting this into (4.47) gives the heat equation (energy conservation):

$$\partial_i(nE) + \partial_i(nE v_i) + \frac{1}{2} \partial_i q_i + \partial_j(v_i P_{ij}) = 0. \quad (4.51)$$

Although the lattice gas may in principle comprise an indefinite number of speeds, from (4.46) we see that the pressure depends upon the square of the bulk velocity; that is, it is the total internal energy of the lattice gas minus the bulk kinetic energy. In a single speed lattice gas, this kind of velocity dependence is anomalous and is a well known deficiency of the lattice gas (see the discussion in subsection §2.3.1). However, for a multispeed lattice gas the existence of this term takes on a physical interpretation. For a classical ideal gas, the pressure is proportional to both the sound speed squared and the temperature

$$p = \rho c_s^2 = n k_B T. \quad (4.52)$$

Since $\rho = mn$, equating (4.46) with the ideal gas law (4.52) gives the total internal energy in terms of the bulk kinetic energy $\frac{1}{2}mv^2$ and the local particle thermal energy $k_B T$

$$E = \frac{g}{2} m v^2 + \frac{k_B T}{\gamma - 1}. \quad (4.53)$$

The Navier-Stokes equation (4.45), the pressure (4.46), and the total energy (4.53)

all explicitly have a factor g in them.¹ If $g = 1$, then a multispeed lattice gas would exactly solve the ideal fluid equations where the physical interpretation of the total internal energy would then be that it partitions into a bulk motion term, or kinetic energy, and a fluctuating motion term, or random heat energy associated with a certain gas temperature. Therefore, the multispeed lattice gas calculation, in the Boltzmann limit, would exactly agree with classical kinetic gas theory (see the expression for the partial pressure of an electron gas given by Li and Wu [59]). One would expect g to approach one only as the number of speeds in the lattice gas model becomes large.

4.5 Determination of Expansion Coefficients

For convenience we will make the following definitions

$$a_0 \equiv \sum_{\sigma} B_{\sigma} \frac{c_{\sigma}^2}{c^2} d_{\sigma} \quad (4.55)$$

$$a_1 \equiv \sum_{\sigma} B_{\sigma} d_{\sigma} (1 - d_{\sigma}) \quad (4.56)$$

$$a_2 \equiv \sum_{\sigma} B_{\sigma} d_{\sigma} (1 - d_{\sigma}) \frac{E_{\sigma}}{k_B T} \quad (4.57)$$

$$a_3 \equiv \sum_{\sigma} B_{\sigma} \frac{c_{\sigma}^2}{c^2} d_{\sigma} (1 - d_{\sigma}) (1 - 2d_{\sigma}) \quad (4.58)$$

$$b_1 \equiv \sum_{\sigma} B_{\sigma} \frac{c_{\sigma}^2}{c^2} d_{\sigma} (1 - d_{\sigma}) \quad (4.59)$$

$$b_2 \equiv \sum_{\sigma} B_{\sigma} \frac{c_{\sigma}^2}{c^2} d_{\sigma} (1 - d_{\sigma}) \frac{E_{\sigma}}{k_B T} \quad (4.60)$$

¹In the Boltzmann limit, the factor g depends on the particle speeds, c_{σ} , and on the density distribution per speed, d_{σ} , by the following complicated expression

$$g = \frac{D}{D+2} \frac{\sum_{\sigma} B_{\sigma} d_{\sigma} \sum_{\sigma} B_{\sigma} (\frac{c_{\sigma}}{c})^4 d_{\sigma} (1 - d_{\sigma}) (1 - 2d_{\sigma})}{[\sum_{\sigma} B_{\sigma} (\frac{c_{\sigma}}{c})^2 d_{\sigma} (1 - d_{\sigma})]^2}. \quad (4.54)$$

This expression is derived in the following section, see (4.80).

$$b_3 \equiv \sum_{\sigma} B_{\sigma} \frac{c_{\sigma}^4}{c^4} d_{\sigma} (1 - d_{\sigma}) (1 - 2d_{\sigma}) \quad (4.61)$$

$$a_4 \equiv \sum_{\sigma} B_{\sigma} \frac{c_{\sigma}^2}{c^2} d_{\sigma} (1 - d_{\sigma}) (1 - 2d_{\sigma}) \frac{E_{\sigma}}{k_B T} \quad (4.62)$$

$$a_5 \equiv \sum_{\sigma} B_{\sigma} \frac{c_{\sigma}^4}{c^4} d_{\sigma} (1 - d_{\sigma}) (1 - 6d_{\sigma} + 6d_{\sigma}^2) \quad (4.63)$$

Defining

$$B \equiv \sum_{\sigma} B_{\sigma} \quad (4.64)$$

the reduced density has the usual form $d = \frac{\sum_{\sigma} B_{\sigma} d_{\sigma}}{B} = \frac{n}{B}$ and the zeroth moment of (4.36) is

$$\frac{1}{B} \sum_{a\sigma} f_a^{\sigma} = \sum_{\sigma} B_{\sigma} \left[d_{\sigma} - \frac{1}{2} d_{\sigma} (1 - d_{\sigma}) (\alpha_2^{\rho} + \beta_2 \frac{\varepsilon_{\sigma}}{k_B T}) \frac{v^2}{c^2} + \frac{c_{\sigma}^2}{2Dc^2} d_{\sigma} (1 - d_{\sigma}) (1 - 2d_{\sigma}) (\alpha_1^v)^2 \frac{v^2}{c^2} \right] = d. \quad (4.65)$$

Using the definitions, (4.65) reduces to

$$a_1 \alpha_2^{\rho} + a_2 \beta_2 - \frac{a_3}{D} (\alpha_1^v)^2 = 0. \quad (4.66)$$

The first moment of (4.36) is

$$\begin{aligned} \frac{1}{B} \sum_{a\sigma} e_{ai}^{\sigma} f_a^{\sigma} &= \sum_{\sigma} B_{\sigma} \left[-\frac{c_{\sigma}^2}{Dc^2} d_{\sigma} (1 - d_{\sigma}) \alpha_1^v \frac{v_i}{c} \right. \\ &\quad - \frac{c_{\sigma}^2}{2Dc^2} d_{\sigma} (1 - d_{\sigma}) \alpha_3^v \frac{v_i v^2}{c^3} \\ &\quad + \frac{c_{\sigma}^2}{2Dc^2} d_{\sigma} (1 - d_{\sigma}) (1 - 2d_{\sigma}) \alpha_1^v (\alpha_2^{\rho} + \beta_2 \frac{\varepsilon_{\sigma}}{k_B T}) \frac{v_i v^2}{c^3} \\ &\quad \left. - \frac{c_{\sigma}^4}{2D(D+2)c^4} d_{\sigma} (1 - d_{\sigma}) (1 - 6d_{\sigma} + 6d_{\sigma}^2) (\alpha_1^v)^3 \frac{v_i v^2}{c^3} \right] \\ &= d \frac{v_i}{c}. \end{aligned} \quad (4.67)$$

Using the definitions, the first-order terms in the velocity of (4.67) reduce to

$$\alpha_1^v = -\frac{Dn}{b_1} \quad (4.68)$$

and the third-order terms in the velocity reduce to

$$b_1 \alpha_3^v - \frac{a_3}{D} \alpha_1^v \alpha_2^\rho - \frac{a_4}{D} \alpha_1^v \beta_2 + \frac{a_5}{D(D+2)} (\alpha_1^v)^3 = 0. \quad (4.69)$$

The second moment of (4.36) is

$$\begin{aligned} \frac{1}{B} \sum_{a\sigma} (e_{ai}^\sigma)^2 f_a^\sigma &= \sum_{\sigma} B_{\sigma} \left[\frac{c_{\sigma}^2}{c^2} d_{\sigma} \right. \\ &\quad - \frac{c_{\sigma}^2}{2c^2} d_{\sigma} (1 - d_{\sigma}) (\alpha_2^\rho + \beta_2 \frac{\varepsilon_{\sigma}}{k_B T}) \frac{v^2}{c^2} \\ &\quad \left. + \frac{c_{\sigma}^4}{2Dc^4} d_{\sigma} (1 - d_{\sigma}) (1 - 2d_{\sigma}) (\alpha_1^v)^2 \frac{v^2}{c^2} \right] \\ &= \frac{dE}{2mc^2}. \end{aligned} \quad (4.70)$$

Using the definitions, the terms independent of the velocity of (4.70) reduce to

$$nE = \frac{1}{2} \sum_{\sigma} mc_{\sigma}^2 B_{\sigma} d_{\sigma} \quad (4.71)$$

and the second-order terms in the velocity reduce to

$$b_1 \alpha_2^\rho + b_2 \beta_2 - \frac{b_3}{D} (\alpha_1^v)^2 = 0. \quad (4.72)$$

The forms of (4.66) and (4.72) are the same, so using (4.68) we may write them in matrix form as

$$\begin{pmatrix} a_1 & a_2 \\ b_1 & b_2 \end{pmatrix} \begin{pmatrix} \alpha_2^\rho \\ \beta_2 \end{pmatrix} = \frac{Dn^2}{b_1^2} \begin{pmatrix} a_3 \\ b_3 \end{pmatrix} \quad (4.73)$$

The solution for α_2^ρ and β_2 is then simply

$$\alpha_2^\rho = \frac{Dn^2}{b_1^2} \frac{a_3 b_2 - a_2 b_3}{a_1 b_2 - a_2 b_1} \quad (4.74)$$

$$\beta_2 = \frac{Dn^2}{b_1^2} \frac{a_1 b_3 - a_3 b_1}{a_1 b_2 - a_2 b_1} \quad (4.75)$$

Using $\alpha_1^v = -\frac{Dn}{b_1}$, (4.72) becomes

$$b_1 \alpha_2^\rho + b_2 \beta_2 = Dd^2 \frac{b_3}{b_1^2} \quad (4.76)$$

which will be of use when we derive an expression for the momentum flux density tensor.

4.6 Momentum Flux Density Tensor

The definition of the momentum flux density tensor (4.39) is the following

$$\Pi_{ij} = mc^2 \sum_{a\sigma} e_{ai}^\sigma e_{aj}^\sigma f_a^\sigma.$$

Substituting into (4.39) the expansion (4.36) for f_a^σ gives

$$\begin{aligned} \Pi_{ij} = & mc^2 \sum_{a\sigma} e_{ai}^\sigma e_{aj}^\sigma \left[d_\sigma - \frac{1}{2} d_\sigma (1 - d_\sigma) (\alpha_2^p + \beta_2 \frac{\varepsilon_\sigma}{k_B T}) \frac{v^2}{c^2} \right] \\ & + mc^2 \sum_{a\sigma} e_{ai}^\sigma e_{aj}^\sigma e_{ak}^\sigma e_{al}^\sigma \frac{1}{2} d_\sigma (1 - d_\sigma) (1 - 2d_\sigma) (\alpha_1^v)^2 \frac{v_k v_l}{c^2}. \end{aligned} \quad (4.77)$$

Using the identities for the products of lattice vectors, we have

$$\begin{aligned} \Pi_{ij} = & \frac{1}{D} \sum_{\sigma} mc_\sigma^2 B_\sigma d_\sigma \delta_{ij} - \frac{m}{2D} (b_1 \alpha_2^p + b_2 \beta_2) v^2 \delta_{ij} \\ & + \frac{m}{2} \frac{D}{D+2} \frac{d^2 b_3}{b_1^2} v^2 \delta_{ij} + m \frac{D}{D+2} \frac{d^2 b_3}{b_1^2} v_i v_j. \end{aligned} \quad (4.78)$$

Using (4.71) and the identity (4.76), this reduces to

$$\Pi_{ij} = \rho \frac{2E}{Dm} \delta_{ij} - \rho g v^2 \frac{\delta_{ij}}{D} + \rho g v_i v_j \quad (4.79)$$

where we have determined the factor g to be

$$g = \frac{D}{D+2} \frac{n b_3}{b_1^2}. \quad (4.80)$$

Now we know that the ideal part of the momentum flux density tensor (2.192) is

$$\Pi_{ij} = p \delta_{ij} + \rho g v_i v_j$$

so equating this with (4.79) gives us an expression for the fluid's pressure

$$p = \frac{2}{D}(nE - \frac{g}{2}\rho v^2) \quad (4.81)$$

For $g = 1$, this is exactly the correct form of the pressure for a thermohydrodynamic fluid.

4.7 Thermohydrodynamic Sound Speed Measurements

In this section we consider the linear response of a multispeed lattice gas to a macroscopic perturbation of the density field. The macroscopic equations of motion are (4.44), respectively

$$\begin{aligned} \partial_t \rho + \partial_i(\rho v_i) &= 0 \\ \partial_t(\rho v_i) + \partial_j(g\rho v_i v_j) &= -c_s^2 \partial_i \left(\frac{\rho E}{\frac{1}{2}mc^2} - g\rho \frac{v^2}{c^2} \right) + \rho \nu \partial^2 v_i \end{aligned}$$

where $n = \rho/m$ has been used. It is sufficient to treat a macroscopic density perturbation on a resting equilibrium state where ρ is uniform and constant, $v = 0$, and the energy E is constant. Then an ε -expansion of the dynamical variables is

$$v_i = \varepsilon u_i \quad (4.82)$$

$$\rho = \rho_o + \varepsilon \varrho, \quad (4.83)$$

where the small fluctuating parts of the velocity and density are denoted u and ϱ , respectively. Consequently, the linear response equations are

$$\partial_t \varrho = -\rho_o \partial_i u_i \quad (4.84)$$

$$\rho_o \partial_t u_i = -\frac{E}{\frac{1}{2}mc^2} c_s^2 \partial_i \varrho + \rho_o \nu_o \partial^2 u_i \quad (4.85)$$

Then, applying ∂_t to the continuity equation and ∂_i to the Navier-Stokes equation allows us to eliminate u_i and to obtain the following second-order equation in ρ

$$\partial_t^2 \rho = \frac{E}{\frac{1}{2}mc^2} c_s^2 \partial^2 \rho + \nu_o \partial^2 \partial_t \rho. \quad (4.86)$$

In an inviscid fluid ($\nu = 0$), ρ would satisfy the wave equation

$$\rho = \rho_o \exp(-i\omega t + i\vec{k} \cdot \vec{x}). \quad (4.87)$$

Given a non-zero perturbation, ρ can be Fourier expanded

$$\rho = \int d\omega dk^3 \tilde{\rho} \exp(-i\omega t + i\vec{k} \cdot \vec{x}) \quad (4.88)$$

and we can replace ρ with $\tilde{\rho}$ by taking $\partial_t \rightarrow -i\omega$ and $\partial_i \rightarrow ik_i$. Equation (4.86) becomes

$$-\omega^2 \tilde{\rho} = -k^2 C_s^2 \tilde{\rho} + i\omega \nu_o k^2 \tilde{\rho}. \quad (4.89)$$

where the thermal sound speed is defined as

$$C_s \equiv c_s \sqrt{\frac{E}{\frac{1}{2}mc^2}} = \sqrt{\frac{2E}{mD}}. \quad (4.90)$$

Dividing out $\tilde{\rho}$ gives a quadratic equation for ω

$$\left(\frac{\omega}{C_s}\right)^2 + i\frac{\nu_o k^2}{C_s} \left(\frac{\omega}{C_s}\right) - k^2 = 0. \quad (4.91)$$

The dispersion relation for $\omega(k)$ is then

$$\omega = \pm C_s k \sqrt{1 + \frac{\nu_o^2 k^2}{4C_s^2}} - i\frac{\nu_o}{2} k^2. \quad (4.92)$$

In the long wavelength limit, (4.92) reduces to linear sound speed dispersion

$$\omega = \pm C_s k. \quad (4.93)$$

The imaginary part of the dispersion relation (4.92), will cause damping in the sound wave.

A simple numerical experiment to test the lattice gas thermohydrodynamic equations (4.46),(4.52), and (4.53) of §4.4 is to measure the sound speed as a function of temperature.² To numerically measure the sound speed of a fluid at rest, it is convenient to set up a sinusoidal density perturbation of a given wavelength. Such a perturbation will give rise to a standing wave whose amplitude fluctuation is easily measured and provides a direct means for measuring the sound speed for a gas with a given density and energy.

A preliminary test has been conducted for a 13-bit 3-speed lattice gas. The lattice size is chosen to be 1024x512 and the perturbation is chosen to have a wavelength of $\lambda = 512$. The density variation occurs along the narrow channel direction so that one full period of the standing wave exists on a toroidal space. For each of the

²Since the lattice gas has a factor g due to the discreteness of space, the Navier-Stokes equation must be rescaled to have the correct form. This may be done by rescaling time and viscosity[41]

$$t \rightarrow \frac{t}{g} \quad (4.94)$$

$$\nu \rightarrow g\nu \quad (4.95)$$

Then the Navier-Stokes equation (4.45) for constant density becomes

$$g\rho\partial_i v_i + \rho g\partial_j (v_i v_j) = -\frac{2}{D}\partial_i \left(nE - \frac{1}{2}\rho g v^2 \right) + g\eta\partial^2 v_i. \quad (4.96)$$

allowing us to identify a scaled pressure

$$p \rightarrow \frac{2}{gD} \left(nE - \frac{1}{2}\rho g v^2 \right). \quad (4.97)$$

Since one would like to write $p = mn(C'_s)^2$, in a reference frame where the fluid is at rest, then

$$C'_s \rightarrow \sqrt{\frac{2E}{gmD}} = \frac{1}{\sqrt{g}}C_s. \quad (4.98)$$

This is a rescaled sound speed in the Galilean invariant frame of reference.

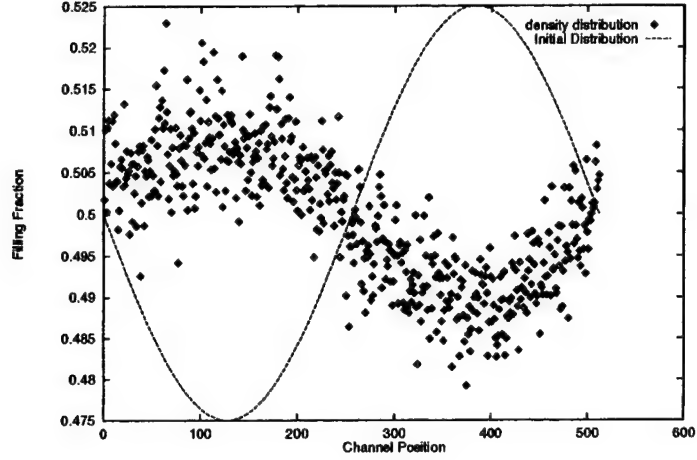


Figure 4.1: Hydrothermal CAM-8 Sound Wave Experiment: Standing wave density profile for a 13-bit 3-speed lattice gas, $d = 0.5$, 5 percent amplitude perturbation, $\lambda = 512$.

512 channel positions an average density can be obtained by summing over 1024 data points. Although the density can be integrated in this way, because of the fluctuations in the lattice gas, the resulting average versus channel position is noisy.

Figure 4.1 shows the integrated standing wave density profile after the wave has oscillated many times. At small time intervals, the first Fourier harmonic is measured by multiplying the density profile by its initial sinusoidal envelope. The fluctuation of this first component will smoothly oscillate with a frequency of $\frac{c}{\lambda}$ (see Figure 4.2). Several measurements were made for a fluid at density, $d = 0.5$, for a range of energies, $E = 0.25, 0.26, \dots, 0.36$. This is the full range of energies available at this density. The resulting sound speed data are presented in Figure 4.3. Viscous damping becomes higher with increasing energy in accordance with the predicted dispersion relation (4.92). This implies that the kinematic viscosity, ν_0 , is strongly energy dependent and increases as the system temperature is raised. This can be qualitatively understood as

follows by considering the 13-bit 3-speed lattice gas. At high energy filling fractions, the population of the fast moving particles increases, thereby reducing the chance of energy mixing collisions. Without these energy mixing collisions, particles can more readily diffuse throughout the fluid, so the mean-free-path, λ , increases. Furthermore, the sound speed increases with temperature; $C_s \propto \sqrt{E}$. These two factors both contribute to the increase of the fluid's kinematic viscosity since $\nu_o \sim C_s \lambda$.

4.8 Rayleigh-Bénard Convection on the CAM-8

A well known fluid instability of a thermohydrodynamic system is Rayleigh-Bénard convection[70, 30]. Rayleigh-Bénard convection is a popular experiment because one can observe the onset of order and then the transition to chaos in the flow patterns [21, 6].

Here the implementation of the two-speed hexagonal lattice gas with a rest particle, includes gravitational forcing, free-slip and no-slip boundaries that may be oriented horizontally, vertically, or inclined $\pm 60^\circ$, and heating and cooling sites to model temperature controlled boundary surfaces. This has been encoded within the site data space of 16-bits per site for simple implementation on the CAM-8. The ability to encode such complex dynamics within 16-bits is one of the remarkable aspects of the lattice gas formalism in terms of efficient memory use, affording us the ability to do flash updating from prestored collision tables. Of the 2^{16} collision table entries, 98 percent are used (that is, are not identity entries) in this model. Similar lattice gas models have been implemented by Burges and Zaleski [20], by Chen *et al.* [27], and by Ernst and Das [35].

To optimize the collision frequency between the fast and slow particles, following

Chen [27] their momenta are chosen to be of unit value. That is, the slow particles have unit mass, $m_1 = 1$ and the fast particles have half the mass, $m_2 = 1/2$. In this way, $p_1 = p_2 = 1$ and their energies are $E_1 = 1$ and $E_2 = 2$. With this convention we have the usual FHP-type collisions [42] between the different speed particles while conserving mass, momentum, and energy. These include head-on 2-body collisions, three-body collisions, collisions with spectators, etc.

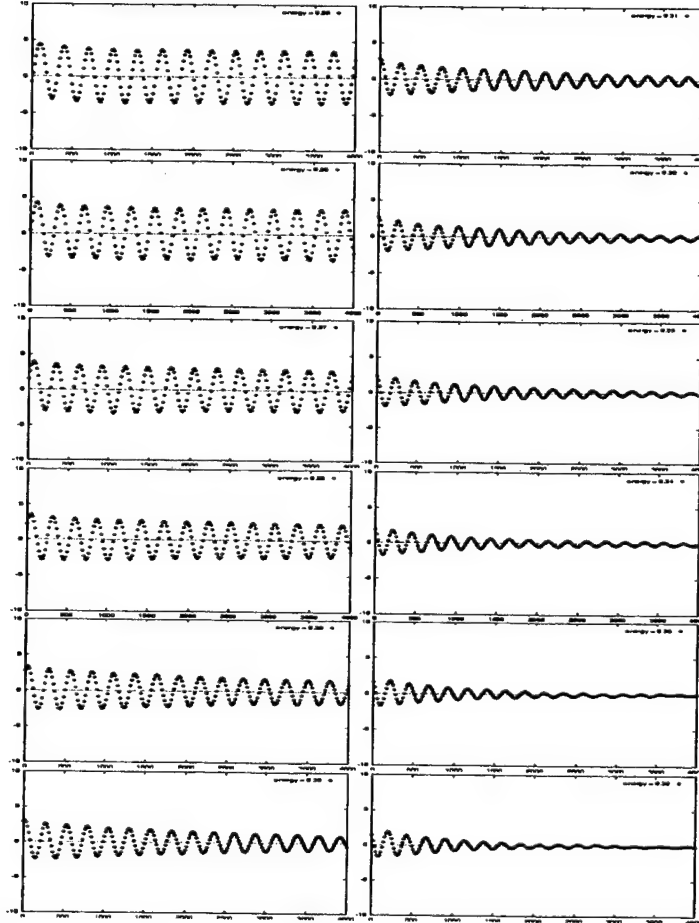


Figure 4.2: Hydrothermal CAM-8 Sound Wave Experiment: Sound wave damping. Oscillations of a standing wave amplitude versus time at $d = 0.5$ for several energies ranging from 0.25 to 0.36 with a 1024×512 lattice size in a simple 13-bit 3-speed model.

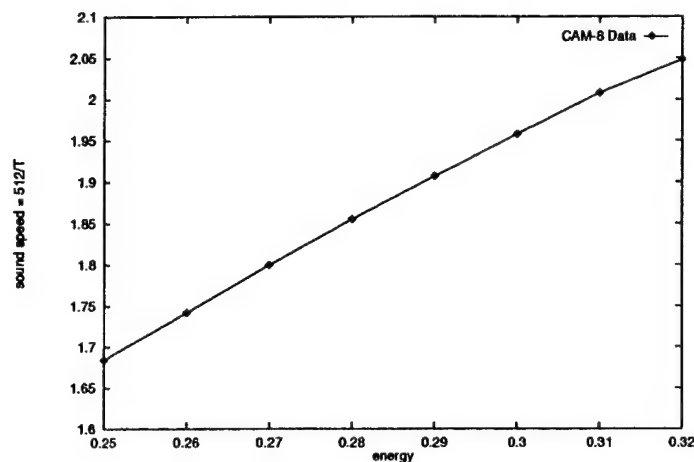


Figure 4.3: Hydrothermal CAM-8 Sound Wave Experiment: Sound versus energy derived from standing waves at $d = 0.5$ for several energies ranging from 0.25 to 0.32 in a simple 13-bit 3-speed lattice gas model.

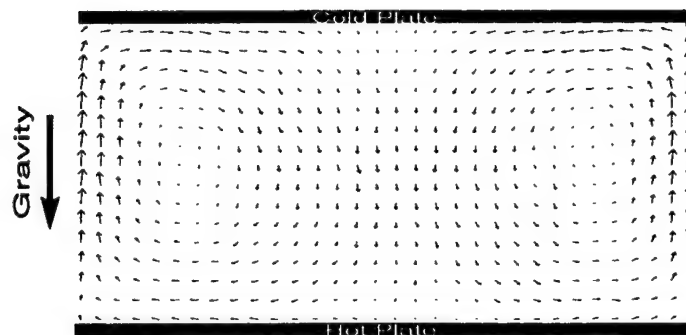


Figure 4.4: Hydrothermal CAM-8 Experiment: Rayleigh-Bénard convection cells at the onset of convection where rolls are first observed in a simple 13-bit 3-speed lattice gas model. Lattice Size: 2048×1024 . Time Average: 100. Spatial Average: 64×64 . Mass Density Fraction= $1/5$. Data presented at 50,000 time steps.

Chapter 5

Integer Lattice Gases ($L > 1$)

Two discrete models for fluid dynamics are the lattice gas automaton (LGA) and lattice-Boltzmann equation (LBE). Each has its own advantages and disadvantages for modeling complex fluids on parallel computers. I have explored a new discrete approach, an *integer lattice gas*, that retains the best features of both [17]. An integer lattice gas uses $L > 1$ bits in binary encoded fashion to represent the particle count in each momentum state of the spatial lattice (in the special case of $L = 1$ the method reduces to LGA). Like the LGA, the integer method: (1) is exactly computed on a discrete spacetime lattice (all the additive conserved quantities, *e.g.* mass and momentum, are kept strictly fixed during the entire course of the calculation—there is no numerical round-off error); (2) microscopically obeys semi-detailed balance; (3) has a mesoscopic limit defined by ensemble averaging; and (4) acts like a fluid in the continuum macroscopic limit (the usual Chapman-Enskog expansion is performed). Like the LBE, the integer method: (1) recovers the correct fluid equations, with full Galilean invariance; (2) achieves a reduction in viscosity; and (3) achieves a considerable noise reduction. Numerical experiments were carried out on parallel computers (CAM-8, CM-5, SP-2) to verify the theoretical analysis of the integer

lattice gas.

LGA has exact conservations, obeys semi-detailed balance, is unconditionally stable, and provides an eligible computer architecture. In LGA, a single bit is used to represent each particle momentum state in a crystallographic spatial lattice. Since the dynamics is computed on the “microscopic” level, the single particle distribution probabilities at the “mesoscopic” level are defined by ensemble averaging. Allocating a bit for every particle momentum state limits the LGA fluid dynamics to low Reynolds numbers. Additionally, there are discretization artifacts, including in particular, a lack of Galilean invariance.

In an effort to repair these problems, in particular to obtain high Reynolds numbers and to recover Galilean invariance, the LBE approach was born. Here one uses floating point numbers to directly represent the mesoscopic particle probability distribution function in the Boltzmann equation and one typically uses the Bhatnager-Gross-Krook approximation to model the collision operator, though this is prone to numerical instabilities. So, as a trade-off to avoid computing any microscopic details, LBE gives up semi-detailed balance and consequently unconditional stability, a problem typical of finite-difference methods.

The integer lattice gas is an alternate route to avoid these problems encountered in LGA and LBE. Since the particle distribution function is known in closed form, a theoretical analysis of the integer lattice gas is possible, and in fact many results obtained in the $L = 1$ case follow in the expected fashion for $L > 1$, (*e.g.* calculation of the kinematic viscosity presented below). Just as the LGA fluid model has been extended to model complex fluids, such as multiphase and immiscible fluids, the integer lattice gas likewise can be extended to model complex fluids. So the lessons

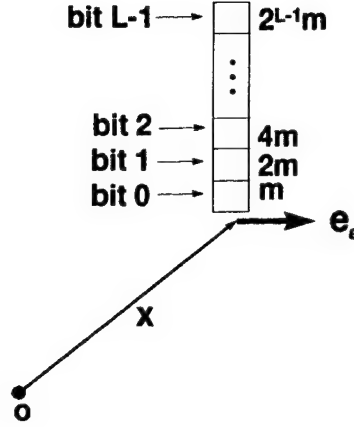


Figure 5.1: Binary exponential encoding and bit layout for an integer lattice gas with L bits per momentum state.

learned for the $L = 1$ case will apply when multiple bits are used to encode the particle occupancies.

5.1 Microdynamics

In the integer lattice gas L bits per site are used in a binary exponential encoding where the least significant bit represents a single particle of mass, m , the next significant bit represents two particles, and the most significant bit represents 2^{L-1} particles, as indicated in Figure 5.1. Now, two indices are used on all variables—the first index is the directional index for the particle's momentum state, and the second index is the bit index. Note that as usual, the first index is taken modulo B , for example

$$n_{al} \equiv n_{\text{mod}_B(a)l}. \quad (5.1)$$

Therefore, the total particle count in a momentum state is obtained by summing

over channel bits where the l^{th} -occupation variable is weighted by 2^l as follows

$$n_a \equiv \sum_{l=0}^{L-1} 2^l n_{al}. \quad (5.2)$$

Similarly, the collision operator for the total particle count is defined by

$$\Omega_a \equiv \sum_{l=0}^{L-1} 2^l \Omega_{al}. \quad (5.3)$$

The local microdynamics consist of collision and streaming phases as usual in lattice gas dynamics. The collisional phase reorders the particle counts locally at each site

$$n'_{al}(\vec{x}, t) = n_{al}(\vec{x}, t) + \Omega_{al}[\vec{n}(\vec{x}, t)], \quad (5.4)$$

and in the streaming phase the particle counts at \vec{x} “hop” to the neighboring site at $\vec{x} + \ell \hat{e}_a$ and time is incremented by τ

$$n_{al}(\vec{x} + \ell \hat{e}_a, t + \tau) = n_{al}(\vec{x}, t). \quad (5.5)$$

Combining these two equations and summing over the bit index, the particle counts obey the usual lattice gas equation:

$$n_a(\vec{x} + \ell \hat{e}_a, t + \tau) = n_a(\vec{x}, t) + \Omega_a[\vec{n}(\vec{x}, t)]. \quad (5.6)$$

This is identical to (2.23) for the $L = 1$ case.

5.2 Mesodynamics

5.2.1 Equilibrium Distribution

The probability of having a bit occupied in an integer lattice gas satisfying semi-detailed balance is still determined by ensemble averaging and must have the form

of a Fermi-Dirac distribution. Since the l^{th} -bit denotes a particle of mass $2^l m$, the Fermi-Dirac distribution is

$$f_{al} \equiv \langle n_{al}(x) \rangle = \frac{1}{\exp(-2^l m(\alpha + c\beta_i e_{ai})) + 1}. \quad (5.7)$$

As usual one may define the mass density in terms of a sum over the ensemble average of occupation variables

$$\rho(x) \equiv \sum_{a=1}^B \sum_{l=0}^{L-1} 2^l m \langle n_{al}(x) \rangle = \sum_{a=1}^B m \langle n_a(x) \rangle, \quad (5.8)$$

and similarly for the momentum density

$$\rho(x)v_i(x) \equiv \sum_{a=1}^B \sum_{l=0}^{L-1} 2^l m c e_{ai} \langle n_{al}(x) \rangle = \sum_{a=1}^B m c e_{ai} \langle n_a(x) \rangle. \quad (5.9)$$

An interesting consequence of binary exponential encoding is that a closed form solution for the equilibrium distribution of the total channel counts is obtained, which of course is not the Fermi-Dirac distribution. For convenience, let us write the distribution function for the individual particles in terms of the fugacity as follows

$$f_{al}(z_a) = \frac{1}{z_a^{-2^l} + 1}. \quad (5.10)$$

The definition of the fugacity is identical to (2.161) for the $L = 1$ case presented above

$$z_a \equiv \exp(\alpha + mc\vec{\beta} \cdot \hat{e}_a). \quad (5.11)$$

The probability of having a particular total channel count must be determined by a weighted sum of L Fermi-Dirac distributions as follows

$$f_{aL}(z_a) \equiv \frac{\sum_{l=0}^{L-1} 2^l f_{al}(z_a)}{\sum_{l=0}^{L-1} 2^l} \quad (5.12)$$

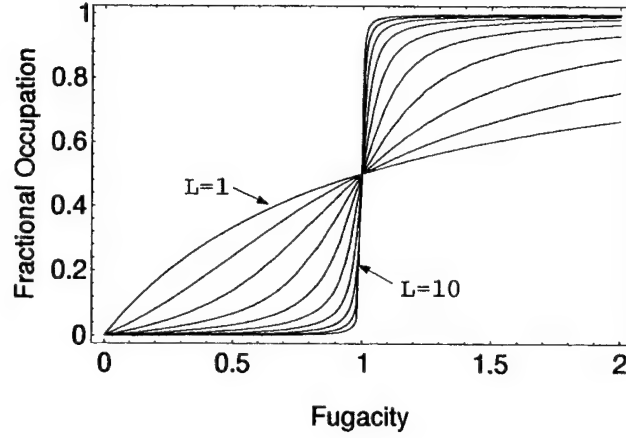


Figure 5.2: Fractional occupation versus fugacity for an integer lattice gas for $L = 1$ to $L = 10$. At high values of L the distribution becomes a step function.

It is worthwhile to find a closed form expansion for (5.12). Using (5.10) with some mathematical manipulations allows us to rewrite the argument of the sum as follows

$$f_{aL}(z_a) = \frac{1}{2^L - 1} \sum_{l=0}^{L-1} \left(\frac{2^l}{z^{-2^l} - 1} - \frac{2^{l+1}}{z^{-2^{l+1}} - 1} \right). \quad (5.13)$$

Now this finite telescoping series (5.13) for the probability of a channel count has the following closed form sum

$$f_{aL}(z_a) = \frac{1}{2^L - 1} \left(\frac{1}{z_a^{-1} - 1} + \frac{2^L}{z_a^{-2^L} - 1} \right). \quad (5.14)$$

This distribution is plotted in Figure 5.2 for several values of L from $L = 1$ to $L = 10$. A quite interesting alternative way to directly arrive at (5.14) is to make use of some reasoning from statistical mechanics. This alternative approach is presented in the following section and sheds light on the behavior of the integer lattice gas equilibrium distribution function.

5.2.2 Boltzmann Equation

A collision state, denoted by s , at some site of the lattice has $B \times L$ bits. We write the collision state as a vector

$$s = (n_{1,0}, \dots, n_{B,0} ; \dots ; n_{1,L-1}, \dots, n_{B,L-1}). \quad (5.15)$$

The probability in the Boltzmann limit for a site of the lattice being in this configuration can be written as usual in factorized form as

$$P_s = \prod_{a=1}^B \prod_{l=0}^{L-1} f_{al}^{n_{al}} (1 - f_{al})^{1-n_{al}}. \quad (5.16)$$

We define the mean field collision operator, in the mean-field limit, in the usual fashion in terms of the Boltzmann probability

$$\Omega_{al}^{mf} = \sum_{ss'} (n'_{al} - n_{al}) P(s, s'). \quad (5.17)$$

We write the distribution function in series with diffusive ordering in $\varepsilon^2 \sim \ell^2 \sim \tau$ as is usual in a Chapman-Enskog expansion: $f_a = f_a^{(0)} + \varepsilon f_a^{(1)} + \dots$. We then make a linear approximation by Taylor expanding the mean field collision operator

$$\Omega_{al}^{mf} \simeq \sum_{b=1}^B J_{al,b} f_b^{(1)}. \quad (5.18)$$

where the Jacobian of the collision operator must now be determined using the chain rule as follows

$$J_{al,b} = \sum_{m=0}^{L-1} \frac{\partial \Omega_{al}^{mf}}{\partial f_{bm}} \frac{\partial f_{bm} / \partial z_b}{\partial f_b / \partial z_b}. \quad (5.19)$$

Note that the partial derivative $\frac{\partial f_{bm}}{\partial f_b}$ is determined by taking a ratio of derivatives of the numerator and denominator with respect to the fugacity z_b . This is mathematically convenient because one knows the analytical form of the distribution function

in terms of the fugacity using (5.10). The Boltzmann equation to order ε^2 is the following

$$\partial_i f_a + c e_{ai} \partial_i f_a + \frac{\ell^2}{2\tau} e_{ai} e_{aj} \partial_i \partial_j f_a = \frac{1}{\tau} \sum_{b=1}^B f_b^{(1)} \underbrace{\sum_{l=0}^{L-1} 2^l J_{al,b}}_{J_{ab}}. \quad (5.20)$$

This is the expected mesoscopic transport equation so long as the following definition holds

$$J_{ab} \equiv \sum_{l=0}^{L-1} 2^l J_{al,b}. \quad (5.21)$$

From this lattice Boltzmann equation the continuum equations are determined by expressing the distribution function in terms of the macroscopic variables of mass density and momentum density.

5.2.3 Chapman-Enskog Expansion

In a fashion identical to the analysis carried out in §2.4.1, for an integer lattice gas the equilibrium probability for finding particles in momentum state $m c e_{ai}$ at position \vec{x} at time t is given by

$$f_a^{(0)} = f_{aL}(z_a) \quad (5.22)$$

whose closed analytical form is written above in (5.14). This is the essential difference from the $L = 1$ case presented in Chapter 2; that is, the form of the distribution function is no longer Fermi-Dirac. Otherwise, all the calculations carried out for the $L = 1$ case carry over directly to the $L > 1$ case treated here. The fugacity is defined as

$$z_a = \exp [m(\alpha^\rho + c \alpha_i^u e_{ai})]. \quad (5.23)$$

Note that α^ρ and α_i^u are functions of $\rho(\vec{x}, t)$ and $v_i(\vec{x}, t)$, as will be shown below. It is straightforward to do a Taylor expansion of the fugacity about $z^o = \exp(m\alpha^\rho)$, which

gives the subsonic limit expansion

$$z_a = z^o \left(1 + m c \alpha_i^u e_{ai} + \frac{1}{2} m^2 c^2 \alpha_i^u \alpha_j^u e_{ai} e_{aj} + \dots \right). \quad (5.24)$$

Inserting the deviation in the fugacity $\delta z \equiv z_a - z^o$ into a Taylor expansion of $f_a^{(0)}$ about z^o then gives

$$\begin{aligned} f_a^{(0)} &= f_{aL}(z^o) + f'_{aL}(z^o) \delta z + \frac{1}{2} f''_{aL}(z^o) \delta z^2 + \dots \\ &= f_{aL}(z^o) + \left[z f'_{aL} \right]_{z=z^o} m c \alpha_i^u e_{ai} + \\ &\quad \frac{1}{2} \left[z f'_{aL} + z^2 f''_{aL} \right]_{z=z^o} m^2 c^2 \alpha_i^u \alpha_j^u e_{ai} e_{aj} + \\ &\quad \mathcal{O}(c^3) \end{aligned} \quad (5.25)$$

Inserting (5.26) into the first moment (2.105) and second moment (2.106) of $f_a^{(0)}$ gives the following expressions for the particle density

$$\rho = m B f_{aL}(z^o) + \frac{m^3 c^2 B}{2D} \left[z f'_{aL} + z^2 f''_{aL} \right]_{z=z^o} (\alpha^u)^2 \quad (5.27)$$

and the momentum density

$$\rho v_i = \frac{m^2 c^2 B}{D} \left[z f'_{aL} \right]_{z=z^o} \alpha_i^u, \quad (5.28)$$

respectively. Manipulating (5.27) and (5.28) allows us to solve for α_i^u and then $f_{aL}(z^o)$

$$f_{aL}(z^o) = d - \frac{D d^2 v^2}{2c^2} \left[\frac{z f'_{aL} + z^2 f''_{aL}}{(z f'_{aL})^2} \right]_{z=z^o}, \quad (5.29)$$

where the reduced density $d \equiv \frac{\rho}{mB}$ is used. Therefore it is possible to express the equilibrium particle distribution as an expansion in ρ and v_i by inserting (5.28) and (5.29) into (5.26) to obtain the desired result for the subsonic expansion about the fluid's equilibrium density $f_{aL}(z^o) = d$:

$$f_{aL}^{(0)}(z_a) = d \left(1 + \frac{D}{c} e_{ai} v_i + g_L \frac{D(D+2)}{2c^2} Q_{aij} v_i v_j \right) + \mathcal{O}(v^3) \quad (5.30)$$

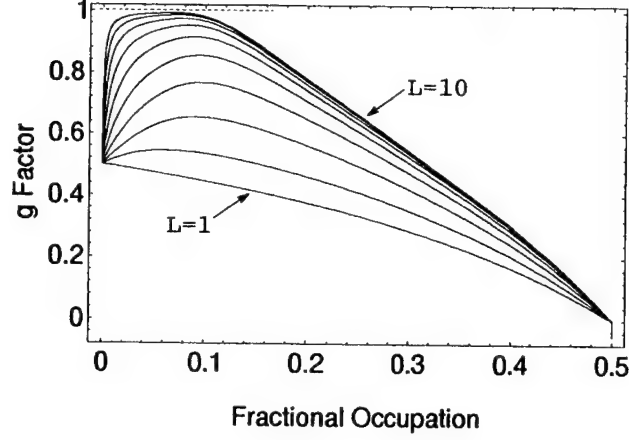


Figure 5.3: Galilean factor versus fractional occupation for an integer lattice gas for $L = 1$ to $L = 10$ for $D = 2$ dimensions. At high values of L the g -factor flattens and approaches a value of $\frac{2D}{D+2}$ at low densities.

where the following identifications are made

$$Q_{aij} \equiv e_{ai}e_{aj} - \frac{\delta_{ij}}{D} \quad (5.31)$$

and Galilean prefactor

$$g_L = \frac{d}{2^L - 1} \frac{D}{D + 2} \left[\frac{z f'_L - z^2 f''_L}{(z f'_L)^2} \right]_{z=z^o}. \quad (5.32)$$

5.2.4 First Correction to the Equilibrium Distribution

We can obtain the mean field collision operator along channel a by summing (5.18) over all particle masses as follows

$$\Omega_a^{\text{mf}} = \sum_{l=0}^{2^L-1} 2^l \Omega_{al}^{\text{mf}} = \sum_{b=1}^B J_{a,b} f_b^{(1)}. \quad (5.33)$$

where (5.21) has been used. As in the $L = 1$ case (2.171) the same propagation equation for $L > 1$ holds true

$$\Omega_a^{\text{mf}}(f) = \ell e_{ai} \partial_i f_a^{(0)} + \mathcal{O}(\epsilon^2). \quad (5.34)$$

Equating our expressions for the mean field collision operator, (5.33) and (5.34)

$$\sum_{b=1}^B J_{ab} f_L^{(1)}(z_b) = e_{ai} \partial_i f_L^{(0)}(z_a), \quad (5.35)$$

the first order correction to the equilibrium distribution function is obtained

$$f_L^{(1)}(z_a) = d\tau D \sum_{b=1}^B J_{ab}^{-1} e_{bi} e_{bi} \partial_i v_j. \quad (5.36)$$

Using the J -theorem (2.175) we write the distribution function to order ϵ as

$$f_L(z_a) = d + d \frac{D}{c} e_{ai} v_i + dg_L \frac{D(D+2)}{2c^2} Q_{aij} v_i v_j - d\lambda \frac{D}{c} e_{ai} e_{ai} \partial_i v_j \quad (5.37)$$

where the eigenvalue λ is given by

$$\lambda = \frac{-\ell}{\sum_{ab} J_{ab} (\hat{e}_a \cdot \hat{e}_b)^2}. \quad (5.38)$$

It is quite remarkable that this expression for the distribution function (5.37) is identical to that given for the $L = 1$ case in (2.187) provided the prefactor is replaced ($g \rightarrow g_L$). The Galilean prefactor g_L is plotted in Figure 5.3 for $L = 1$ up to $L = 10$. Galilean invariance is recovered exactly in two dimensions for low densities at large L values, since $2D/(D+2) = 1$ for $D=2$. In three dimensions, particular densities give $g_L = 1$, since $2D/(D+2) > 1$ for $D=3$.

Remark:

A critical value of $d_c \sim 0.1$ is observed where g_L becomes flat for large L values. This is a kind of symmetry breaking in the Galilean invariance that occurs for an integer

Table 5.1: All terms of the grand partition function for a simple integer lattice gas ($B = 1$, $V = 2$, $L = 2$)

N	$\{n\}$	Degeneracy	z-factor
6	$\{3, 3\}$	1	z^6
5	$\{2, 3\}$	2	$2z^5$
4	$\{2, 2\}$	1	$3z^4$
	$\{3, 1\}$	2	
3	$\{2, 1\}$	2	$4z^3$
	$\{3, 0\}$	2	
2	$\{2, 0\}$	2	$3z^2$
	$\{1, 1\}$	1	
1	$\{1, 0\}$	2	$2z^1$
0	$\{0, 0\}$	1	1

lattice gas. The fact that Galilean invariance is recovered at low densities is consistent with the earlier observation that the integer lattice gas becomes identically a Bose-Einstein lattice gas at large L and low densities. The critical value $d_c \sim 0.1$ occurs at fractional occupations where the integer distribution function departs from the Bose-Einstein distribution function. See Figure 5.5.

5.2.5 Statistical Mechanics

The results for the integer lattice gas system contained in the subsection entitled “Bose-Einstein Statistics” and in the subsection entitled “Galilean Invariance” of this section §5.2.5 are fascinating. The $L \rightarrow \infty$ case is treated, and it is shown that the system obeys Bose-Einstein statistics. In expression (2.91), summing over all possible

configurations will give all possible polynomials with unit coefficients in the fugacity.¹ Therefore, (2.91) can be simplified by doing a binary count over all integer powers of the fugacity by exchanging the sum and product as follows

$$\Xi = \prod_{xa} \sum_{n=0}^{2^L-1} z_a^n. \quad (5.39)$$

This is the most compact and useful form of the grand partition function. Notice that in (5.39) the exponent is now independent of a since we are directly counting all integer powers of the fugacity going from the empty system $n = 0$ up to the completely filled system at $n = 2^L - 1$.

The grand partition function can then be re-expressed as

$$\begin{aligned} \Xi &= \prod_{xa} \sum_{n=0}^{2^L-1} z_a^n \\ &= \prod_{xa} \prod_{l=0}^{L-1} \sum_{n=0}^1 z_a^{2^l n} \end{aligned} \quad (5.40)$$

$$= \prod_{xa} \prod_{l=0}^{L-1} (1 + z_a^{2^l}). \quad (5.41)$$

¹As a concrete example consider an integer lattice gas with $B = 1$, $V = 2$, and $L = 2$. For simplicity consider a system at rest with $V_i = 0$. The Hamiltonian and total density are

$$H = \sum_x E n(\vec{x}) \quad \rho_{\text{tot}} = \sum_x m n(\vec{x}).$$

The fugacity is $z = \exp(-\beta E + \mu m)$. Summing the z -factors from Table 5.1 in the text above, the grand partition function is

$$\begin{aligned} \Xi &= \sum_{\{n\}} \prod_x z^n \\ &= 1 + 2z + 3z^2 + 4z^3 + 3z^4 + 2z^5 + z^6 = (1 + z + z^2 + z^3)^2 \\ &= \left(\sum_{n=0}^{2^L-1} z^n \right)^V = \prod_x \sum_{n=0}^{2^L-1} z^n. \end{aligned}$$

This simple example shows how the sum and product are to be interchanged.

Note that in the second line above the sum $\sum_{n=0}^{2^L-1}$ was written as $\prod_{l=0}^{L-1} \sum_{n=0}^1$. In the present case, base two is the correct choice, however this type of re-expression of the sum can be accomplished in any base.² The logarithm of the grand partition function is

$$\log \Xi = \sum_{xa} \sum_{l=0}^{L-1} \log(1 + z_a^{2^l}). \quad (5.42)$$

Since $\partial z_a / \partial \beta = -E_a z_a$, then expected energy is

$$\langle E \rangle = -\frac{\partial \log \Xi}{\partial \beta} = \sum_{xa} \sum_{l=0}^{L-1} \frac{2^l z_a^{2^l}}{1 + z_a^{2^l}} E_a. \quad (5.43)$$

The expected energy is also

$$\langle E \rangle = \sum_{xa} F_L(z) E_a, \quad (5.44)$$

so the distribution is immediately identified

$$F_L(z_a) = \sum_{l=0}^{L-1} \frac{2^l z_a^{2^l}}{1 + z_a^{2^l}}. \quad (5.45)$$

This is a sum over Fermi-Dirac functions where the l^{th} -level is exponentially weighted

²As a concrete example note that

$$\begin{aligned} \sum_{n=0}^{2^3-1} z^n &= 1 + z^2 + z^3 + z^4 + z^5 + z^6 + z^7 \\ &= (1+z)(1+z^2)(1+z^4) \\ &= \prod_{l=0}^3 (1 + z^{2^l}) = \prod_{l=0}^3 \sum_{n=0}^1 z^{2^l n} \\ \sum_{n=0}^{3^2-1} z^n &= 1 + z^2 + z^3 + z^4 + z^5 + z^6 + z^7 + z^8 \\ &= (1+z+z^2)(1+z^3+z^6) \\ &= \prod_{l=0}^1 (1 + z^{3^l} + z^{(3^l)^2}) = \prod_{l=0}^1 \sum_{n=0}^2 z^{3^l n}. \end{aligned}$$

by 2^l . Consider the identity for a finite geometric series

$$\sum_{n=0}^{N-1} x^n = \frac{1-x^N}{1-x} \quad (5.46)$$

for any x . Using this identity, the grand partition function (5.39) can be written as

$$\begin{aligned} \Xi &= \prod_{xa} \sum_{n=0}^{2^L-1} z_a^n \\ &= \prod_{xa} \frac{1-z_a^{2^L}}{1-z_a} \end{aligned} \quad (5.47)$$

Note that since z_a is not a function of x , the grand partition function sums to the following closed analytical form

$$\Xi = \prod_a \left(\frac{1-z_a^{2^L}}{1-z_a} \right)^V. \quad (5.48)$$

$$\rightarrow \log \Xi = \sum_{xa} \left[\log(1+z_a^{2^l}) - \log(1+z_a) \right]. \quad (5.49)$$

Since $\partial z_a / \partial \beta = -E_a z_a$, then

$$-\frac{\partial \log \Xi}{\partial \beta} = \sum_{xa} \left(\frac{z_a}{1-z_a} - \frac{2^L z_a^{2^L}}{1+z_a^{2^L}} \right) E_a. \quad (5.50)$$

The expected energy is then

$$\langle E \rangle \equiv -\frac{\partial \log \Xi}{\partial \beta} = \sum_{xa} F_L(z) E_a, \quad (5.51)$$

where the distribution is immediately identified

$$F_L(z_a) = \frac{1}{z_a^{-1}-1} - \frac{2^L}{z_a^{-2^L}+1}. \quad (5.52)$$

This is a closed form analytic expression for the distribution function.³ The results of this section have been worked out elsewhere [17] but are included here for completeness to aid in the subsequent development. The fractional occupation is obtained

³Equating the result (5.45) with (5.52), we find the following identity

$$\sum_{l=0}^{L-1} \frac{2^l z_a^{2^l}}{1+z_a^{2^l}} = \frac{1}{z_a^{-1}-1} - \frac{2^L}{z_a^{-2^L}+1}. \quad (5.53)$$

from (5.52) by dividing by the maximum number of particles per channel which is $2^L - 1$ so that

$$f_L(z_a) \equiv \frac{1}{2^L - 1} \left(\frac{1}{z_a^{-1} - 1} - \frac{2^L}{z_a^{-2^L} + 1} \right). \quad (5.55)$$

This is identical to (5.14).

Fermi-Dirac Statistics ($L = 1$ Limit)

Consider a single-speed $L = 1$ lattice gas. It is quite simple to check the single particle distribution is the Fermi-Dirac function, (2.97), by evaluating F_L at $L = 1$

$$F_1(z) = \lim_{L \rightarrow 1} F_L(z) \quad (5.56)$$

$$= \lim_{L \rightarrow 1} \left(\frac{1}{z^{-1} - 1} - \frac{2^L}{z^{-2^L} + 1} \right) \quad (5.57)$$

$$= \frac{1}{z^{-1} - 1} - \frac{2}{z^{-2} + 1} \quad (5.58)$$

$$= \frac{1}{z^{-1} + 1}. \quad (5.59)$$

Q.E.D.

Bose-Einstein Statistics

Consider a single speed $L = \infty$ integer lattice gas. In this case the grand partition function can be straightforwardly calculated. To begin with, one may derive, in the usual fashion of the statistical mechanics for a system of bosonic particles, the grand

This is expected since the L.H.S. can be written as a telescoping series

$$\sum_{l=0}^{L-1} \frac{2^l z_a^{2^l}}{1 + z_a^{2^l}} = \sum_{l=0}^{L-1} \left(\frac{2^l}{z^{-2^l} - 1} - \frac{2^{l+1}}{z^{-2^{l+1}} - 1} \right). \quad (5.54)$$

partition function as follows

$$\begin{aligned}\Xi &= \prod_{\alpha} \sum_{n=0}^{\infty} z_{\alpha}^n \\ &= \prod_{\alpha} \frac{1}{1 - z_{\alpha}}\end{aligned}\tag{5.60}$$

$$\longrightarrow \log \Xi = \sum_{\alpha} \log \left(\frac{1}{1 - z_{\alpha}} \right)\tag{5.61}$$

Since $\partial z_{\alpha} / \partial \beta = -E_{\alpha} z_{\alpha}$, then

$$-\frac{\partial \log \Xi}{\partial \beta} = \sum_{\alpha} \frac{z_{\alpha}}{1 - z_{\alpha}} E_{\alpha}.\tag{5.62}$$

The expected energy is then

$$\langle E \rangle \equiv -\frac{\partial \log \Xi}{\partial \beta} = \sum_{\alpha} F_{\infty}(z) E_{\alpha},\tag{5.63}$$

where the Bose-Einstein distribution is immediately identified

$$F_{\infty}(z_{\alpha}) = \frac{1}{z_{\alpha}^{-1} - 1}.\tag{5.64}$$

This is a well known result. The Bose-Einstein distribution function is plotted versus occupation number in Figure 5.4. This function diverges for unit fugacity.

It is possible to obtain the Bose-Einstein distribution (5.64) by taking the $L = \infty$ limit of the integer lattice gas distribution function (5.52) as follows

$$F_{\infty}(z) = \lim_{L \rightarrow \infty} F_L(z)\tag{5.65}$$

$$= \lim_{L \rightarrow \infty} \left(\frac{1}{z^{-1} - 1} - \frac{2^L}{z^{-2^L} + 1} \right)\tag{5.66}$$

$$= \frac{1}{z^{-1} - 1} - \lim_{L \rightarrow \infty} \frac{2^L z^{2^L}}{1 + z^{2^L}}\tag{5.67}$$

The first term on the R.H.S. is the Bose-Einstein function and the second term vanishes. To see why this is indeed the case, let us examine the limits of the numerator

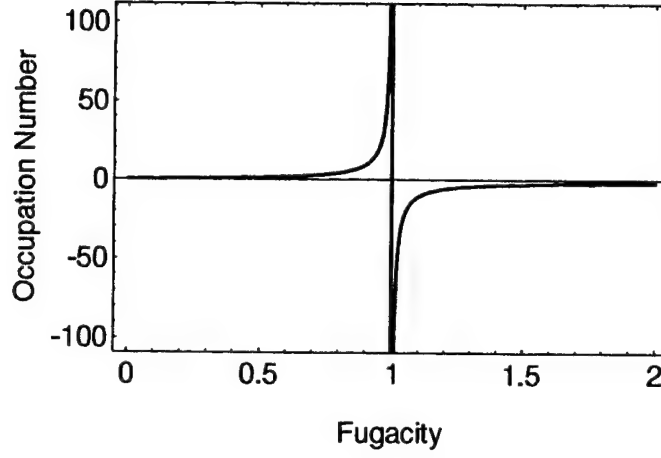


Figure 5.4: Occupation number versus fugacity for a Bose-Einstein lattice gas.

and denominator separately. For the case when $z \geq 1$ the Bose-Einstein function diverges (in fact in the first derivation of the Bose-Einstein distribution (5.64), the geometric series is only finite in the case of $z < 1$). Consider the situation where $z < 1$. Making a variable substitution $m = 2^L$, the limit of the numerator is

$$\lim_{L \rightarrow \infty} 2^L z^{2^L} = \lim_{m \rightarrow \infty} \frac{m}{z^{-m}} = \frac{\infty}{\infty}, \quad (5.68)$$

which is indeterminate. Therefore, we can use L'Hospital's rule to evaluate this

$$\lim_{m \rightarrow \infty} \frac{m}{z^{-m}} = \frac{1}{\lim_{m \rightarrow \infty} z^{-m} \log z} = \frac{1}{\infty} = 0. \quad (5.69)$$

The limit of the denominator is simply unity

$$\lim_{L \rightarrow \infty} (1 + z^{2^L}) = \lim_{m \rightarrow \infty} (1 + z^m) = 1. \quad (5.70)$$

Then

$$\lim_{L \rightarrow \infty} \frac{2^L z^{2^L}}{1 + z^{2^L}} = \frac{0}{1} = 0. \quad (5.71)$$

Therefore

$$F_{\infty}(z) = \frac{1}{z^{-1} - 1}. \quad (5.72)$$

This is the expected result.⁴

To understand the limiting behavior of the integer lattice gas versus a Bose-Einstein lattice gas it is sufficient to graphically plot their respective distribution functions for several different values of L . To make the comparison it is necessary that the Bose-Einstein fractional occupation is defined as

$$f_{\infty}(z) \equiv \frac{1}{2^L - 1} \left(\frac{1}{z^{-1} - 1} \right). \quad (5.73)$$

A plot of the Bose-Einstein fractional occupation (5.73) for several values of L is plotted in Figure 5.5. For comparison purposes, the integer lattice gas fractional occupation (5.14) is overplotted. The two distribution functions (5.73) and (5.14) become identical for large L values. It is clear from Figure 5.5 that for practical purposes an $L = 16$ integer lattice gas⁵, for example, would be a very good model of a Bose-Einstein lattice gas.⁶

⁴The identity that a weighted Fermi-Dirac series of rational fractions converges to the Bose-Einstein distribution is known, see identity 1.121.2 on page 22 of Gradshteyn and Ryzhik [43]: for $x^2 < 1$,

$$\frac{1}{x - 1} = \sum_{l=0}^{\infty} \frac{2^l}{x^{2^l} + 1}.$$

⁵ $L = 16$ is a convenient choice for a computer implementation since two-byte integers can be used to encode the momentum states.

⁶The local collision operator for an $L = 24$ integer lattice gas has been implemented by a polytope acceptance-rejection technique [17].

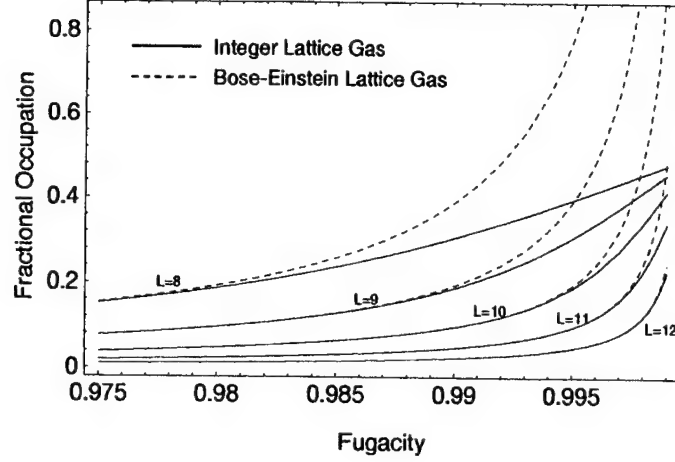


Figure 5.5: Fractional occupation versus fugacity for a Bose-Einstein lattice gas and an integer lattice gas in $D = 2$ dimensions ranging from $L = 8, \dots, 12$. The two distribution functions become identical at large L values.

Galilean Invariance

It is straightforward to calculate the Galilean prefactor for the Bose-Einstein lattice gas. We will need the first and second derivatives of $F_\infty(z)$ with respect to the fugacity. These derivatives are

$$F'_\infty(z) = \frac{1}{(1-z)^2} \quad (5.74)$$

$$F''_\infty(z) = \frac{2}{(1-z)^3}. \quad (5.75)$$

Then the Galilean prefactor as a function of the fugacity is

$$g_\infty(z) = F_\infty \frac{D}{D+2} \left[\frac{zF'_\infty + z^2 F''_\infty}{(zF'_\infty)^2} \right] = \frac{D}{D+2} (1+z). \quad (5.76)$$

A parametric plot of the Galilean prefactor, $g_\infty(z)$, versus the occupation number, $F_\infty(z)$, using the fugacity as the parameter is given in Figure 5.6. The Galilean

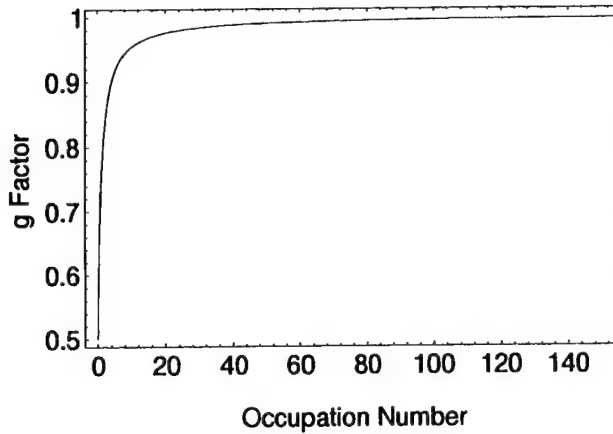


Figure 5.6: Galilean prefactor versus occupation number for a Bose-Einstein lattice gas in $D = 2$ dimensions. Galilean invariance emerges for large occupation numbers.

prefactor becomes a constant at high occupations, which occurs at $z = 1$ since the distribution function is singular there

$$\lim_{z \rightarrow 1} g_{\infty} = \frac{2D}{D+2}. \quad (5.77)$$

In two-dimensions ($D = 2$) the Galilean prefactor becomes unity and invariance is recovered in the macroscopic limit in the sense that the dynamics is identical in all moving frames of reference.

5.3 Macrodynamics

This section on the macroscopic dynamical behavior of the integer lattice gas closely parallels the treatment presented for the $L = 1$ case of §2.5. Therefore in this section I will give just an abridged version of the macroscopic analysis.

The macroscopic equations of motion are determined from mass conservation (con-

tinuity equation)

$$\partial_t \rho + \partial_i (\rho v_i) = 0 \quad (5.78)$$

and momentum conservation (Euler's equation)

$$\partial_t (\rho v_i) + \partial_j \Pi_{ij} = 0. \quad (5.79)$$

The momentum flux density is

$$\Pi_{ij} = p \delta_{ij} + g_L \rho v_i v_j - \frac{\rho c}{D+2} \left(\lambda - \frac{\ell}{2} \right) \partial_j v_i. \quad (5.80)$$

With sound speed $c_s \equiv \frac{c}{\sqrt{D}}$, the pressure is

$$p = \rho c_s^2 \left(1 - g_L \frac{v^2}{c^2} \right). \quad (5.81)$$

Inserting (5.80) into Euler's equation (5.79), the Navier-Stokes equation for viscous incompressible flow emerges

$$\rho \partial_t v_i + g_L \rho v_j \partial_j v_i = -\partial_i p + \eta \partial^2 v_i, \quad (5.82)$$

with shear viscosity

$$\eta = \frac{\rho c}{D+2} \left(\lambda - \frac{\ell}{2} \right). \quad (5.83)$$

This completes the analysis of the integer lattice gas.

Chapter 6

The Simplest Integer Lattice Gas ($L = 2$)

6.1 Introduction

The simplest integer lattice gas is an $L = 2$ model in two dimensions on the triangular lattice with lattice coordination number $B = 6$. With two bits per channel, one can encode up to three particles in each momentum state so there can be up to 18 particles per site. The total number of on-site particle configurations is $2^{BL} = 4096$. The number of equivalence classes is 1097, with 693 containing more than one member and with 404 trivial equivalence classes containing only a single member. Of the 693 contributing equivalence classes, 128 are independent modulo the isometries of the triangular lattice. That is, the total momentum vectors of the contributing equivalence classes all reside in an angular sector ranging from 0 to $\frac{2\pi}{B}$ radians. The number of independent equivalence classes is further reduced by the constraint of particle-hole symmetry. I provide a complete list of all the independent equivalence classes for the $L = 2$ integer lattice gas (see Appendix E). There are 71 such equivalence classes enumerated below ranging from two particles per site up to half-filling,

or nine particles per site. The largest equivalence class has 18 members. For a two dimensional isothermal fluid, there are three additive conserved quantities that are invariant with respect to the dynamics. These are the mass, m , and two components of the momentum, p_x and p_y . Letting N_{EC} denote the number of members contained in an equivalence class, each equivalence class is specified in the following fashion

$$\{N_{EC}, m, 2p_x, \frac{\sqrt{3}}{2}p_y, \underbrace{\{n_0, n_1, \dots, n_B\}, \dots, \{n_0, n_1, \dots, n_B\}}_{N_{EC}-\text{number of members}}\}$$

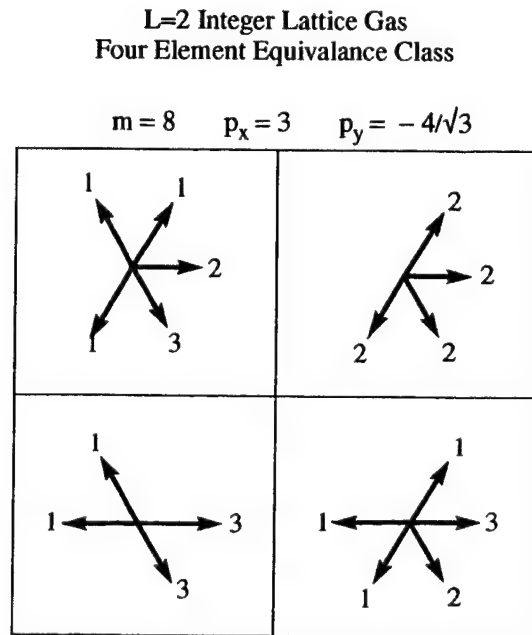


Figure 6.1: An example equivalence class for an $L = 2$ integer lattice gas for $D = 2$ and $B = 6$ that has eight particles and nonzero momentum components.

As an example of this notation, consider the FHP lattice lattice gas described in Chapter 3. With only two-body and three-body symmetric collisions, the FHP lattice

gas uses only two equivalence classes each with zero momentum

$$\{3, 2, 0, 0, \{0, 0, 1, 0, 0, 1\}, \{0, 1, 0, 0, 1, 0\}, \{1, 0, 0, 1, 0, 0\}\},$$

$$\{2, 3, 0, 0, \{0, 1, 0, 1, 0, 1\}, \{1, 0, 1, 0, 1, 0\}\}.$$

This collision set is depicted in Figure 3.2 of §3.2.2, and is a subset of the full collision set for the $L = 2$ generalization presented here. Using the same notational format, the list given in Appendix E defines the full collision set for the $L = 2$ integer lattice gas. Here, for illustrative purposes, consider the following four-element equivalent class which is only one of the equivalence classes of the $L = 2$ integer lattice gas for $D = 2$ and $B = 6$ presented in the appendix. This equivalence class has eight particles with nonzero x and y components for the total momentum at a site:

$$\{4, 8, 6, 2, \{2, 1, 1, 0, 1, 3\}, \{2, 2, 0, 0, 2, 2\}, \{3, 0, 1, 1, 0, 3\}, \{3, 1, 0, 1, 1, 2\}\}.$$

This equivalence class is depicted in Figure 6.1. In an implementation of this collision table on the CAM-8 prototype, a uniform transition matrix is used of the type given in §2.1.3. That is, the probability of a member of a particular equivalence class transitioning to another configuration within that equivalence class is chosen randomly and uniformly. So the transition probability equals the inverse of the size of the equivalence class: $\frac{1}{\|T\|}$. The model therefore satisfies detailed balance. Furthermore, an auxiliary local rule is used to generate random numbers in a reversible fashion. The update procedure for a local collision is carried out as follows. The local state is examined and its mass and momentum are computed to determine its equivalence class. A precomputed table is read that provides the size of the equivalence class. The local random number is then taken modulo the equivalence class size minus one

to choose another member of the equivalence class to replace the current local configuration. With a reversible random number generator, all the integer lattice gas dynamics in turn remain reversible.

Remark:

A quite interesting and natural property of this computational construction is that on the one hand the transition matrix describes a statistical detailed balance process while on the other hand the actual computer implementation of the integer lattice gas is in fact absolutely reversible and deterministic.

The reversibility of the model was demonstrated on the CAM-8 prototype as is customarily done to check the consistency of the computer implementation. A more complete description of the computer implementation of this integer lattice gas, applicable to the workstation or the CAM-8, is given in Appendix E.

6.2 A Numerical Test of the Kinematic Shear Viscosity

In this section I wish to demonstrate the consistency of mean-field analysis of the integer lattice gas given in the previous chapter using the $L = 2$ integer lattice gas by comparing the theoretical prediction of the kinematic shear viscosity with numerically measured values of the shear viscosity. First of all, it is necessary to determine an explicit expression for the kinematic viscosity for the particular $L = 2$ collision set provided earlier in this chapter. We begin by inserting (5.17) into (5.19) to allow us to write the Jacobian of the collision operator in terms of the fugacity as follows

$$J_{ab}(z) = \sum_{ss'} (n'_a - n_a) \sum_m \frac{\partial P(s, s')}{\partial f_{bm}} \frac{\partial f_{bm} / \partial z_b}{\partial f_b / \partial z_b}$$

$$\begin{aligned}
&= \frac{1}{z F_L'} \sum_{ss'} (n'_a - n_a) n_b P(s, s') \\
&= \frac{1}{z F_L'} \left(\frac{1-z}{1-z^{2^L}} \right)^B \sum_{ss'} (n'_a - n_a) n_b z^p,
\end{aligned} \tag{6.1}$$

where $p = p(s)$ is the total particle count in collision $s \rightarrow s'$. Therefore, $J_{ab}(z)$ is specified in terms of a complex rational polynomial function of the fugacity. Inserting (5.38) into (5.83) the kinematic viscosity $\nu \equiv \frac{\eta}{\rho}$ in turn is known as a function of the fugacity

$$\nu(z) = \frac{l^2}{\tau} \frac{1}{D+2} \left(\frac{-1}{\sum_{ab} J_{ab}(z) (\hat{e}_a \cdot \hat{e}_b)^2} - \frac{1}{2} \right). \tag{6.2}$$

Inserting (6.1) this can be rewritten as

$$\nu(z) = \frac{l^2}{\tau} \frac{1}{D+2} \left[\left(\frac{1-z^{2^L}}{1-z} \right)^B \frac{-z F_L'}{\sum_{ab} \sum_{ss'} (n'_a - n_a) n_b z^p (\hat{e}_a \cdot \hat{e}_b)^2} - \frac{1}{2} \right]. \tag{6.3}$$

Using the full collision set given in the previous section, the sum over collision events in the denominator of the above expression will be a 16th-order polynomial¹ in z

$$\begin{aligned}
\sum_{ab} \sum_{ss'} (n'_a - n_a) n_b z^p (\hat{e}_a \cdot \hat{e}_b)^2 &= -6z^2 - 54z^3 - 219z^4 - 571.285714z^5 - 1086.9z^6 \\
&\quad - 1688.683516z^7 - 2218.651948z^8 - 2466z^9 \\
&\quad - 2218.651948z^{10} - 1688.683516z^{11} - 1086.9z^{12} \\
&\quad - 571.285714z^{13} - 219z^{14} - 54z^{15} - 6z^{16}.
\end{aligned} \tag{6.4}$$

Note that the coefficients are symmetric about half-filling, z^9 . For an $L = 2$ integer lattice gas the fractional occupation as a function of the fugacity is

$$f_{L=2}(z) = \frac{1}{3} \left(\frac{z}{1-z} - \frac{4z^4}{1-z^4} \right). \tag{6.5}$$

¹The lowest order non-zero coefficient will be quadratic corresponding to two-body collisions and likewise because of particle-hole symmetry the highest order non-zero coefficient will be $(2^L - 1)B - 2 = 16$, corresponding to the collision of two holes.

Therefore, it is straightforward to plot the kinematic viscosity $\nu(z)$ as a function of the fractional occupation $f(z)$ parametrically in the fugacity (see the solid curve in Figure 6.3).

The numerical data overplotted in Figure 6.3 was computed on the CAM-8 prototype. A numerical simulation of the $L = 2$ integer lattice gas was carried out on a 512×512 space. A sinusoidal velocity profile with wavelength equaling the size of the space is used as an initial condition for a range of densities from $d = 0.1$ up to $d = 0.9$ in steps of $\Delta d = 0.05$. The resulting Navier-Stokes dynamics causes an exponential decay of the velocity sinusoid by viscous damping. A similar numerical experiment was carried out for the usual $L = 1$ case; see Method 2 of §3.3.1. On a log-linear plot the decay of the amplitude of the sinusoidal profile is extremely linear (see Figure 6.2) and gives an accurate measurement of the decay time constant which equals $k^2\nu$. Consequently, this allows us to determine the kinematic viscosity ν numerically in a straightforward manner. The comparison of the mean-field theory and numerical experiment is quite good for medium densities, as can be seen in Figure 6.3. The departure of theory from experiment at low and high densities is typical for this kind of comparison and also exists for an $L = 1$ lattice gas. However the departure for the $L = 2$ lattice gas is greater than expected and perhaps is due to correlations that are neglected in the mean-field calculation.

6.3 Channel Sampling Algorithm

I have implemented a two-dimensional $L = 4$ integer lattice-gas on a triangular lattice. In this case the number of collision configurations is $2^{4 \times 6} = 16m$. This is small enough to store in a lookup table format so that the full collision set is implemented as in the

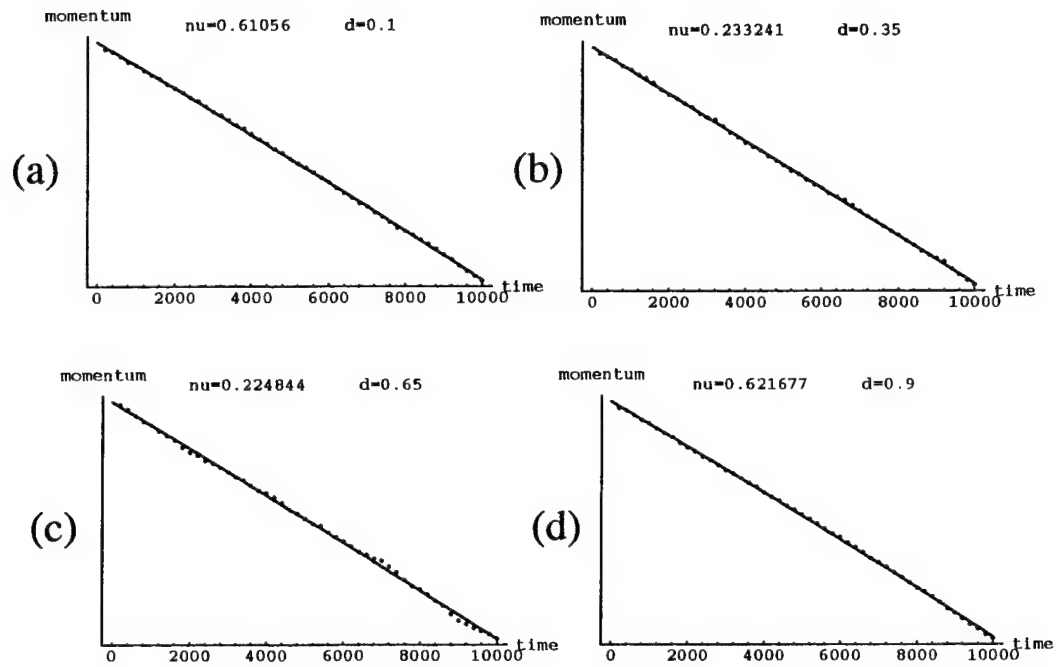


Figure 6.2: Log-log plot of the decay of a sinusoidal velocity profile for an $L = 2$ integer lattice gas with a full collision set with statistical detailed-balance. The decay of velocity profiles at four different densities, $d = 0.1, 0.25, 0.65$, and 0.9 , are plotted. The linear fit is extremely good at all densities. The data were computed on the CAM-8 on a 512×512 simulation space. At each density 50 data points were taken at intervals of 200 time steps.

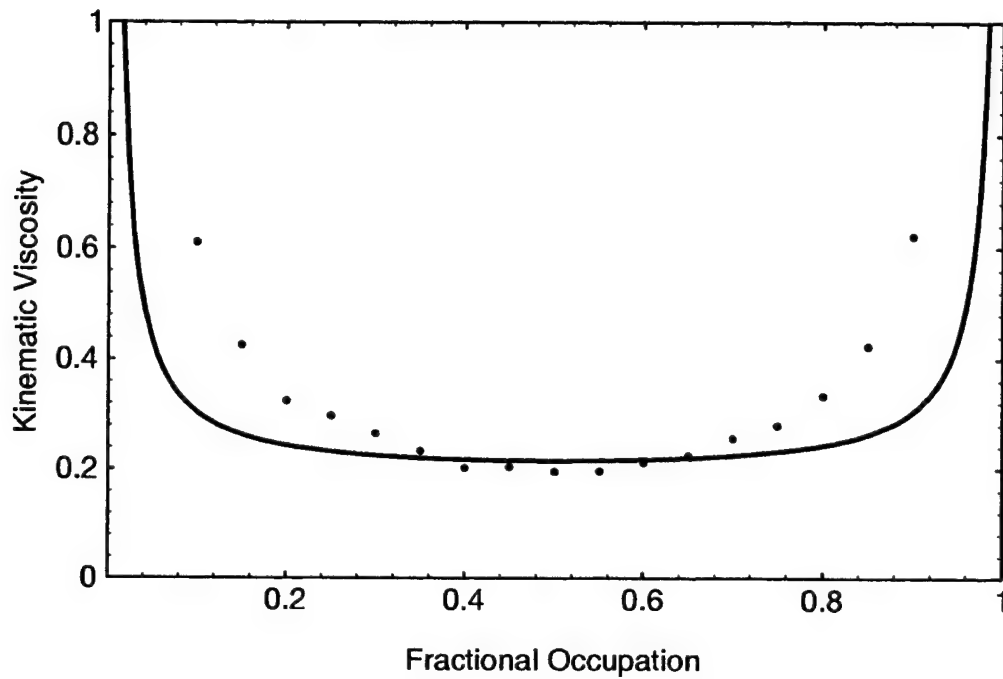


Figure 6.3: Kinematic viscosity versus fractional occupation, or reduced density, of an $L = 2$ integer lattice gas with a full collision set with statistical detailed-balance. The solid curve represents a mean-field theoretical predictions and the data points represent numerical measurements carried out on the CAM-8 uses the method of a decaying sinusoidal velocity profile. The simulation was carried out on a 512 space. The comparison of theory and numerical experiment is good at medium densities.

$L = 2$ example given above. However, for cases with larger values of L , storing the full lookup table is impractical. Therefore, an alternative method that is suitable for large L integer lattice gases is presented here.

In an integer lattice gas a group of L bits is used to encode a particle count in each momentum state. We refer to this group of bits as a *channel*. To reduce the size of the lookup table, one selects only subsets of the channels for updating in a successive manner. Enough channel subsets are selected so that all channels have the opportunity for updating. An example of this algorithm is described in this section for an implementation on the CAM-8 prototype; it is constrained to no more than $2^{16} = 64k$ collision configurations.

Let us denote the channels by n_1, n_2, \dots, n_6 and the rest-particle channel by n_0 . Let $\{\vec{n}\}$ denote set of a four channels, where $\vec{n} = (n_A, n_B, n_C, n_D)$. If d is the background density, define the particle deviations A, B, C , and D , as follows

$$n_A = 2^L d + A \tag{6.6}$$

$$n_B = 2^L d + B \tag{6.7}$$

$$n_C = 2^L d + C \tag{6.8}$$

$$n_D = 2^L d + D. \tag{6.9}$$

$$\tag{6.10}$$

A *collision set* has the property that the first two channels of the set form a pair, the AB -pair, and the last two channels in the set form a pair, the CD -pair, in such a way that a four-channel HPP-type collision can occur between the two pairs. For example, $\{n_1, n_2, n_3, n_4\}$ is an appropriate collision set. So only those operations that act on a collision set $\{A, B, C, D\}$ that transfers particles between the AB -pair and

the CD -pair are used. The collision operator is

$$\Omega = \frac{1}{2^{3L}} \left[n_A n_B (2^L - n_C)(2^L - n_D) - n_C n_D (2^L - n_A)(2^L - n_B) \right]. \quad (6.11)$$

We can also write this collision operator as follows

$$\Omega = (A+B-C-D)d(1-d) + \frac{1}{2^L}(AB-CD)(1-2d) - \frac{1}{2^{2L}} [AB(C+D) + CD(A+B)]. \quad (6.12)$$

This way of writing Ω shows its explicit dependence on d . The practicality of this form of the collision operator comes from the fact that one can use the bits in an integer lattice gas simulation to directly encode the deviations of the particle counts from their mean value. In this way a greater “dynamic range” is achieved. The look-up tables generated depend on the background density. This is a unique feature of an integer lattice gas.

Since finite integer mathematics is used, there may be some numerical round-off error in doing the divisions in (6.11). This is corrected by the following procedure. The particle count that passes from one pair to the other is called the *transfer amount* and is denoted \mathcal{T} . If $\Omega < 0$ then

$$\mathcal{T} = \min(A, B, 2^L - C, 2^L - D, \Omega), \quad (6.13)$$

or else for $\Omega > 0$ then

$$\mathcal{T} = \min(2^L - A, 2^L - B, C, D, \Omega). \quad (6.14)$$

This ensures the transfer amount does not exceed either the number of particles in the losing channels or the number of holes in the gaining channels. Then if the update procedure

$$A' = A - \mathcal{T} \quad (6.15)$$

$$B' = B - \mathcal{T} \quad (6.16)$$

$$C' = C + \mathcal{T} \quad (6.17)$$

$$D' = D + \mathcal{T} \quad (6.18)$$

$$(6.19)$$

is used, the dynamics is unconditionally stable.

A complete collision operator to take us from one input state at time t to an output state at time $t + \tau$ is constructed by choosing a number of collision sets and then arranging them in a particular sequence. With $B = 6$ channels there are three possible collision sets (see Figure 3.1). They are

$$\{n_1, n_4, n_3, n_6\}$$

$$\{n_1, n_4, n_5, n_2\}$$

$$\{n_5, n_2, n_3, n_6\}.$$

If a rest particle channel, n_0 , is included, then there are six additional possible collisions sets. They are

$$\{n_5, n_0, n_4, n_6\}$$

$$\{n_1, n_3, n_2, n_0\}$$

$$\{n_5, n_1, n_6, n_0\}$$

$$\{n_3, n_0, n_2, n_4\}$$

$$\{n_1, n_0, n_2, n_6\}$$

$$\{n_5, n_3, n_4, n_0\}.$$

We define a *forward* collision sequence, denoted by \vec{n}_f , by the following 9 collision sets

$$\{n_5, n_0, n_4, n_6\}$$

$$\{n_1, n_3, n_2, n_0\}$$

$$\{n_1, n_4 n_3, n_6\}$$

$$\{n_5, n_1, n_6, n_0\}$$

$$\{n_3, n_0, n_2, n_4\}$$

$$\{n_1, n_4, n_5, n_2\}$$

$$\{n_1, n_0, n_2, n_6\}$$

$$\{n_5, n_3, n_4, n_0\}$$

$$\{n_5, n_2, n_3, n_6\}$$

The *reverse* collision sequence, denoted by \vec{n}_r , is a sequence in just the reverse order of \vec{n}_f . For the purpose of analytical calculations, the microdynamical update equation with a recursive collision operator is the following

$$n = n + \Omega[(\vec{n} + \Omega[\vec{n}_f])_r]. \quad (6.20)$$

The transition probability for a particular collision will then be $T(n \rightarrow n') = \frac{1}{2}$.

In the computer implementation of an integer lattice gas, I actually use the following decomposition in time. On even time steps the forward collision sequence is used and on odd time steps the reverse collision sequence is used.

$$n(1) = n(0) + \Omega[\vec{n}(0)_f] \quad (6.21)$$

$$n(2) = n(1) + \Omega[\vec{n}(1)_r]. \quad (6.22)$$

$$(6.23)$$

It is necessary to use this alternating method to ensure that chirality effects do not induce any spurious invariants.

Examples of $L = 2$ and $L = 4$ integer lattice gas simulations are given in Figures 6.5 and 6.4 illustrating the Von Karman instability. In fact the latter simulation illustrates the transition from laminar to chaotic flow. This significance of this numerical test is to verify that the integer lattice gas behaves as a Navier-Stokes fluid as predicted and to provide a qualitative test of the model. The $L = 2$ integer lattice gas using the table lookup algorithm described in Appendix E. This $L = 2$ integer lattice gas was only a few times slower than the $L = 1$ gas. The $L = 4$ integer lattice gas running on the CAM-8 using the channel sampling algorithm described in this section was an order of magnitude slower than an $L = 1$ lattice gas on the CAM-8.

Note that here, a novel technique is used to visualize the flow past the cylindrical obstacle. A second lattice gas with attractive nonlocal interparticle interaction "floats", in its liquid phase, above the integer lattice gas. This liquid is injected on the left side of the simulation space at regular intervals and is advected by the local momentum of the integer lattice gas. Bulk momentum is filtered on the right side of the simulation to eliminate periodicity. The liquid flow does not affect the hydrodynamics of the integer lattice gas and is simply a passive fluid. Surface tension in the liquid allows a natural type of streamline visualization very much in analogy with inserting tracer ink into water flow.

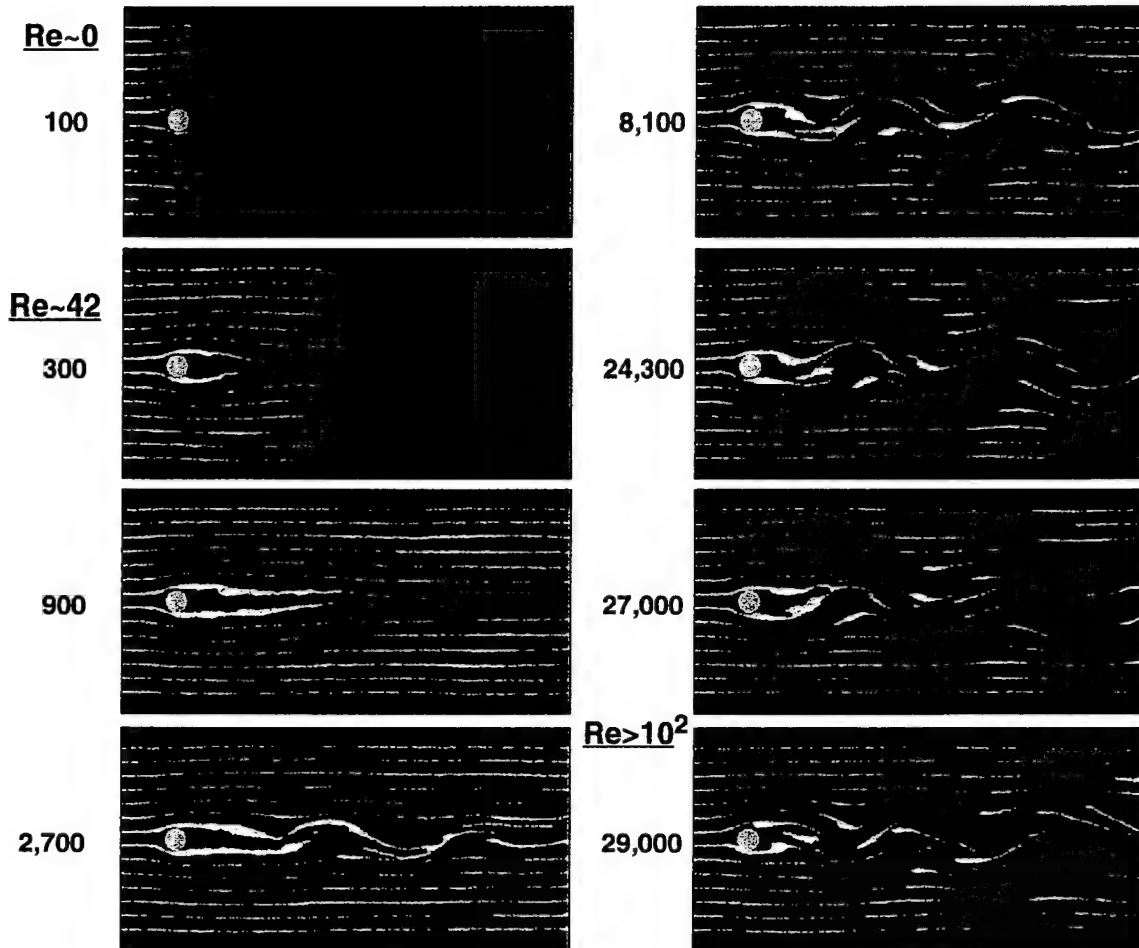


Figure 6.4: Simulation on the CAM-8 prototype of flow past a cylinder. An $L = 2$ integer lattice gas on a triangular lattice using uniform sampling by table lookup for detailed balanced collisions on a 2048×1024 lattice was used. Time series plots from laminar flow, $Re = 0$, through the vortex shedding regime, $Re > 42$, to the vortex street flow regime are shown. Fluid streamlines are illustrated using a liquid tracer fluid (an $L = 1$ long range lattice gas) with no coarse-graining. The first frame shown is at $t = 100$ and the last frame is at $t = 29,000$. The gas is at rest at $t = 0$, $v = 0$, and is quickly accelerated to a steady state low Mach number background flow.

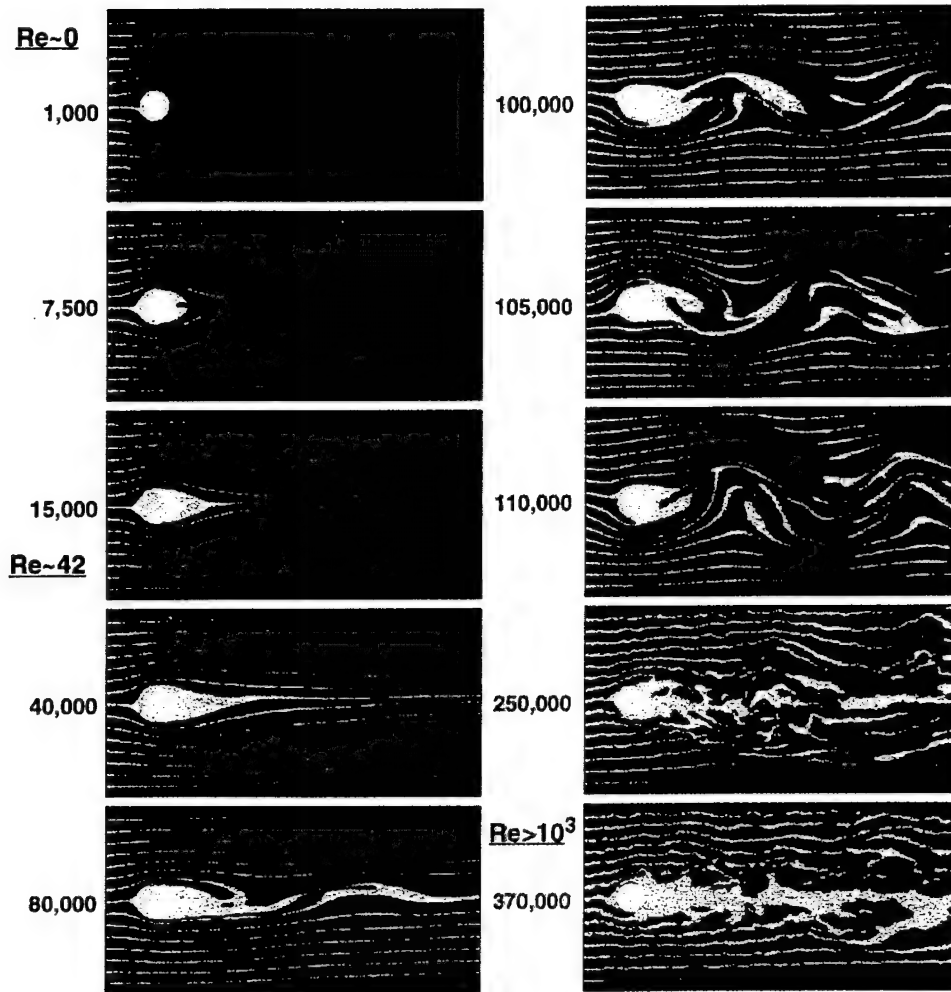


Figure 6.5: Simulation on the CAM-8 prototype of flow past a cylinder. An $L = 4$ integer lattice gas on a triangular lattice using a four channel sampling algorithm on a 2048×1024 lattice was used. Time series plots from laminar flow, $Re = 0$, through the vortex shedding regime, $Re > 42$, to the chaotic flow regime, $Re > 10^3$ are shown. Fluid streamlines are illustrated using a liquid tracer fluid (an $L = 1$ long range lattice gas) with no coarse-graining. The first frame shown is at $t = 1000$ and the last frame is at $t = 370,000$. The gas is at rest at $t = 0$, $v = 0$, and is accelerated linearly to $v = 0.4c$ at $t = 370,000$. The diameter of cylindrical obstacle is $d = 128$. The critical Reynolds number for vortex shedding, $Re = 42$, occurs at approximately $t \sim 40,000$. The maximum Reynolds number achieved in simulation is $Re \sim 1000$.

Chapter 7

Conclusion

7.1 Discussion

In this volume I have given a self-contained review of the foundations of the lattice gas subject. Therefore, this volume will serve as the basis for more advanced lattice gas applications treated subsequently. I have included enough material for the reader to understand how viscous hydrodynamic systems can be modeled by this discrete particle dynamics on a crystallographic spacetime lattice using only local collisions and streaming. This is ideally suited to parallel computation and even offers a paradigm for a new fine-grained parallel computing architecture, which has taken the form of the CAM-8 prototype lattice gas machine used to carry out the computations presented in this volume.

I have given a brief history of the subject and have tried to explain my motivation for working with lattice gases, including the conceptual simplicity and the inherent efficiency beyond continuum molecular dynamics. I have introduced this discrete lattice based formalism by telescoping upwards in scale from the microscopic domain of a discrete transport equation, to the mesoscopic domain of the lattice Boltzmann equation, up to the viscous and incompressible Navier-Stokes equation in the macroscopic

domain. I have shown that all the coefficients in the Chapman-Enskog expansion, used as a bridge between mesoscopic and macroscopic regimes, are completely determined, including the shear viscosity transport coefficient. Consequently, the lattice gas particle dynamics are completely defined by the geometry of the spacetime lattice.

I used lattice-tensors, formed by products of the lattice vectors summed over all lattice directions and have shown that when these lattice-tensors are isotropic the correct macroscopic equation of motion ensues. The choice of lattice is the triangular lattice in two dimensions and the face centered hypercubic lattice projected onto three dimensions since in these cases the lattice-tensors are isotropic. Given a lattice, all the properties of the system were fixed.

The form of the macroscopic hydrodynamics is determined by the invariants of the dynamics: mass, momentum, and energy. Therefore, the lattice gas method is a first principles description of fluid dynamics. Yet I believe it will find its greatest application in various generalized forms not treated in this volume, in particular: first the generalization to include nonlocal interparticle interaction so that complex hydrodynamics can be modeled at scales beyond that achieved by a traditional molecular dynamics treatment; and second the generalization to lattice based quantum computations where quantum behavior can be numerically captured that is otherwise impossible by classical means. These two generalization of the lattice gas methodology presented here each deserve their own place and so volume II treats multiphase fluids and volume III treats quantum fluids.

Nevertheless, a contribution of this first volume to lattice gas theory is a statistical mechanics treatment of lattice gases that is based on a grand partition function for the system. In this first volume, the main result is a generalization of a Boolean lattice gas

to an integer lattice gas. By this generalization to the integer case, Galilean invariance is restored and a slight reduction in viscosity is achieved. Moreover, there is significant reduction in noisy density fluctuations. These gains are important to a community interested in modeling for quantitative purposes. And finally, the integer lattice gas retains detailed-balance in its collisions, and in turn, so does its total dynamics. One achievement presented in here is the mean-field calculation of the shear viscosity of an integer lattice gas that is done in arbitrary dimensions. Verification of the prediction is by comparison with exact numerical experiment, where the kinematic viscosity of an $L = 2$ integer lattice gas fluid is measured on the CAM-8.

At the outset of my exploration of the integer lattice gas system, I had hoped that a natural cross-over from Fermi-Dirac statistics to Bose-Einstein statistics would be seen by going from the $L = 1$ limit to the infinite L limit. Remarkably, this hope has in fact been realized. The Bose-Einstein distribution function is indeed recovered in the $L = \infty$ limit. The statistics of integers is interesting in this context, and the fractional distribution function is representable in simple closed form. In Volume II, lattice-gas statistical mechanics is very useful since it allows us to perform a Mayer cluster expansion of the equilibrium pressure and consequently perturbatively determine the equation of state for a nonideal lattice gas fluid.

7.2 Summary of Lattice Gas Systems for Viscous Fluids

7.2.1 Classical Integer Lattice Gas

$$n'_a(\vec{x} + \ell \hat{e}_a, t + \tau) = n_a(\vec{x}, t) + \Omega_a[\vec{n}(\vec{x}, t)],$$

for momentum directions $a = 1, \dots, B$ where the occupation variable is

$$n_a = \sum_{l=0}^{L-1} 2^l n_{al},$$

and the collision operator is

$$\Omega_a = \sum_{l=0}^{L-1} 2^l \Omega_{al}.$$

7.2.2 Multispeed Lattice Gas

$$n_a^\sigma(\vec{x} + \ell \vec{e}_a^\sigma, t + \tau) = n_a^\sigma(\vec{x}, t) + \Omega_a^\sigma(\vec{n}(\vec{x}, t)). \quad (7.1)$$

for momentum directions $a = 1, \dots, B$ and speeds $\sigma = 0, 1, \dots, M$.

References

- [1] B.J. Alder and T.E. Wainwright. Velocity autocorrelations for hard spheres. *Physical Review Letters*, 18(23):988–990, 1967.
- [2] Frank J. Alexander, Shiyi Chen, and J.D. Sterling. Lattice boltzmann thermohydrodynamics. *Physical Review E*, 47(4):R2249–R2252, 1993.
- [3] Cécile Appert, Daniel Rothman, and Stéphane Zaleski. A liquid-gas model on a lattice. In Gary D. Doolean, editor, *Lattice Gas Methods: Theory, Applications, and Hardware*, pages 85–96. Special Issues of Physica D, MIT/North Holland, 1991.
- [4] Cécile Appert and Stéphane Zaleski. Lattice gas with a liquid-gas transition. *Physical Review Letters*, 64:1–4, 1990.
- [5] Cécile Appert and Stéphane Zaleski. Dynamical liquid-gas phase transition. *Journal de Physique II*, 3:309–337, 1993.
- [6] Gregory L. Baker and Jerry P. Gollub. *Chaotic Dynamics an introduction*. Cambridge University Press, 1990.
- [7] Adriano Barenco, Charles H. Bennett, Richard Cleve, David P. DeVincenzo, Norman H. Margolus, Peter W. Shor, Tycho Sleator, John Smolin, and Harald Weinfurter. Elementary gates for quantum computation. *Physical Review A*, 52(5):3457–3467, 1995.
- [8] Charles H. Bennett. Logical reversibility of computation. *IBM Journal of Research and Development*, 6:525–532, 1979.
- [9] Charles H. Bennett. Thermodynamics of computation—a review. *International Journal of Theoretical Physics*, 21:219–253, 1982.
- [10] P.L. Bhatnager, E.P. Gross, and M. Krook. A model for collision processes. in gases. i. small amplitude processes in charged and neutral one-component systems. *Physical Review*, 94(3):511–525, 1954.

- [11] Michael Biafore. Cellular automata for nanometer-scale computation. *Physica D*, 70(3/4), 1994.
- [12] Bruce M. Boghosian. Correlations and renormalization in lattice gases. *Physical Review E*, 1994. To appear.
- [13] Bruce M. Boghosian. Correlations and renormalization in lattice gases. *Physical Review E*, 52(1), July 1995. comp-gas/9403003.
- [14] Bruce M. Boghosian. Lattice gases illustrate the power of cellular automata in physics. *Computers in Physics*, 5(6), Nov/Dec 1991.
- [15] Bruce M. Boghosian, Peter V. Coveney, and Andrew N. Emerton. A lattice-gas model of microemulsions. *Proceedings of the Royal Society*, 1996. To appear, comp-gas/9507001.
- [16] Bruce M. Boghosian and Washington Taylor IV. A quantum lattice-gas model for the many-particle schrodinger equation. *Submitted to Physical Review*, 1996. quant-ph/9604035.
- [17] Bruce M. Boghosian, Jeffrey Yepez, Francis J. Alexander, and Norman H. Margolus. Integer lattice gas. *Physical Review E*, To appear 1997. comp-gas/9602001.
- [18] R. Brito and M.H. Ernst. Lattice gases in slab geometries. *Physical Review A*, 44(12):8384–8687, 1991.
- [19] R. Brito and M.H. Ernst. Ring kinetic theory for tagged-particle problems in lattice gases. *Physical Review A*, 46(2):875–887, 1992.
- [20] Christopher Burges and Stéphane Zaleski. Buoyant mixtures of cellular automaton gases. *Complex Systems*, 1:31–50, 1987.
- [21] Giorgio Careri. *Order And Disorder In Matter*. The Benjamin/Cummings Publishing Company, 1984.

- [22] Hudong Chen, Shiyi Chen, Gary D. Doolen, Y.C. Lee, and H.A. Rose. Multithermodynamic phase lattice-gas automata incorporating interparticle potentials. *Physical Review A*, 40(5):2850–2853, 1989. Rapid Communications.
- [23] Hudong Chen, Shiyi Chen, and William H. Matthaeus. Recovery of the navier-stokes equations using a lattice-gas boltzmann method. *Physical Review A*, 45(8):R5339–R5342, 1992.
- [24] Hudong Chen and William H. Matthaeus. New cellular automaton model for magnetohydrodynamics. *Physical Review Letters*, 58(18):1845–1848, 1987.
- [25] Hudong Chen and William H. Matthaeus. An analytic theory and formulation of a local magnetohydrodynamic lattice gas model. *Physics of Fluids*, 31(6):1439–1455, 1988.
- [26] S. Chen, G.D. Doolean, K. Eggert, D. Grunau, and E.Y. Loh. Local lattice-gas model for immiscible fluids. *Physical Review A*, 43(12):7053–7056, 1991.
- [27] Shiyi Chen, Hudong Chen, Gary D. Doolen, Semion Gutman, and Minxu Lee. A lattice gas model for thermohydrodynamics. *Journal of Statistical Physics*, 62(5/6):1121–1151, 1991.
- [28] Shiyi Chen, Hudong Chen, Daniel Martínez, and William Matthaeus. Lattice boltzmann model for simulation of magnetohydrodynamics. *Physical Review Letters*, 67(27):3776–3779, 1991.
- [29] Shiyi Chen, Karen Diemer, Gary D. Doolen, and Kenneth Eggert. Lattice gas automata for flow through porous media. In Gary D. Doolean, editor, *Lattice Gas Methods: Theory, Applications, and Hardware*, pages 72–84. Special Issues of Physica D, MIT/North Holland, 1991.
- [30] E.G.D. Cohen. The kinetic theory of fluids—an introduction. *Physics Today*, pages 64–73, January 1984.
- [31] David G. Cory, Amr F. Fahmy, and Timothy F. Havel. Ensemble quantum computing by nuclear magnetic resonance spectroscopy. Technical report tr-10-96, Harvard University Center for Research in Computing Technology, Aiken

Computation Laboratory, 33 Oxford Street, Cambridge, MA 02138, December 1996.

- [32] D. Dab and Anna Lawniczak. Cellular automaton model for reactive systems. *Physical Review Letters*, 64:2462–2465, 1990.
- [33] P.G. Drazin and W.H. Reid. *Hydrodynamic Stability*. Cambridge University Press, 1981.
- [34] Artur Ekert and Richard Jozsa. Quantum computation and shor's factoring algorithm. *Reviews of Modern Physics*, 68(3):733–753, 1996.
- [35] M.H. Ernst and Shankar P. Das. Thermal cellular automata fluids. *Journal of Statistical Physics*, 66(1/2):465–483, 1992.
- [36] M.H. Ernst and Shankar P. Das. Thermal cellular automata fluids. *Journal of Statistical Physics*, 66(1/2):465–483, 1992.
- [37] M.H. Ernst, E.H. Hauge, and J.M.M van Leeuwen. Asymptotic time behavior of correlation functions. *Physical Review Letters*, 25(18):1254–1256, 1970.
- [38] Richard P. Feynman. Simulating physics with computers. *International Journal of Theoretical Physics*, 21(6/7):467–488, 1982.
- [39] Richard P. Feynman. Quantum mechanical computers. *Optics News*, 11(2):11–20, 1985.
- [40] Edward Fredkin and Tommaso Toffoli. Conservative logic. *International Journal of Theoretical Physics*, 21(3/4):219–253, 1982.
- [41] Uriel Frisch, Dominique d'Humières, Brosl Hasslacher, Pierre Lallemand, Yves Pomeau, and Jean-Pierre Rivet. Lattice gas hydrodynamics in two and three dimensions. *Complex Systems*, 1:649–707, 1987.
- [42] Uriel Frisch, Brosl Hasslacher, and Yves Pomeau. Lattice-gas automata for the navier-stokes equation. *Physical Review Letters*, 56(14):1505–1508, 1986.

- [43] I.S. Gradshteyn and I.M. Ryzhik. *Table of Integrals, Series, and Products*. Academic Press, Orlando, Florida 32887, alan jeffrey corrected and enlarged edition, 1980.
- [44] P. Grosfils, J.P. Boon, and P. Lallemand. 19-bit thermal lattice-gas automaton. *Journal of Statistical Physics*, 1993.
- [45] Daryl Grunau, Shiyi Chen, and Kenneth Eggert. A lattice boltzmann model for multiphase fluid flows. *Physics of Fluids A*, 5(10):2557–2562, 1993.
- [46] Andrew K. Gustensen and Daniel H. Rothman. A galilean-invariant immiscible lattice gas. *Physica*, D(47):53–63, 1991.
- [47] Andrew K. Gustensen and Daniel H. Rothman. A lattice-gas model for three immiscible fluids. *Physica*, D(47):47–52, 1991.
- [48] J. Hardy, O. de Pazzis, and Y. Pomeau. Molecular dynamics of a classical lattice gas: Transport properties and time correlation functions. *Physical Review A*, 13(5):1949–1961, 1976.
- [49] Detlef Heitmann and Jorg P. Kotthaus. The spectroscopy of quantum dot arrays. *Physics Today*, 46(6):56–63, 1993.
- [50] Michel Hénon. Viscosity of a lattice gas. In Gary D. Doolean, editor, *Lattice Gas Methods for Partial Differential Equations*, pages 179–207. Santa Fe Institute, Addison-Wesley Publishing Company, 1990.
- [51] Washington Taylor IV and Bruce M. Boghosian. Renormalization of lattice gas transport coefficients. Technical Report Series TMC-208, Thinking Machines Corporation, September 1991. Also presented by Boghosian at the International Conference on Pattern Formation and Lattice-Gas Automata, June 1993.
- [52] Leo P. Kadanoff, Guy R. McNamara, and Gianluigi Zanetti. A poiseuille viscometer for lattice gas automata. *Complex Systems*, 1:709–803, 1987.

- [53] Ray Kapral and Anna Lawniczak. Bibliography for special 1994 lattice gas issue of the fields institute series. In Ray Kapral and Anna Lawniczak, editors, *Proceedings of the Pattern Formation and Lattice-Gas Automata NATO Advanced Research Workshop*. Fields Institute for Research in Mathematical Sciences, American Mathematical Society, 1993.
- [54] Ray Kapral, Anna Lawniczak, and P. Masiar. Oscillations and waves in a reactive lattice-gas automaton. *Physical Review Letters*, 66:2539–2542, 1991.
- [55] George Em Karniadakis and Steven A. Orszag. Nodes, modes and flow codes. *Physics Today*, 46(3):34–42, 1993.
- [56] T.R. Kirkpatrick and M.H. Ernst. Kinetic theory for lattice-gas cellular automata. *Physical Review A*, 44(12):8051–8061, 1991.
- [57] L.D. Landau and E.M. Lifshitz. *Fluid Mechanics*, volume 6 of *Course of Theoretical Physics*. Pergamon Press, 2nd edition, 1987.
- [58] Anna Lawniczak, D. Dab, and Ray Kapral. Reactive lattice-gas automata. *Physica D*, 47:132–138, 1991.
- [59] Chihwen Li and Chwan-Hwa Wu. A particle-in-cell fluid model for radio frequency glow discharges. *Computers in Physics*, 7(3):363–375, 1993.
- [60] Richard L. Liboff. *Introduction to the Theory of Kinetic Equations*. Robert E. Krieger Publishing Company, 1979.
- [61] Seth Lloyd. A technologically feasible quantum computer. Complex System Group T-13, Los Alamos National Laboratory, Preprint.
- [62] Norman Margolus. Physics-like models of computation. *Physica*, 10D:81–95, 1984.
- [63] Norman Margolus. Parallel quantum computation. In W.H. Zurek, editor, *Complexity, Entropy, and the Physics of Information, SFI Studies in the Sciences of Complexity, vol. VIII*, pages 273–287. Addison-Wesley, 1990.

- [64] Norman Margolus. Cam-8: a computer architecture based on cellular automata. *American Mathematical Society*, 6, 1996. Fields Institute Communications.
- [65] Norman Margolus and Tommaso Toffoli. Cellular automata machines. In Gary D. Doolean, editor, *Lattice Gas Methods for Partial Differential Equations*, pages 219–249. Santa Fe Institute, Addison-Wesley Publishing Company, 1990. The first 8-module CAM-8 prototype was operational in the fall of 1992.
- [66] Norman Margolus, Tommaso Toffoli, and Gérard Vichniac. Cellular-automata supercomputers for fluid-dynamics modeling. *Physical Review Letters*, 56(16):1694–1696, 1986.
- [67] Danial O. Martinez, Shiyi Chen, and William H. Matthaeus. Lattice boltzmann magnetohydrodynamics. *Physics of Plasmas*, 1(6):1850–1867, 1994.
- [68] Danial O. Martinez, William H. Matthaeus, Shiyi Chen, and Dave Montgomery. Comparison of spectral method and lattice boltzmann simulations of two-dimensional hydrodynamics. *Physics of Fluids*, 6(3):1285–1298, 1994.
- [69] Guy R. McNamara and Gianluigi Zanetti. Use of the boltzmann equation to simulate lattice-gas automata. *Physical Review Letters*, 61(20):2332–2335, 1988.
- [70] Christiane Normand and Yves Pomeau. Convective instability: A physicist's approach. *Reviews of Modern Physics*, 49(3):581–624, 1977.
- [71] A.J.H. Ossendrijver, A. Santos, and M.H. Ernst. Lattice gases with static disorder: Renormalization of mean field theory. *Journal of Statistical Physics*, 71(5/6):1015–1042, 1993.
- [72] Norman H. Packard and Stephen Wolfram. Two-dimensional cellular automata. *Journal of Statistical Physics*, 38(5/6):901–946, 1985.
- [73] Yves Pomeau. A new kinetic theory for a dense classical gas. *Physics Letters*, 27A(9):601–602, 1968.

- [74] J.P. Rivet and U. Frisch. Lattice gas automata in the boltzmann approximation. *Comptes Rendus*, 302(II):p. 267, 1986. In French. Translation appears in *Lattice Gas Methods for Partial Differential Equations*, SFI SISOC, Eds. Doolen et al., Addison-Wesley Publishing Co., 1990.
- [75] Daniel Rothman. Macroscopic laws for immiscible two-phase flow in porous media: results from numerical experiments. *Journal of Geophysical Research*, 95:8663, 1990.
- [76] Daniel H. Rothman. Negative-viscosity lattice gases. *Journal of Statistical Physics*, 56(3/4):517–524, 1989.
- [77] Daniel H. Rothman and Stéphane Zaleski. Lattice-gas models of phase separation: interfaces, phase transitions, and multiphase flow. *Reviews of Modern Physics*, 1994.
- [78] Xiaowen Shan and Hudong Chen. Lattice boltzmann model for simulating flows with multiple phases and components. *Physical Review E*, 47(3):1815–1819, 1993.
- [79] Xiaowen Shan and Hudong Chen. Simulation of nonideal gases and liquid-gas phase transitions by the lattice boltzmann equation. *Physical Review E*, 49(4):2941–2948, 1994.
- [80] Tsutomu Shimomura, Gary D. Doolen, Brosl Hasslacher, and Castor Fu. Calculations using lattice gas techniques. In Gary D. Doolean, editor, *Lattice Gas Methods for Partial Differential Equations*, pages 3–9. Santa Fe Institute, Addison-Wesley Publishing Company, 1990.
- [81] Peter W. Shor. Algorithms for quantum computation: Discrete log and factoring. Private communication, 1994.
- [82] Peter W. Shor. Polynomial-time algorithms for prime factorization and discrete logarithms on a quantum computer. In *Proceedings of the 35th Annual Symposium on Foundations of Computer Science*, pages 124–134. Santa Fe, NM, IEEE Computer Society Press, 1994.

- [83] J.A. Somers and R.C. Rem. The construction of efficient collision tables for fluid flow computations with cellular automata. In P. Manneville, N. Boccara, G.Y. Vichniac, and R. Bidaux, editors, *Cellular Automata and Modeling of Complex Physical Systems*, pages 161–177. Springer-Verlag, February 1989. Proceedings of the Winter School, Les Houches, France.
- [84] Sauro Succi. Lattice boltzmann equation for quantum mechanics. *Physica D*, 69:327–332, 1993.
- [85] Sauro Succi. Numerical solution of the schrodinger equation using discrete kinetic theory. *Unpublished*, 1996.
- [86] Christopher Teixeira. *Continuum Limit Of Lattice Gas Fluid Dynamics*. PhD thesis, Massachusetts Institute of Technology, Department of Nuclear Engineering, 1992. Kim Molvig Thesis Supervisor.
- [87] TMC. *C* Programming Guide*. Thinking Machines Corporation, Cambridge, Massachusetts USA, 1990. Version 6.0.
- [88] Tommaso Toffoli. Computation and construction universality of reversible cellular automata. *Journal of Computer and System Sciences*, 15(2):213–231, 1977.
- [89] Tommaso Toffoli. Cam: A high-performance cellular-automaton machine. *Physica*, 10D:195–204, 1984. A demonstration TM-gas experiment was part of the CAMForth software distribution.
- [90] Tommaso Toffoli. Cellular automata as an alternative to (rather than an approximation of) differential equations in modeling physics. *Physica*, 10D:117–127, 1984.
- [91] Tommaso Toffoli. Fine-grained parallel supercomputer. Technical report PL-TR-95-2013, Phillips Laboratory, Contract No. F196828-94-C-0068 Step Research 26 Athens Street, Cambridge, MA 02138, November 1994.
- [92] Tommaso Toffoli and Norman Margolus. *Cellular Automata Machines*. MIT Press Series in Scientific Computation. The MIT Press, 1987.

- [93] René van Roij. Ring kinetic theory of the boghosian-levermore cellular automaton. Master's thesis, Institute for Theoretical Physics University of Utrecht, August 1992. Supervisor: Prof M.H. Ernst.
- [94] Gerard Y. Vichniac. Simulating physics with cellular automata. *Physica*, 10D:96–116, 1984.
- [95] Stephen Wolfram. Statistical mechanics of cellular automata. *Reviews of Modern Physics*, 55(3):601–644, 1983.
- [96] Stephen Wolfram. Universality and complexity in cellular automata. *Physica*, 10D:1–35, 1984.
- [97] Stephen Wolfram. Cellular automaton fluids 1: Basic theory. *Journal of Statistical Physics*, 45(3/4):471–526, 1986.
- [98] Stephen Wolfram and James B. Salem. Thermodynamics and hydrodynamics with cellular automata. In Stephen Wolfram, editor, *Theory and Applications of Cellular Automata*, pages 362–365. World Scientific, 1986. Submitted November 1985.
- [99] Jeffrey Yepez. Lattice-gas crystallization. *Journal of Statistical Physics*, 81(1/2):255–294, 1994.
- [100] Jeffrey Yepez. Lattice gas dynamics: Volume 1 viscous fluids. Technical report PL-TR-96-2122(I), Air Force Research Laboratory, AFRL/VSBE Hanscom AFB, MA 01731, October 1995.
- [101] Jeffrey Yepez. Long-range lattice-gas simulation on the cam-8 prototype. Technical report PL-TR-95-2132, Phillips Laboratory, PL/GPA Hanscom AFB, MA 01731, September 1995.
- [102] Jeffrey Yepez. Lattice gas dynamics: Volume 2 multiphase fluids. Technical report PL-TR-96-2122(II), Air Force Research Laboratory, AFRL/VSBE Hanscom AFB, MA 01731, November 1996. Currently in draft.

- [103] Jeffrey Yepez. Lattice gas dynamics: Volume 3 quantum fluids. Technical report PL-TR-96-2122(III), Air Force Research Laboratory, AFRL/VSBE Hanscom AFB, MA 01731, November 1996. Currently in draft.
- [104] Jeffrey Yepez. A lattice-gas with long-range interactions coupled to a heat bath. *American Mathematical Society*, 6:261–274, 1996. Fields Institute Communications.
- [105] Jeffrey Yepez. Lattice gas for superfluid helium ii. *International Journal of Theoretical Physics*, Submitted 1996. Presented at the Sixth International Conference on Discrete Models for Fluid Mechanics, Boston University Center for Computational Science, August 1996.
- [106] Jeffrey Yepez, Guy P. Seeley, and Norman Margolus. Lattice-gas automata fluids on parallel supercomputers. 1993. Los Alamos Archive: Comp-Gas.
- [107] Jeffrey Yepez, Guy P. Seeley, and George Mou. Lattice-gas automata on parallel architectures. In *Proceedings of International Symposium on Parallel Computation*, pages 522–525, 1993. Beijing, China.

Appendix A

The Cellular Automata Machine CAM-8

To better understand the lattice gas paradigm as a possible computing architecture, a prototype machine has been constructed, called the cellular automata machine CAM-8 and is shown in figure A.1. The CAM-8 architecture [65, 64] is the latest in a line of cellular automata machines developed by the Information Mechanics Group at MIT [89, 92, 66]. The CAM-8 architecture itself is a simple digital electronic realization of the lattice gas scheme, and in the early 1990's was tested against other parallel supercomputers and is optimal at performing lattice gas simulations [107]. Lattice gas data streaming and collisions are directly implemented in the architecture.

One can think of the discrete memory space within the CAM-8 as an artificial microworld. This provides several compelling opportunities. First of all, the discrete microworld paradigm with simple local rules governing the system's evolution made it quite straightforward to construct the fine-grained parallel CAM-8 out of elementary "chunks".¹ Figure A.2 is a schematic diagram of a CAM-8 system. On the left is a

¹An expanded machine, called the CAM-8-64 [91], in 1994 was designed to incorporate a billion sites using the standard CAM-8 module. A new design using RAMBus memory chips and field programmable gate arrays has recently been completed by Margolus and is two orders of magnitude

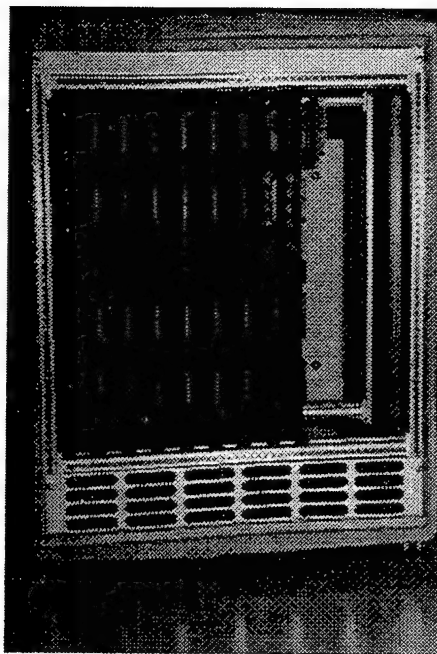


Figure A.1: MIT Laboratory for Computer Science cellular automata machine CAM-8. This 8 module prototype can evolve a D-dimensional cellular space with 32 million sites where each site has 16 bits of data with a site update rate of 200 million per second. The communication network is a Cartesian three-dimensional mesh. Crystallographic lattice geometries can be directly embedded into the CAM-8.

single hardware module—the elementary “chunk” of the architecture. On the right is an indefinitely extendable array of modules (in the CAM-8 prototype the array is actually three-dimensional). A uniform spatial calculation is divided up evenly among these modules, with each module containing a volume of 16 million lattice sites. These sites are scanned in a sequential pipelined fashion. In the diagram, a solid lines between modules indicates a local *mesh* interconnection. These wires are used for spatial data movements.²

faster than the CAM-8.

²There is also a tree network (not shown) connecting all modules to the front-end host, a SPARC workstation with a custom SBus interface card, that controls the CAM-8. It downloads a bit-mapped

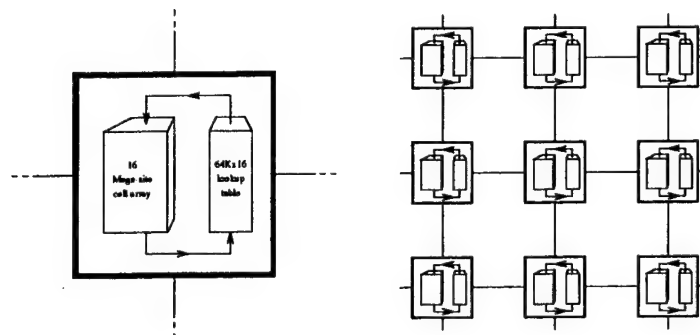


Figure A.2: CAM-8 system diagram. (a) A single processing node, with DRAM site data flowing through an SRAM lookup table and back into DRAM. (b) Spatial array of CAM-8 nodes, with nearest-neighbor (mesh) interconnect (1 wire/bit-slice in each direction).

The CAM-8 uses custom VLSI chips to control data movement and commodity dynamics random access memory (DRAM) to store its state data. Each site of the lattice has 16 bits (or a multiple thereof). A 16-bit lattice site is also referred to as a *cell*. Each bit of a cell is part of an entire bit plane of the lattice which is stored in a single DRAM chip. Therefore, a bit plane can be “translated” through the lattice arbitrarily by off-setting the pointer to the zeroth memory address in the DRAM chip. The translation vectors for the bit planes are termed *kicks*. The specification of the x,y, and z components of the kicks for each bit plane (or hyperplane) defines the lattice geometry. The kicks can be changed during the simulation. Thus, the data movement in the CAM-8 is quite general. Once the kicks are specified, the coding of

pattern as the initial condition for the simulations. It also sends a “step-list” to the CAM-8 to specify the sequence of kicks and scans that evolve the lattice gas in time. One can view the lattice gas simulation in real-time since a custom video module captures site data for display on a VGA monitor, a useful feature for lattice gas algorithm development, test and evaluation. The CAM-8 has built-in 25-bit event counters allowing real-time measurements without slowing the lattice gas evolution. This feature is used to do real-time coarse-grain block averaging of the occupation variables and to compute the components of the momentum vectors for each block. The amount of coarse-grained data is sufficiently small to be transferred back to the front-end host for graphical display as an evolving flow field within an X-window.

the lattice gas streaming is completed. In effect, the kicks determine all the global permutations of the data.

The CAM-8 runs through its discrete dynamics with absolutely no round-off error so that in a lattice gas simulation all additive conserved quantities are kept exactly fixed throughout the course of a simulation. Its processors are ultimately simple, each able to act on only a small number of bits of information at a time. This is sufficient for a classical lattice gas algorithm that only permutes bits, never creating or destroying bits of information, just shuffling them about. Permutations achieve particle-conserving reversible dynamics and are used in all classical lattice gas implementations on the CAM-8. Local permutations of data occur within the cells. These permutations are the computational metaphor for physical collisions between particles. The CAM-8 uses commodity static random access memory (SRAM) to store all the local state transitions, or local rules.³

Within a CAM-8 classical lattice gas simulation, all information is exactly preserved in time, and as a consequence of this fact, at any point in a simulation one can decide to reverse the computation: the state of the artificial microworld evolves back to its initial state. Therefore the dynamics has a time-reversal invariance, or in other words, the algorithm is logically invertible. Because of algorithm reversibility, CAM-8 lattice gas simulations are unconditionally stable, since transitions from one state to the next are unitary operations. Unconditional stability in a numerical treatment is

³All local permutations are implemented in look-up tables. All possible physical events with a certain input configuration and a certain output configuration are precomputed and stored in SRAM, for fast table look-up. The width of the CAM-8 look-up tables is 16-bits, or 64K entries. This is a reasonable width satisfying the opposing considerations of model complexity versus memory size limitations for the SRAM. Site permutations of data wider than 16-bits must be implemented in several successive table look-up passes. Since the look-up tables are double buffered, a scan of the space can be performed while a new look-up table is loaded for the next scan.

a highly valuable and desirable characteristic. Yet the CAM-8, which is a classical computer, is it not limited to performing only unitary operations on its 16-bit cell (*i.e.* permutations), it can do general mappings which are irreversible. Therefore, the CAM-8 dissipates heat like any conventional computer, but an optimal lattice gas computer would dissipate no heat as it processed through its simulation.

Appendix B

Discrete Mathematics for Lattice Calculations

B.1 Discrete Fourier Transform

Since a discrete Fourier transform is used in the course of the development in the text of this dissertation, we review it in this appendix for completeness. Consider a quantity $A(\vec{x})$ defined over the entire lattice. The discrete transform and its inverse in one dimension are

$$A(k_n) = \frac{1}{\sqrt{V}} \sum_{\{x_l\}} e^{ik_n x_l} A(x_l) \quad (\text{B.1})$$

$$A(x_n) = \frac{1}{\sqrt{V}} \sum_{\{k_l\}} e^{-ik_l x_n} A(k_l). \quad (\text{B.2})$$

The possible k -vectors are $k_n = 2n\pi/V\ell$ and the lattice vectors are $x_n = \ell n$, where $n = 1, \dots, V$ and ℓ is the cell size. The generalization to D dimensions is straightforward.

Inserting (B.2) into (B.1) gives

$$A(k_n) = \frac{1}{\sqrt{V}} \sum_{\{x_l\}} e^{ik_n x_l} \left[\frac{1}{\sqrt{V}} \sum_{\{k_m\}} e^{-ik_m x_l} A(k_m) \right] \quad (\text{B.3})$$

$$= \sum_{\{k_m\}} A(k_m) \left[\frac{1}{V} \sum_{\{x_l\}} e^{i(k_n - k_m)x_l} \right] \quad (\text{B.4})$$

For the R.H.S. of this last expression to equal $A(k_n)$, the quantity in brackets must be a Kronecker delta. Therefore, the resolution of the identity is

$$\frac{1}{V} \sum_{\{x_l\}} e^{i(k_n - k_m)x_l} = \delta_{nm}. \quad (\text{B.5})$$

Similarly, inserting (B.1) into (B.2) gives

$$A(x_n) = \frac{1}{\sqrt{V}} \sum_{\{k_l\}} e^{-ik_l x_n} \left[\frac{1}{\sqrt{V}} \sum_{\{x_m\}} e^{ik_l x_m} A(x_m) \right] \quad (\text{B.6})$$

$$= \sum_{\{x_m\}} A(x_m) \left[\frac{1}{V} \sum_{\{k_l\}} e^{ik_l(x_m - x_n)} \right]. \quad (\text{B.7})$$

Again, for the R.H.S. of this last expression to equal $A(x_n)$, the quantity in brackets must be a Kronecker delta. Therefore, the resolution of the identity is

$$\frac{1}{V} \sum_{\{k_n\}} e^{ik_n(x_m - x_n)} = \delta_{mn}. \quad (\text{B.8})$$

B.2 Integration by Parts on a Lattice

We will need the following theorem for the discrete analog of integration by parts in calculus.

Theorem: INTEGRATION BY PARTS ON A LATTICE.

The sum over the product of two quantities where one of the quantities is differentiated is equal to minus the sum over the product of the two quantities where the derivative is exchanged to act on the other quantity, provided that the product vanishes at the outer boundary of the lattice. That is,

$$\sum_{\{\vec{x}\}} \left. \frac{\partial u(\vec{x})}{\partial x_i} \right|_{\vec{x} \text{ on lattice}} v(\vec{x}) = - \sum_{\{\vec{x}\}} u(\vec{x}) \left. \frac{\partial v(\vec{x})}{\partial x_i} \right|_{\vec{x} \text{ on lattice}}. \quad (\text{B.9})$$

Proof:

The theorem follows directly from the theorem of integration by parts in calculus by converting the sum into an integral according to the recipe (2.44) given above

$$\sum_{\{\vec{x}\}} \left. \frac{\partial(uv)}{\partial x_i} \right|_{\vec{x} \text{ on lattice}} = \left[\frac{1}{\ell^3} \int d^D x \frac{\partial(uv)}{\partial x_i} \right]_{\vec{x} \text{ on lattice}} = 0. \quad (\text{B.10})$$

Note that the R.H.S is always equals zero because of periodic boundary conditions,

$$uv|_{\text{at periodic boundary}} = 0. \quad (\text{B.11})$$

Expanding the derivative of the product then gives

$$\left[\frac{1}{\ell^3} \int d^D x \left(\frac{\partial u}{\partial x_i} v + u \frac{\partial v}{\partial x_i} \right) \right]_{\vec{x} \text{ on lattice}} = 0. \quad (\text{B.12})$$

Finally, (2.44) is used again now to convert the integrals back to sums

$$\rightarrow \sum_{\{\vec{x}\}} \left[\left. \frac{\partial u}{\partial x_i} \right|_{\vec{x} \text{ on lattice}} v(\vec{x}) + u(\vec{x}) \left. \frac{\partial v}{\partial x_i} \right|_{\vec{x} \text{ on lattice}} \right] = 0. \quad (\text{B.13})$$

This completes the proof. Q.E.D. \square

B.3 Discrete Green's Function

Let us define a *discrete Green's function* of Poisson's equation, denoted $g(\vec{x}, \vec{x}')$, as follows

$$\frac{\partial^2 g(\vec{x}, \vec{x}')}{\partial x_i^2} = \delta_{xx'}, \quad (\text{B.14})$$

where the Konecker delta, $\delta_{xx'}$, is one if $x = x'$ and zero otherwise. There is an implied summation $\partial^2/\partial x_i^2 = \partial^2/\partial x_1^2 + \dots + \partial^2/\partial x_D^2 = \nabla^2$. A useful reflection symmetry of the Green function is

$$\frac{\partial g(\vec{x}, \vec{x}')}{\partial x_i} = - \frac{\partial g(\vec{x}, \vec{x}')}{\partial x'_i}. \quad (\text{B.15})$$

Note that (B.15) is an expression of the fact that the Green function, which is a scalar, depends only on the separation $x - x'$. Let us see why this is so.

Using (B.2) for the discrete inverse Fourier transform, write the discrete Green function as

$$g(\vec{x}, \vec{x}') = \frac{1}{\sqrt{V}} \sum_{\vec{k}} e^{-i\vec{k} \cdot (\vec{x} - \vec{x}')} g(\vec{k}). \quad (\text{B.16})$$

Inserting (B.16) into (B.14) gives

$$-\frac{1}{\sqrt{V}} \sum_{\vec{k}} k^2 e^{-i\vec{k} \cdot (\vec{x} - \vec{x}')} g(\vec{k}) = \delta_{\vec{x}\vec{x}'}. \quad (\text{B.17})$$

Equating (B.17) with (B.8) implies that the discrete Green function must be of the form ($\vec{k} \neq \vec{0}$)

$$g(\vec{k}) = -\frac{1}{k^2 \sqrt{V}}. \quad (\text{B.18})$$

This is the Green function in k -space. Using (B.1), the Fourier transform of (B.18) gives the desired result for the Green function in x -space

$$g(\vec{x}, \vec{x}') = -\frac{1}{V} \sum_{\vec{k}} \frac{e^{-i\vec{k} \cdot (\vec{x} - \vec{x}')}}{k^2}. \quad (\text{B.19})$$

We do indeed see that $g(\vec{x}, \vec{x}')$ is only a function of the separation distance between \vec{x} and \vec{x}' .

Appendix C

The Parallel C-Star Language on the CM-5: A Network Communications Test

A parallel version of the C-language developed by Thinking Machines Corporation is the C* language[87]. This is a well developed language in spirit very close to its predecessor – it is as concise as the C-language itself. It offers many useful constructs making the coding of algorithms for parallel data very efficient. As typical of most parallel languages, an array operation is handled in a single instruction — for the most part programming loops do not appear in the code. Most parallel computation is achieved by data movement. The geometry of the problem is specified at the onset by defining your the data structure's *shape*. This is usually a D-dimensional array with a certain size in each dimension. The shape definition defines all the needed communication topology for the compiler. It is possible to declare boolean shapes in C*. We have used this feature to encode each bit plane of the lattice-gas. This is a convenient feature of the language making efficient use of memory. Normally, in a lattice-gas code, one must extract and insert individual bits at the lattice sites. The option of working directly with boolean arrays has therefore simplified the coding

effort substantially. If individual elements of a parallel array must be accessed, C* uses the syntax of parallel left indexing. Right indexing of arrays is reserved for its usual C-language meaning. We use right indexed arrays to represent the individual bit planes of the lattice gas.

An example of using a square shape with a lattice size of 1024 and using right indexing for the 6 FHP bit planes is given in the following code fragment

```
#define LATTICE_SIZE 1024
#define PILE_SIZE    6

shape      [LATTICE_SIZE][LATTICE_SIZE]Lattice ;

bool:Lattice  lattice0 [PILE_SIZE], lattice1 [PILE_SIZE] ,
              lattice_next0 [PILE_SIZE], lattice_next1 [PILE_SIZE] ;
```

We have implemented a two-dimensional hexagonal lattice embedded into a three-dimensional mesh. This implementation is isomorphic to our implementation in CAM-Forth on the CAM-8 and GCC/DPEAC on the CM-5. Streaming of pleat 0 and pleat 1 are coded separately. We give a C* code fragment for this embedding. Note that the comments to the right of the lines correspond exactly to the kick components listed in Table 3.1. The C* code for streaming pleat 0 is the following

```
/* 0, 0, 1 */      lattice_next1 [0] = lattice0 [0] ;
/* 0,-1, 1 */      to_torus_dim ( &lattice_next1 [1] , lattice0 [1] , 1, -1 ) ;
/* 0,-1, 0 */      to_torus_dim ( &lattice_next0 [2] , lattice0 [2] , 1, -1 ) ;
/* 1,-1, 1 */      to_torus_dim ( &lattice0 [3] , lattice0 [3] , 0, 1 ) ;
                   to_torus_dim ( &lattice_next1 [3] , lattice0 [3] , 1, -1 ) ;
/* 1, 0, 1 */      to_torus_dim ( &lattice_next1 [4] , lattice0 [4] , 0, 1 ) ;
/* 0, 1, 0 */      to_torus_dim ( &lattice_next0 [5] , lattice0 [5] , 1, 1 ) ;
```

and the likewise, the code for streaming pleat 1 is the following

```
/* -1, 1,-1 */     to_torus_dim ( &lattice1 [0] , lattice1 [0] , 0, -1 ) ;
                   to_torus_dim ( &lattice_next0 [0] , lattice1 [0] , 1, 1 ) ;
/* -1, 0,-1 */     to_torus_dim ( &lattice_next0 [1] , lattice1 [1] , 0, -1 ) ;
/* 0,-1, 0 */      to_torus_dim ( &lattice_next1 [2] , lattice1 [2] , 1, -1 ) ;
/* 0, 0,-1 */      lattice_next0 [3] = lattice1 [3] ;
/* 0, 1,-1 */      to_torus_dim ( &lattice_next0 [4] , lattice1 [4] , 1, 1 ) ;
/* 0, 1, 0 */      to_torus_dim ( &lattice_next1 [5] , lattice1 [5] , 1, 1 ) ;
```

With a few C* lines of code one can completely implement hexagonal lattice-gas streaming. We have used the C* command *to-torus-dim(destination pointer, source, axis, distance)* to shift the bit planes with toroidal boundary conditions. This is an efficient communication routine for sending data in a regular fashion using grid communications. The partitioning of the space between processors is handled completely by the C* compiler. We will see how efficiently the compiler does this partitioning in the discussion to follow.

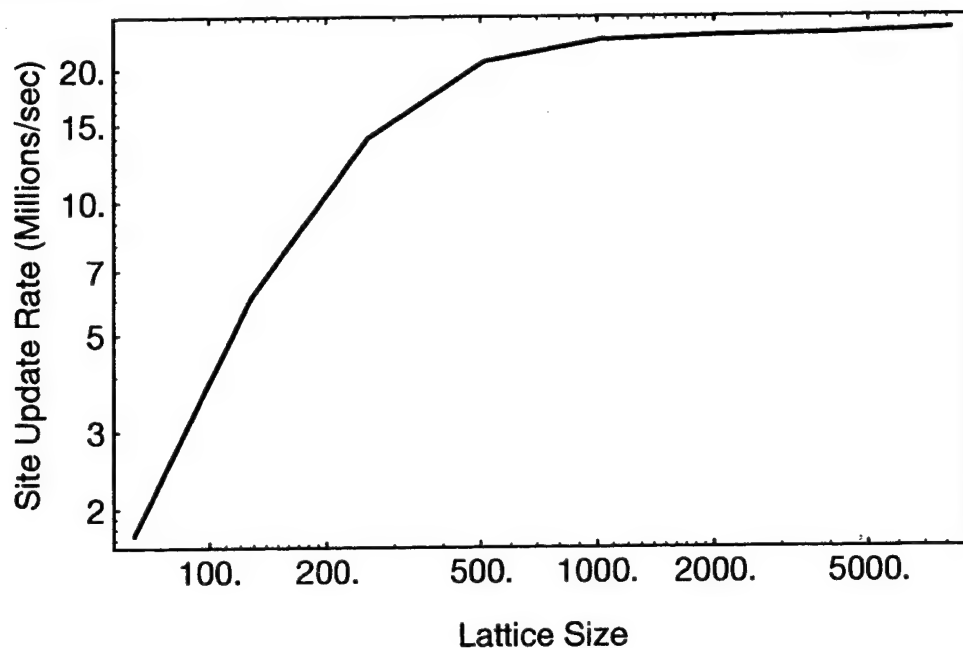


Figure C.1: Performance runs on a 256-node CM-5 for an FHP hexagonal lattice embedded into a 3D mesh. Performance significantly suffers by communication overhead for small lattice sizes.

We have tested our C* implementation for different situations. Given a certain lattice size, for example 1024×2048 , we have found the performance of the CM-5 to vary linearly with the number of processing nodes. This linear variation is expected

so long as the lattice size is sufficiently large. To determine a reasonable lattice size, we have performed repeated simulations with different lattice sizes but with a fixed number of processors. The results obtained for a fixed 256-node partition of the CM-5 is given in figure C.1, in which we plotted simulation site update rates for lattice sizes $64 \times 128, 128 \times 256, \dots, 8192 \times 16384$. For small lattice sizes, the performance is very poor, on the order of a million site updates per seconds. This is because the streaming is limited by processor to processor communication bandwidth. As the lattice size increases, the number of sites interior to the node grows and the number of sites on the partition boundary decreases. Consequently, the site update rate continuously improves with larger lattices. The update rate asymptotically approaches about 25 million site updates per second. This is equivalent to approximately 100,000 site updates per processing node. This is roughly the maximum update rate achievable on a SPARCstation 1. A full 512-node partition has a peak rate of about 50 million site updates per second, which is about one quarter the speed of the CAM-8.

Appendix D

Mach Number Expansion of the Fermi-Dirac Distribution Function

D.1 Expanding the Single-Speed Fermi-Dirac Distribution Function

We begin with the most general form of the single particle distribution function, appropriate for single speed lattice gases: the Fermi-Dirac distribution. Write the distribution as a function of the sum of scalar collision invariants, $\alpha + \beta e_{ai} v_i$, as follows

$$f_a = \frac{1}{1 + e^{\alpha + \beta e_{ai} v_i}}. \quad (\text{D.1})$$

Expand the α and β as follows

$$\alpha = \alpha_0 + \frac{1}{2} \alpha_2 v^2 + \mathcal{O}(v^4) \quad (\text{D.2})$$

$$\beta = \beta_1 + \frac{1}{2} \beta_3 v^2 + \mathcal{O}(v^4). \quad (\text{D.3})$$

A Taylor expansion to fourth order in v_i of (D.1) about zero velocity is the following

$$\begin{aligned}
f_a = d & \quad (D.4) \\
& -d(1-d)\beta_1 e_{ai} \frac{v_i}{c} \\
& -\frac{1}{2}d(1-d)\alpha_2 \frac{v^2}{c^2} \\
& +\frac{1}{2}d(1-d)(1-2d)\beta_1^2 e_{ai} e_{aj} \frac{v_i v_j}{c^2} \\
& -\frac{1}{2}d(1-d)\beta_3 e_{ai} \frac{v_i v^2}{c^3} \\
& +\frac{1}{2}d(1-d)(1-2d)\beta_1 \alpha_2 e_{ai} \frac{v_i v^2}{c^3} \\
& -\frac{1}{6}d(1-d)(1-6d+6d^2)\beta_1^3 e_{ai} e_{aj} e_{ak} \frac{v_i v_j v_k}{c^3} \\
& +O(v^4)
\end{aligned}$$

where $d = f_a|_{v=0}$. The coefficients can be determined by taking the first three moments of the distribution function and equating them to the particle number density ($m \sum_a f_a = \rho$), the momentum density ($mc \sum_a e_{ai} f_a = \rho v_i$) and the moment density flux tensor ($mc^2 \sum_a e_{ai} e_{aj} f_a = \Pi_{ij}$). The zeroth moment of (D.4) is

$$\frac{1}{B} \sum_a f_a = d - \frac{1}{2}d(1-d)\alpha_2 \frac{v^2}{c^2} + \frac{1}{2D}d(1-d)(1-2d)\beta_1^2 \frac{v^2}{c^2} = d \quad (D.5)$$

$$\rightarrow \alpha_2 = \frac{(1-2d)\beta_1^2}{D} \quad (D.6)$$

The first moment of (D.4) is

$$\frac{1}{B} \sum_a e_{ai} f_a = -\frac{1}{D}d(1-d)\beta_1 \frac{v_i}{c} \quad (D.7)$$

$$\begin{aligned}
& +d(1-d) \frac{v_i v^2}{c^3} \left[-\frac{1}{2Dc^2}\beta_3 + \frac{1}{2D}(1-2d)\beta_1 \alpha_2 - \frac{3}{2D(D+2)}(1-6d+6d^2)\beta_1^3 \right] \\
& = d \frac{v_i}{c}. \quad (D.8)
\end{aligned}$$

This implies the following

$$\beta_1 = -\frac{D}{1-d} \quad (\text{D.9})$$

$$\alpha_2 = \frac{D(1-2d)}{(1-d)^2}. \quad (\text{D.10})$$

Substituting these last two expressions into (D.4), causes the ideal part of the lattice gas distribution function to become

$$(f_a^{eq})_{LGA}^{ideal} = \frac{n}{B} + \frac{nD}{cB} e_{ai} v_i + g \frac{nD(D+2)}{2c^2 B} \hat{e}_{ai} \hat{e}_{aj} v_i v_j - g \frac{n(D+2)}{2c^2 B} v^2, \quad (\text{D.11})$$

where

$$g \equiv \frac{D}{D+2} \frac{1-2d}{1-d}. \quad (\text{D.12})$$

The second moment of (D.4) is

$$\begin{aligned} \frac{1}{B} \sum_a e_{ai} e_{aj} f_a^{eq} &= \sum_a e_{ai} e_{aj} d \left[1 - \frac{g}{2} (D+2) \frac{v^2}{c^2} + \frac{g}{2} D(D+2) e_{ak} e_{al} \frac{v_k v_l}{c^2} \right] \\ &= \frac{d}{D} (1 - g \frac{v^2}{c^2}) \delta_{ij} - g d v_i v_j. \end{aligned} \quad (\text{D.13})$$

To summarize, using $\rho = mn$ for the density and $c_s = \frac{c}{\sqrt{D}}$ for the sound speed, the following hold true

$$m \sum_a (f_a^{eq})^{ideal} = \rho \quad (\text{D.14})$$

$$mc \sum_a e_{ai} (f_a^{eq})^{ideal} = \rho v_i \quad (\text{D.15})$$

$$mc^2 \sum_a e_{ai} e_{aj} (f_a^{eq})^{ideal} = \rho c_s^2 (1 - g \frac{v^2}{c^2}) \delta_{ij} + g \rho v_i v_j \quad (\text{D.16})$$

D.2 Single Particle Distribution Function from Symmetry

Begin by expanding the momentum flux density tensor to all the possible products involving the $E^{(n)}$ tensors that contract to a second rank tensor

$$\Pi_{ij} = mc^2 d \left(E_{ij} + \frac{\epsilon^{(1)}}{c} E_{ijk} v_k + \frac{\epsilon_1^{(2)}}{c^2} E_{ijkl} v_k v_l + \frac{\epsilon_2^{(2)}}{c^2} E_{ij} v_k v_k - \frac{\lambda_1^{(2)}}{c} E_{ijkl} \partial_k v_l - \frac{\lambda_2^{(2)}}{c} E_{ij} \partial_k v_k \right), \quad (\text{D.17})$$

where the superscripts on the constants ϵ and λ denote the order of the particular terms. We will see that the tensor expansion (D.17) to fourth-rank in E is sufficient to give the full Navier-Stokes equation. Fix two constants of (D.17) by looking at the trace of the momentum flux tensor which, by (2.105), is proportional to the particle mass density

$$\Pi_{ii} = mc^2 \sum_a f_a = \rho c^2 \quad (\text{D.18})$$

or since by definition $\rho = mn$ reduces to

$$n = d \left(E_{ii} + \frac{\epsilon^{(1)}}{c} E_{iik} v_k + \frac{\epsilon_1^{(2)}}{c^2} E_{iikl} v_k v_l + \frac{\epsilon_2^{(2)}}{c^2} E_{ii} v_k v_k - \frac{\lambda_1^{(2)}}{c} E_{iikl} \partial_k v_l - \frac{\lambda_2^{(2)}}{c} E_{ii} \partial_k v_k \right). \quad (\text{D.19})$$

Using (2.19) and (2.20), then (D.19) becomes

$$n = d \left[B + \left(\frac{\epsilon_1^{(2)}}{c^2} \frac{B}{D} + B \frac{\epsilon_2^{(2)}}{c^2} \right) v_k v_k - \left(\frac{\lambda_1^{(2)}}{c} \frac{B}{D} + B \frac{\lambda_2^{(2)}}{c} \right) \partial_k v_k \right]. \quad (\text{D.20})$$

The last two terms must vanish. This implies the following constraint on the constant coefficients

$$d = \frac{n}{B} \quad (\text{D.21})$$

$$\epsilon_2^{(2)} = -\frac{\epsilon_1^{(2)}}{D} \quad (\text{D.22})$$

$$\lambda_2^{(2)} = -\frac{\lambda_1^{(2)}}{D}. \quad (\text{D.23})$$

Call d the *reduced density*. The form of (D.17) then simplifies to

$$\Pi_{ij} = \frac{\rho c^2}{B} \left[E_{ij} + \frac{\epsilon^{(1)}}{c} E_{ijk} v_k + \frac{\epsilon^{(2)}}{c^2} \left(E_{ijkl} v_k v_l - \frac{1}{D} E_{ij} v_k v_k \right) - \frac{\lambda^{(2)}}{c} \left(E_{ijkl} \partial_k v_l - \frac{1}{D} E_{ij} \partial_k v_k \right) \right]. \quad (\text{D.24})$$

Since $\Pi_{ij} = mc^2 \sum_a e_{ai} e_{aj} f_a$, it immediately follows from (D.24) how to write the equivalent expansion for the single particle distribution function f_a

$$f_a = \frac{n}{B} \left[1 + \frac{\epsilon^{(1)}}{c} e_{ak} v_k + \frac{\epsilon^{(2)}}{c^2} \left(e_{ak} e_{al} v_k v_l - \frac{1}{D} v_k v_k \right) - \frac{\lambda^{(2)}}{c} \left(e_{ak} e_{al} \partial_k v_l - \frac{1}{D} \partial_k v_k \right) \right]. \quad (\text{D.25})$$

It is possible to determine the value of the constant $\epsilon^{(1)}$ by multiplying (D.25) by \hat{e}_a , summing over lattice directions a , and equating the result to (2.106) ($\sum_a e_{ai} f_a = n \frac{v_i}{c}$)

$$\sum_a e_{ai} f_a = \frac{n}{B} \frac{\epsilon^{(1)}}{c} \sum_a e_{ai} e_{ak} v_k = \frac{n \epsilon^{(1)}}{D c} v_i, \quad (\text{D.26})$$

which implies that $\epsilon^{(1)} = D$. Using (2.19) and (2.20), multiplying (D.25) by $e_{ai} e_{aj}$, and summing over lattice directions a , then (D.25) gives us the following

$$\begin{aligned} \sum_a e_{ai} e_{aj} f_a = & \frac{n}{B} \left\{ \frac{B}{D} \delta_{ij} + \frac{\epsilon^{(2)}}{c^2} \left[\frac{B}{D(D+2)} (\delta_{ij} \delta_{kl} + \delta_{ik} \delta_{jl} + \delta_{il} \delta_{kj}) v_k v_l - \frac{B}{D^2} \delta_{ij} v_k v_k \right] - \right. \\ & \left. \frac{\lambda^{(2)}}{c} \left[\frac{B}{D(D+2)} (\delta_{ij} \delta_{kl} + \delta_{ik} \delta_{jl} + \delta_{il} \delta_{kj}) \partial_k v_l - \frac{B}{D^2} \delta_{ij} \partial_k v_k \right] \right\} \end{aligned}$$

or

$$\sum_a e_{ai} e_{aj} f_a = \frac{n}{D} \delta_{ij} + \frac{2n \epsilon^{(2)}}{D(D+2)c^2} \left[v_i v_j - \frac{1}{D} \delta_{ij} v^2 \right] + \frac{2n \lambda^{(2)}}{D(D+2)c} \left[\frac{1}{2} (\partial_i v_j + \partial_j v_i) - \frac{1}{D} \delta_{ij} \partial_k v_k \right]. \quad (\text{D.27})$$

The value of the constant $\epsilon^{(2)}$ is determined by equating this result for $\sum_a e_{ai} e_{aj} f_a$ to (2.117). In the incompressible fluid limit, the divergence of the velocity field

vanishes; $\partial_k v_k = 0$. Therefore fix the constant coefficient $\epsilon^{(2)} = \frac{1}{2}D(D+2)$ to write the shear viscosity as

$$\eta = \frac{\rho \lambda^{(2)} c}{D(D+2)}. \quad (\text{D.28})$$

The expansion for f_a , (D.25), becomes

$$f_a = \frac{n}{B} + \frac{nD}{cB} e_{ak} v_k + \frac{nD(D+2)}{2c^2 B} \left(e_{ak} e_{al} v_k v_l - \frac{1}{D} v_k v_k \right) - \frac{n\lambda^{(2)}}{cB} e_{ak} e_{al} \partial_k v_l. \quad (\text{D.29})$$

Therefore, the ideal part of (D.29) is

$$(f_a^{eq})^{ideal} = \frac{n}{B} + \frac{nD}{cB} e_{ai} v_i + \frac{nD(D+2)}{2c^2 B} \hat{e}_{ai} \hat{e}_{aj} v_i v_j - \frac{n(D+2)}{2c^2 B} v^2 \quad (\text{D.30})$$

and in summary using $\rho = mn$ for the density and $c_s = \frac{c}{\sqrt{D}}$ for the sound speed this satisfies

$$m \sum_a (f_a^{eq})^{ideal} = \rho \quad (\text{D.31})$$

$$mc \sum_a e_{ai} (f_a^{eq})^{ideal} = \rho v_i \quad (\text{D.32})$$

$$mc^2 \sum_a e_{ai} e_{aj} (f_a^{eq})^{ideal} = \rho c_s^2 \left(1 - \frac{v^2}{c^2} \right) \delta_{ij} + \rho v_i v_j. \quad (\text{D.33})$$

We can identify the pressure

$$p = \rho c_s^2 \left(1 - \frac{v^2}{c^2} \right). \quad (\text{D.34})$$

It appears to have a spurious dependence on the square of the velocity field, $(1 - \frac{v^2}{c^2})$, as did the pressure in the lattice gas calculation in the previous section. Here the factor g does not appear since the particle distribution function is Boltzmann distributed. It is possible to fix this anomaly in the fluid pressure at the expense of redefining the density. Chen et al. [23] have introduced a pressure-corrected equilibrium distribution to have the following Chapman-Enskog expansion

$$(f_a^{eq})_{PC}^{ideal} = \frac{n}{B} + \frac{nD}{cB} e_{ai} v_i + \frac{nD(D+2)}{2c^2 B} \hat{e}_{ai} \hat{e}_{aj} v_i v_j - \frac{nD}{2c^2 B} v^2 \quad (\text{D.35})$$

which satisfies

$$m \sum_a (f_a^{\epsilon q})_{PC}^{ideal} = \rho \left(1 - \frac{v^2}{c^2}\right) \quad (D.36)$$

$$mc \sum_a e_{ai} (f_a^{\epsilon q})_{PC}^{ideal} = \rho v_i \quad (D.37)$$

$$mc^2 \sum_a e_{ai} e_{aj} (f_a^{\epsilon q})_{PC}^{ideal} = \rho c_s^2 \delta_{ij} + \rho v_i v_j. \quad (D.38)$$

Here the definition of the density is modified by the $1 - \frac{v^2}{c^2}$ factor. By this point all the constant coefficients of the expansion (D.17) are determined except for the coefficient $\lambda^{(2)}$.

Appendix E

Integer Lattice Gas Implementation

The full set of equivalence classes modulo the triangular lattice isometries and particle-hole symmetry for the $L = 2$ integer lattice gas with $D = 2$ and $B = 6$ is listed below. Note that the first two equivalence classes have zero total momentum, for two and three particles respectively, and have only one particle per site. These are the equivalence classes for the FHP $L = 1$ lattice gas [42], which therefore is clearly a subset of the $L = 2$ integer lattice gas. The format for this table is given in §6.1.

{3, 2, 0, 0, {0, 0, 1, 0, 0, 1}, {0, 1, 0, 0, 1, 0}, {1, 0, 0, 1, 0, 0}},
{2, 3, 0, 0, {0, 1, 0, 1, 0, 1}, {1, 0, 1, 0, 1, 0}},
{3, 3, 2, 0, {0, 0, 1, 0, 0, 2}, {0, 1, 0, 0, 1, 1}, {1, 0, 0, 1, 0, 1}},
{2, 3, 3, 1, {0, 1, 0, 0, 0, 2}, {2, 0, 0, 0, 1, 0}},
{6, 4, 0, 0, {0, 0, 2, 0, 0, 2}, {0, 1, 1, 0, 1, 1}, {0, 2, 0, 0, 2, 0},
{1, 0, 1, 1, 0, 1}, {1, 1, 0, 1, 1, 0}, {2, 0, 0, 2, 0, 0}},
{4, 4, 2, 0, {0, 1, 0, 1, 0, 2}, {1, 0, 1, 0, 1, 1},
{1, 1, 0, 0, 2, 0}, {2, 0, 0, 1, 1, 0}},
{3, 4, 3, 1, {1, 0, 1, 0, 0, 2}, {1, 1, 0, 0, 1, 1}, {2, 0, 0, 1, 0, 1}},
{4, 4, 4, 0, {0, 0, 1, 0, 0, 3}, {0, 1, 0, 0, 1, 2},
{1, 0, 0, 1, 0, 2}, {2, 0, 0, 0, 2, 0}},
{2, 4, 4, 2, {1, 1, 0, 0, 0, 2}, {3, 0, 0, 0, 1, 0}},
{2, 4, 5, 1, {0, 1, 0, 0, 0, 3}, {2, 0, 0, 0, 1, 1}},
{6, 5, 0, 0, {0, 1, 1, 1, 0, 2}, {0, 2, 0, 1, 1, 1}, {1, 0, 2, 0, 1, 1},
{1, 1, 0, 2, 0, 1}, {1, 1, 1, 0, 2, 0}, {2, 0, 1, 1, 1, 0}},
{7, 5, 2, 0, {0, 0, 2, 0, 0, 3}, {0, 1, 1, 0, 1, 2},
{0, 2, 0, 0, 2, 1}, {1, 0, 1, 1, 0, 2}, {1, 1, 0, 1, 1, 1}},

{2, 0, 0, 2, 0, 1}, {2, 0, 1, 0, 2, 0}},
 {6, 5, 3, 1, {0, 1, 1, 0, 0, 3}, {0, 2, 0, 0, 1, 2}, {1, 1, 0, 1, 0, 2},
 {2, 0, 1, 0, 1, 1}, {2, 1, 0, 0, 2, 0}, {3, 0, 0, 1, 1, 0}},
 {4, 5, 4, 0, {0, 1, 0, 1, 0, 3}, {1, 0, 1, 0, 1, 2}, {1, 1, 0, 0, 2, 1},
 {2, 0, 0, 1, 1, 1}},
 {4, 5, 4, 2, {0, 2, 0, 0, 0, 3}, {2, 0, 1, 0, 0, 2},
 {2, 1, 0, 0, 1, 1}, {3, 0, 0, 1, 0, 1}},
 {4, 5, 5, 1, {1, 0, 1, 0, 0, 3}, {1, 1, 0, 0, 1, 2}, {2, 0, 0, 1, 0, 2},
 {3, 0, 0, 0, 2, 0}},
 {3, 5, 6, 0, {0, 1, 0, 0, 1, 3}, {1, 0, 0, 1, 0, 3}, {2, 0, 0, 0, 2, 1}},
 {2, 5, 6, 2, {1, 1, 0, 0, 0, 3}, {3, 0, 0, 0, 1, 1}},
 {12, 6, 0, 0, {0, 0, 3, 0, 0, 3}, {0, 1, 2, 0, 1, 2}, {0, 2, 0, 2, 0, 2},
 {0, 2, 1, 0, 2, 1}, {0, 3, 0, 0, 3, 0}, {1, 0, 2, 1, 0, 2},
 {1, 1, 1, 1, 1, 1}, {1, 2, 0, 1, 2, 0}, {2, 0, 1, 2, 0, 1},
 {2, 0, 2, 0, 2, 0}, {2, 1, 0, 2, 1, 0}, {3, 0, 0, 3, 0, 0}},
 {9, 6, 2, 0, {0, 1, 1, 1, 0, 3}, {0, 2, 0, 1, 1, 2}, {1, 0, 2, 0, 1, 2},
 {1, 1, 0, 2, 0, 2}, {1, 1, 1, 0, 2, 1}, {1, 2, 0, 0, 3, 0},
 {2, 0, 1, 1, 1, 1}, {2, 1, 0, 1, 2, 0}, {3, 0, 0, 2, 1, 0}},
 {8, 6, 3, 1, {0, 2, 0, 1, 0, 3}, {1, 0, 2, 0, 0, 3}, {1, 1, 1, 0, 1, 2},
 {1, 2, 0, 0, 2, 1}, {2, 0, 1, 1, 0, 2}, {2, 1, 0, 1, 1, 1},
 {3, 0, 0, 2, 0, 1}, {3, 0, 1, 0, 2, 0}},
 {8, 6, 4, 0, {0, 1, 1, 0, 1, 3}, {0, 2, 0, 0, 2, 2}, {1, 0, 1, 1, 0, 3},
 {1, 1, 0, 1, 1, 2}, {2, 0, 0, 2, 0, 2}, {2, 0, 1, 0, 2, 1},
 {2, 1, 0, 0, 3, 0}, {3, 0, 0, 1, 2, 0}},
 {5, 6, 4, 2, {1, 1, 1, 0, 0, 3}, {1, 2, 0, 0, 1, 2}, {2, 1, 0, 1, 0, 2},
 {3, 0, 1, 0, 1, 1}, {3, 1, 0, 0, 2, 0}},
 {5, 6, 5, 1, {0, 2, 0, 0, 1, 3}, {1, 1, 0, 1, 0, 3}, {2, 0, 1, 0, 1, 2},
 {2, 1, 0, 0, 2, 1}, {3, 0, 0, 1, 1, 1}},
 {3, 6, 5, 3, {1, 2, 0, 0, 0, 3}, {3, 0, 1, 0, 0, 2}, {3, 1, 0, 0, 1, 1}},
 {4, 6, 6, 0, {1, 0, 1, 0, 1, 3}, {1, 1, 0, 0, 2, 2}, {2, 0, 0, 1, 1, 2},
 {3, 0, 0, 0, 3, 0}},
 {3, 6, 6, 2, {2, 0, 1, 0, 0, 3}, {2, 1, 0, 0, 1, 2}, {3, 0, 0, 1, 0, 2}},
 {3, 6, 7, 1, {1, 1, 0, 0, 1, 3}, {2, 0, 0, 1, 0, 3}, {3, 0, 0, 0, 2, 1}},
 {12, 7, 0, 0, {0, 1, 2, 1, 0, 3}, {0, 2, 1, 1, 1, 2}, {0, 3, 0, 1, 2, 1},
 {1, 0, 3, 0, 1, 2}, {1, 1, 1, 2, 0, 2}, {1, 1, 2, 0, 2, 1},
 {1, 2, 0, 2, 1, 1}, {1, 2, 1, 0, 3, 0}, {2, 0, 2, 1, 1, 1},
 {2, 1, 0, 3, 0, 1}, {2, 1, 1, 1, 2, 0}, {3, 0, 1, 2, 1, 0}},
 {13, 7, 2, 0, {0, 1, 2, 0, 1, 3}, {0, 2, 0, 2, 0, 3}, {0, 2, 1, 0, 2, 2},
 {0, 3, 0, 0, 3, 1}, {1, 1, 1, 1, 1, 2}, {1, 2, 0, 1, 2, 1},
 {2, 0, 1, 2, 0, 2}, {2, 0, 2, 0, 2, 1}, {2, 1, 0, 2, 1, 1},
 {2, 1, 1, 0, 3, 0}, {3, 0, 0, 3, 0, 1}, {3, 0, 1, 1, 2, 0},
 {1, 0, 2, 1, 0, 3}},
 {10, 7, 3, 1, {0, 2, 1, 0, 1, 3},
 {0, 3, 0, 0, 2, 2}, {1, 1, 1, 1, 0, 3}, {1, 2, 0, 1, 1, 2},
 {2, 0, 2, 0, 1, 2}, {2, 1, 0, 2, 0, 2}, {2, 1, 1, 0, 2, 1},
 {2, 2, 0, 0, 3, 0}, {3, 0, 1, 1, 1, 1}, {3, 1, 0, 1, 2, 0}},
 {9, 7, 4, 0, {0, 2, 0, 1, 1, 3}, {1, 0, 2, 0, 1, 3}, {1, 1, 0, 2, 0, 3},
 {1, 1, 1, 0, 2, 2}, {1, 2, 0, 0, 3, 1}, {2, 0, 1, 1, 1, 2},

{2, 1, 0, 1, 2, 1}, {3, 0, 0, 2, 1, 1}, {3, 0, 1, 0, 3, 0}},
 {7, 7, 4, 2, {0, 3, 0, 0, 1, 3}, {1, 2, 0, 1, 0, 3}, {2, 0, 2, 0, 0, 3},
 {2, 1, 1, 0, 1, 2}, {2, 2, 0, 0, 2, 1}, {3, 0, 1, 1, 0, 2},
 {3, 1, 0, 1, 1, 1}},
 {7, 7, 5, 1, {1, 1, 1, 0, 1, 3}, {1, 2, 0, 0, 2, 2}, {2, 0, 1, 1, 0, 3},
 {2, 1, 0, 1, 1, 2}, {3, 0, 0, 2, 0, 2}, {3, 0, 1, 0, 2, 1},
 {3, 1, 0, 0, 3, 0}},
 {3, 7, 5, 3, {2, 1, 1, 0, 0, 3}, {2, 2, 0, 0, 1, 2}, {3, 1, 0, 1, 0, 2}},
 {6, 7, 6, 0, {0, 2, 0, 0, 2, 3}, {1, 1, 0, 1, 1, 3}, {2, 0, 0, 2, 0, 3},
 {2, 0, 1, 0, 2, 2}, {2, 1, 0, 0, 3, 1}, {3, 0, 0, 1, 2, 1}},
 {4, 7, 6, 2, {1, 2, 0, 0, 1, 3}, {2, 1, 0, 1, 0, 3}, {3, 0, 1, 0, 1, 2},
 {3, 1, 0, 0, 2, 1}},
 {3, 7, 7, 1, {2, 0, 1, 0, 1, 3}, {2, 1, 0, 0, 2, 2}, {3, 0, 0, 1, 1, 2}},
 {2, 7, 7, 3, {3, 0, 1, 0, 0, 3}, {3, 1, 0, 0, 1, 2}},
 {3, 7, 8, 0, {1, 1, 0, 0, 2, 3}, {2, 0, 0, 1, 1, 3}, {3, 0, 0, 0, 3, 1}},
 {2, 7, 8, 2, {2, 1, 0, 0, 1, 3}, {3, 0, 0, 1, 0, 3}},
 {18, 8, 0, 0, {0, 1, 3, 0, 1, 3}, {0, 2, 1, 2, 0, 3}, {0, 2, 2, 0, 2, 2},
 {0, 3, 0, 2, 1, 2}, {0, 3, 1, 0, 3, 1}, {1, 0, 3, 1, 0, 3},
 {1, 1, 2, 1, 1, 2}, {1, 2, 0, 3, 0, 2}, {1, 2, 1, 1, 2, 1},
 {1, 3, 0, 1, 3, 0}, {2, 0, 2, 2, 0, 2}, {2, 0, 3, 0, 2, 1},
 {2, 1, 1, 2, 1, 1}, {2, 1, 2, 0, 3, 0}, {2, 2, 0, 2, 2, 0},
 {3, 0, 1, 3, 0, 1}, {3, 0, 2, 1, 2, 0}, {3, 1, 0, 3, 1, 0}},
 {14, 8, 2, 0, {0, 2, 1, 1, 1, 3}, {0, 3, 0, 1, 2, 2}, {1, 0, 3, 0, 1, 3},
 {1, 1, 1, 2, 0, 3}, {1, 1, 2, 0, 2, 2}, {1, 2, 0, 2, 1, 2},
 {1, 2, 1, 0, 3, 1}, {2, 0, 2, 1, 1, 2}, {2, 1, 0, 3, 0, 2},
 {2, 1, 1, 1, 2, 1}, {2, 2, 0, 1, 3, 0}, {3, 0, 1, 2, 1, 1},
 {3, 0, 2, 0, 3, 0}, {3, 1, 0, 2, 2, 0}},
 {12, 8, 3, 1, {0, 3, 0, 1, 1, 3}, {1, 1, 2, 0, 1, 3}, {1, 2, 0, 2, 0, 3},
 {1, 2, 1, 0, 2, 2}, {1, 3, 0, 0, 3, 1}, {2, 0, 2, 1, 0, 3},
 {2, 1, 1, 1, 1, 2}, {2, 2, 0, 1, 2, 1}, {3, 0, 1, 2, 0, 2},
 {3, 0, 2, 0, 2, 1}, {3, 1, 0, 2, 1, 1}, {3, 1, 1, 0, 3, 0}},
 {11, 8, 4, 0, {0, 2, 1, 0, 2, 3}, {0, 3, 0, 0, 3, 2}, {1, 1, 1, 1, 1, 3},
 {1, 2, 0, 1, 2, 2}, {2, 0, 1, 2, 0, 3}, {2, 0, 2, 0, 2, 2},
 {2, 1, 0, 2, 1, 2}, {2, 1, 1, 0, 3, 1}, {3, 0, 0, 3, 0, 2},
 {3, 0, 1, 1, 2, 1}, {3, 1, 0, 1, 3, 0}},
 {8, 8, 4, 2, {1, 2, 1, 0, 1, 3}, {1, 3, 0, 0, 2, 2}, {2, 1, 1, 1, 0, 3},
 {2, 2, 0, 1, 1, 2}, {3, 0, 2, 0, 1, 2}, {3, 1, 0, 2, 0, 2},
 {3, 1, 1, 0, 2, 1}, {3, 2, 0, 0, 3, 0}},
 {8, 8, 5, 1, {0, 3, 0, 0, 2, 3}, {1, 2, 0, 1, 1, 3}, {2, 0, 2, 0, 1, 3},
 {2, 1, 0, 2, 0, 3}, {2, 1, 1, 0, 2, 2}, {2, 2, 0, 0, 3, 1},
 {3, 0, 1, 1, 1, 2}, {3, 1, 0, 1, 2, 1}},
 {5, 8, 5, 3, {1, 3, 0, 0, 1, 3}, {2, 2, 0, 1, 0, 3}, {3, 0, 2, 0, 0, 3},
 {3, 1, 1, 0, 1, 2}, {3, 2, 0, 0, 2, 1}},
 {6, 8, 6, 0, {1, 1, 1, 0, 2, 3}, {1, 2, 0, 0, 3, 2}, {2, 0, 1, 1, 1, 3},
 {2, 1, 0, 1, 2, 2}, {3, 0, 0, 2, 1, 2}, {3, 0, 1, 0, 3, 1}},
 {4, 8, 6, 2, {2, 1, 1, 0, 1, 3}, {2, 2, 0, 0, 2, 2}, {3, 0, 1, 1, 0, 3},
 {3, 1, 0, 1, 1, 2}},
 {2, 8, 6, 4, {3, 1, 1, 0, 0, 3}, {3, 2, 0, 0, 1, 2}},

{5, 8, 7, 1, {1, 2, 0, 0, 2, 3}, {2, 1, 0, 1, 1, 3}, {3, 0, 0, 2, 0, 3},
 {3, 0, 1, 0, 2, 2}, {3, 1, 0, 0, 3, 1}},
 {2, 8, 7, 3, {2, 2, 0, 0, 1, 3}, {3, 1, 0, 1, 0, 3}},
 {3, 8, 8, 0, {2, 0, 1, 0, 2, 3}, {2, 1, 0, 0, 3, 2}, {3, 0, 0, 1, 2, 2}},
 {2, 8, 8, 2, {3, 0, 1, 0, 1, 3}, {3, 1, 0, 0, 2, 2}},
 {2, 8, 9, 1, {2, 1, 0, 0, 2, 3}, {3, 0, 0, 1, 1, 3}},
 {16, 9, 0, 0, {0, 2, 2, 1, 1, 3}, {0, 3, 0, 3, 0, 3}, {0, 3, 1, 1, 2, 2},
 {1, 1, 2, 2, 0, 3}, {1, 1, 3, 0, 2, 2}, {1, 2, 1, 2, 1, 2},
 {1, 2, 2, 0, 3, 1}, {1, 3, 0, 2, 2, 1}, {2, 0, 3, 1, 1, 2},
 {2, 1, 1, 3, 0, 2}, {2, 1, 2, 1, 2, 1}, {2, 2, 0, 3, 1, 1},
 {2, 2, 1, 1, 3, 0}, {3, 0, 2, 2, 1, 1}, {3, 0, 3, 0, 3, 0},
 {3, 1, 1, 2, 2, 0}},
 {16, 9, 2, 0, {0, 2, 2, 0, 2, 3},
 {0, 3, 0, 2, 1, 3}, {0, 3, 1, 0, 3, 2}, {1, 1, 2, 1, 1, 3},
 {1, 2, 0, 3, 0, 3}, {1, 2, 1, 1, 2, 2}, {1, 3, 0, 1, 3, 1},
 {2, 0, 2, 2, 0, 3}, {2, 0, 3, 0, 2, 2}, {2, 1, 1, 2, 1, 2},
 {2, 1, 2, 0, 3, 1}, {2, 2, 0, 2, 2, 1}, {3, 0, 1, 3, 0, 2},
 {3, 0, 2, 1, 2, 1}, {3, 1, 0, 3, 1, 1}, {3, 1, 1, 1, 3, 0}},
 {12, 9, 3, 1, {0, 3, 1, 0, 2, 3}, {1, 2, 1, 1, 1, 3}, {1, 3, 0, 1, 2, 2},
 {2, 0, 3, 0, 1, 3}, {2, 1, 1, 2, 0, 3}, {2, 1, 2, 0, 2, 2},
 {2, 2, 0, 2, 1, 2}, {2, 2, 1, 0, 3, 1}, {3, 0, 2, 1, 1, 2},
 {3, 1, 0, 3, 0, 2}, {3, 1, 1, 1, 2, 1}, {3, 2, 0, 1, 3, 0}},
 {11, 9, 4, 0, {0, 3, 0, 1, 2, 3}, {1, 1, 2, 0, 2, 3}, {1, 2, 0, 2, 1, 3},
 {1, 2, 1, 0, 3, 2}, {2, 0, 2, 1, 1, 3}, {2, 1, 0, 3, 0, 3},
 {2, 1, 1, 1, 2, 2}, {2, 2, 0, 1, 3, 1}, {3, 0, 1, 2, 1, 2},
 {3, 0, 2, 0, 3, 1}, {3, 1, 0, 2, 2, 1}},
 {8, 9, 4, 2, {1, 3, 0, 1, 1, 3}, {2, 1, 2, 0, 1, 3}, {2, 2, 0, 2, 0, 3},
 {2, 2, 1, 0, 2, 2}, {2, 3, 0, 0, 3, 1}, {3, 0, 2, 1, 0, 3},
 {3, 1, 1, 1, 1, 2}, {3, 2, 0, 1, 2, 1}},
 {8, 9, 5, 1, {1, 2, 1, 0, 2, 3}, {1, 3, 0, 0, 3, 2}, {2, 1, 1, 1, 1, 3},
 {2, 2, 0, 1, 2, 2}, {3, 0, 1, 2, 0, 3}, {3, 0, 2, 0, 2, 2},
 {3, 1, 0, 2, 1, 2}, {3, 1, 1, 0, 3, 1}},
 {4, 9, 5, 3, {2, 2, 1, 0, 1, 3}, {2, 3, 0, 0, 2, 2}, {3, 1, 1, 1, 0, 3},
 {3, 2, 0, 1, 1, 2}},
 {8, 9, 6, 0, {0, 3, 0, 0, 3, 3}, {1, 2, 0, 1, 2, 3},
 {2, 0, 2, 0, 2, 3}, {2, 1, 0, 2, 1, 3}, {2, 1, 1, 0, 3, 2},
 {3, 0, 0, 3, 0, 3}, {3, 0, 1, 1, 2, 2}, {3, 1, 0, 1, 3, 1}},
 {6, 9, 6, 2, {1, 3, 0, 0, 2, 3}, {2, 2, 0, 1, 1, 3}, {3, 0, 2, 0, 1, 3},
 {3, 1, 0, 2, 0, 3}, {3, 1, 1, 0, 2, 2}, {3, 2, 0, 0, 3, 1}},
 {2, 9, 6, 4, {2, 3, 0, 0, 1, 3}, {3, 2, 0, 1, 0, 3}},
 {4, 9, 7, 1, {2, 1, 1, 0, 2, 3}, {2, 2, 0, 0, 3, 2}, {3, 0, 1, 1, 1, 3},
 {3, 1, 0, 1, 2, 2}},
 {2, 9, 7, 3, {3, 1, 1, 0, 1, 3}, {3, 2, 0, 0, 2, 2}},
 {4, 9, 8, 0, {1, 2, 0, 0, 3, 3}, {2, 1, 0, 1, 2, 3}, {3, 0, 0, 2, 1, 3},
 {3, 0, 1, 0, 3, 2}},
 {2, 9, 8, 2, {2, 2, 0, 0, 2, 3}, {3, 1, 0, 1, 1, 3}},
 {2, 9, 9, 1, {3, 0, 1, 0, 2, 3}, {3, 1, 0, 0, 3, 2}},
 {2, 9, 10, 0, {2, 1, 0, 0, 3, 3}, {3, 0, 0, 1, 2, 3}}

A simple, albeit memory intensive, algorithm that I have employed to implement $L = 2$, $L = 3$, and $L = 4$ integer lattice gases uses a table lookup approach, similar to that employed in the well known $L = 1$ case. For $L > 1$ however, more than a single lookup table is required. The algorithm presented here offers two advantages: it is quite simple, and it provides statistically detailed balance in a straightforward fashion.

The first step is to generate a binary sequence of integers from 0 to 2^{BL} ; this is the first table, termed the *configuration table*.¹ For each entry in the configuration table an equivalence class tag is then computed. The equivalence class tag, denoted I_{EC} , is an integer that encodes the configuration's mass and momentum. For the example of the $L = 2$ integer lattice gas given above, where $B = 6$ and $D = 2$, the equivalence class tag may be defined as

$$I_{\text{EC}} \equiv A m + B (2p_x) + C \left(\frac{\sqrt{3}}{2} p_y \right), \quad (\text{E.1})$$

where the constant coefficients A , B , and C are chosen so that I_{EC} is always a positive integer. The second step is to use (E.1) to generate a second table, termed the *tag table* that corresponds one-to-one with the configuration table. Note that the tag table will have many duplicate tags since several configurations can have the same tag. In fact, grouping all the common tags together is the way to find all the configurations that are members of an equivalence class.

¹Note that for $B = 6$ and $L = 4$, the total amount of memory needed to sort a single table is 3×2^{24} bytes, or 48 megabytes. Therefore, since several tables are required in this algorithm, it is not possible on current day supercomputers to simulate integer lattice gases with $L > 4$. To overcome this deficiency, a polytope sampling algorithm was developed that trades off memory for time [17]. Since computational time is crucial for numerical efficiency, the polytope sampling method has not been competitive for smaller values of L but is necessary for large L .

The tag table just described is then sorted. In the C language this can be easily done by calling a quick sort routine. The configuration table must be sorted along the way as the tag table is sorted to keep all the tags and configurations in one-to-one correspondence. At this point, all the configurations are now ordered in equivalence class groupings so that each entry in the configuration table is now juxtaposed to entries in the same equivalence class. Another table is needed to continue the algorithm construction.

The third step is to count the number of similar equivalence tags and to generate a table that gives for each entry in the configuration table the size of the equivalence class that contains that entry. This table is termed the *size table*. With a counter initially set to zero, the size table is generated by sequentially scanning through the tag table and incrementing the counter each time a duplicate tag is found. When a new tag is encountered, this indicates the end of an equivalence class has been reached, so the contents of the counter is just the size of the previous equivalence class, N_{EC} . Before the counter is zeroed out to begin counting the size of the next equivalence class, its value is repeatedly back copied N_{EC} -times into the size table so that there is a one-to-one correspondence to each entry of the configuration table.

Finally, the tag table is regenerated; it is in unsorted fashion again so that it can serve as the main lookup table of the lattice gas simulation. Each tag is replaced with the address of the first entry of the equivalence class with which this tag is associated. The tag table is now a *pointer table* and can be used for table lookup purposes.

The configuration table, the size table, and the pointer table are computed before the integer lattice gas simulation begins and need be computed only a single time; therefore, they impose no computational overhead.

A collision takes place as follows. The incoming site data, s , is used as an address into the pointer table. The outgoing site data, s' , now points to the first element in its equivalence class in the configuration table, s_{base} ,

$$s' = s_{\text{base}}. \quad (\text{E.2})$$

Then s is also used to address the size table so that the size of the equivalence class containing this configuration can be fetched, $N_{\text{EC}}(s)$. A large random number, denoted R , is generated and then taken modulo the size of the equivalence class to obtain a small random number, denoted r ,

$$r = (R \bmod N_{\text{EC}}(s)). \quad (\text{E.3})$$

Note that $0 \leq r \leq N_{\text{EC}}(s) - 1$. The final outgoing site data, s' , is then easily computed by using r as a memory offset from the base address

$$s' = s_{\text{base}} + r. \quad (\text{E.4})$$

In this way, integer lattice gases for $L \leq 4$ can be efficiently simulated on a computer by table lookup.

Appendix F

Counting States in Quantum Mechanics

In quantum mechanics, in the canonical ensemble the partition function is

$$Q = \sum_j \exp\left(-\frac{E_j}{kT}\right), \quad (\text{F.1})$$

where j sums over all accessible energy states. Denoting the energy eigenstates by $\psi_j(x)$ in the position representations, the Schrödinger eigenequation is

$$\hat{H}\psi_j(x) = E_j\psi_j(x). \quad (\text{F.2})$$

The energy eigenfunctions are orthonormalized so

$$\int dx \psi_i^*(x) \psi_j(x) = \delta_{ij}. \quad (\text{F.3})$$

Then the canonical partition function can be rewritten by inserting one into the integrand

$$Q = \sum_j \exp\left(-\frac{E_j}{kT}\right) \int dx \psi_j^*(x) \psi_j(x) \quad (\text{F.4})$$

$$= \sum_j \int dx \psi_j^*(x) \exp\left(-\frac{\hat{H}}{kT}\right) \psi_j(x) \quad (\text{F.5})$$

Now we would like to convert the sum over energy levels into a sum over momentum states (actually into an integration over momentum states since we are considering motion in a continuum). To this end, consider the complete set of orthonormal momentum eigenfunctions

$$\varphi(x, p) = \frac{1}{h^{\frac{3N}{2}}} \exp\left(2\pi i \frac{px}{h}\right). \quad (\text{F.6})$$

The energy eigenfunctions can be expressed as a linear combination of the momentum eigenfunctions as follows

$$\psi_j(x) = \frac{1}{h^{\frac{3N}{2}}} \int dp A_j(p) \exp\left(2\pi i \frac{px}{h}\right). \quad (\text{F.7})$$

Note that the orthonormality condition on the energy eigenfunctions implies that the coefficients satisfy

$$\sum_j A_j^*(p) A_j(p') = \delta(p - p'). \quad (\text{F.8})$$

The partition function can now be rewritten as

$$\begin{aligned} Q &= \sum_j \int dx \left[\frac{1}{h^{\frac{3N}{2}}} \int dp A_j^*(p) \exp\left(-2\pi i \frac{px}{h}\right) \right] \exp\left(-\frac{\hat{H}}{kT}\right) \left[\frac{1}{h^{\frac{3N}{2}}} \int dp' A_j(p') \exp\left(2\pi i \frac{p'x}{h}\right) \right] \\ &= \frac{1}{h^{3N}} \int dx \int dp \exp\left(-2\pi i \frac{px}{h}\right) \exp\left(-\frac{\hat{H}}{kT}\right) \exp\left(2\pi i \frac{px}{h}\right). \end{aligned} \quad (\text{F.9})$$

In the classical limit, the integrand simplifies to the usual Boltzmann weight

$$\exp\left(-2\pi i \frac{px}{h}\right) \exp\left(-\frac{\hat{H}}{kT}\right) \exp\left(2\pi i \frac{px}{h}\right) \rightarrow \exp\left(\frac{-H}{kT}\right) \quad (\text{F.10})$$

so the classical partition function for an N -particle system in the canonical ensemble becomes

$$Q_{\text{classical}} = \frac{1}{h^{3N}} \int dx \int dp \exp\left(\frac{-H}{kT}\right). \quad (\text{F.11})$$

The remarkable point, which is quite well known, is that h^3 is seen to be the “smallest unit” of phasespace.